DEVELOPMENT OF NEW DIELECTRIC MATERIALS

FOR PULSED POWER APPLICATIONS

A Thesis Presented to the Faculty of the Graduate School

of University of Missouri-Columbia

In Partial Fulfillment

Of the Requirements for the Degree

Masters of Science

by

Jason A. Smith

Dr. Randy Curry, Thesis Supervisor

May 2012

The undersigned, appointed by the dean of the Graduate School, have

examined this thesis entitled

DEVELOPMENT OF NEW DIELECTRIC MATERIALS

FOR PULSED POWER APPLICATIONS

presented by Jason A. Smith

a candidate for the degree of Masters of Science

and hereby certify that, in their opinion, it is worthy of acceptance.

_____

Dr. Randy Curry

_____

Dr. Robert O'Connell

_____

Dr. Thomas Clevenger

ACKNOWLEDGMENTS

I would like to thank Andy Erickson and Dr. Larry Ussery at Los Alamos National Laboratory for supporting me in my plans of going to graduate school. I would also like to extend thanks to Dr. Randy Curry, Dr. Thomas Clevenger, Dr. Robert O'Connell, Peter Norgard, Kevin O'Conner, Chris Yeckel, Mark Nichols, and the many other individuals who have helped me in various capacities in this project. I would also like to thank my parents, Michael and Jo Ellen Smith, and my family and friends for their encouragement and love. Most importantly, I would like to thank Jesus Christ for carrying me through everything that I do.

TABLE OF CONTENTS

LIST OF FIGURES

Figure Page

Chapter 1 - INTRODUCTION

1.1 THE NEED FOR NEW MATERIALS

The current pace of technological development in today's world dictates a constant need for new devices that are smaller, faster, smarter, and stronger. As a result, there are many technological fields that need new materials in order to meet the specifications of the future. New material development lays the foundation for implementing new ideas and technology in industrial, commercial, and governmental sectors.

Pulsed power and high power radio frequency (RF) technologies are now being built into mobile applications such as the Active Denial System (ADS). The ADS system that utilizes electromagnetic radiation at 95 GHz to heat the water molecules located within the top layers of skin. The ADS system, shown on a vehicular plat- form in Figure 1.1, serves as non-lethal way of dispersing crowds and discouraging aggressive behavior [1].

Another project in the field of pulsed power is the U.S. Navy's development of an electromagnetic rail gun (EMRG) [2]. This project is for military applications and utilizes an 11 MJ capacitor bank to accelerate a 1 kg projectile to 2 km/s. Using current technologies, the capacitor bank fills a large room.

Figure 1. 1: The Active Denial System (ADS) on a vehicle for portable use [1]

One of the dominant limiting factors of the ADS system and the EMRG system is their size. In order to reduce the size of this system, new materials which include new dielectric materials need to be developed to increase efficiency and reduce energy requirements.

1.2 NANOMATERIALS

"New materials can often be critical enabling drivers for new systems and applications with significant effects [4]." There is currently a large technological push for new "nanomaterials" which are materials that have particle sizes or structures on the billionth of a meter scale (10^{-9} m). Because of the reduced size of particles, the surface

area to volume ratio is much greater, which can give these particles a different set of material properties than particles of larger size.

Figure 1. 2: The capacitor bank that powers the Navy's Electromagnetic Railgun (EMRG) [3]

One example of new nanomaterials is carbon nanotubes. Carbon nanotubes have gained a large amount of attention in the last ten years because of their unique characteristics. Single-walled carbon nanotubes (SWCNT) are carbon atoms that form together into tube shaped structures that are about 0.6 to 1.8 nm in diameter. These SWCNTs, which is represented in Figure 1.3, can be 20 times stronger than steel with a density that is half that of aluminum. They also can exhibit higher current carrying capabilities, emit light at lower voltages than many current light emitting materials, and

conduct heat better than diamond. These characteristics could enable SWCNTs to be used to make stronger mechanical materials, more sensitive sensors, smaller and more efficient computer memory, and better batteries [5].

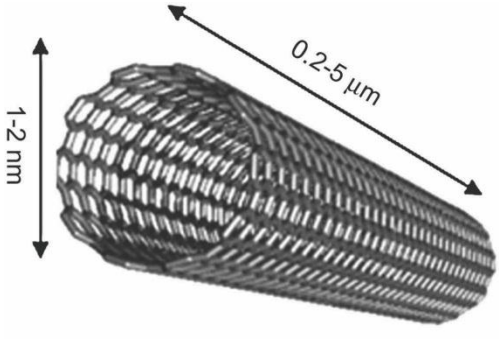

Figure 1. 3: An illustration of a Single Walled Carbon Nanotube (SWCNT) [6]

Another important nanomaterial research area is the formation of semiconductor "quantum dots". These dots are faceted crystals that have a diameter that can be as small as a few nanometers. One of the important characteristics of these dots the size of their band gaps, which is the amount of energy needed to excite a bound electron into a conduction state, can be tightly controlled. The size of the band gap is related to the size of the crystal. As a result, these quantum dots can exhibit particular optical properties, illustrated in Figure 1.4, which can enable them to be used in high quality dyes, laser applications, cell imagery, and solar energy [4].

These small quantum dots also exhibit a large amount of quantum behavior. This quantum behavior in quantum dots is being investigated for the purpose of developing new materials in the field of quantum computing. Typical computers utilize capacitors to

store bits of information [7]. The goal of quantum computers is to store information in the quantum spin of a quantum material. Quantum dots may be stable and predictable enough to assign a spin state and then read that state [7].

Nanopowders are also being investigated as a new source of improved specifications in today's technology. Nanopowders are solid powders that have a grain size on the nanometer scale. New varieties of nanopowders are now becoming available because of advances in manufacturing that have enabled their production on a larger and more affordable scale. As the price comes down, the chances of success of these new materials in replacing currently used materials increases. Largely because of the surface area to volume ratio, different nanopowders can possess unique chemical, electrical, and physical characteristics.

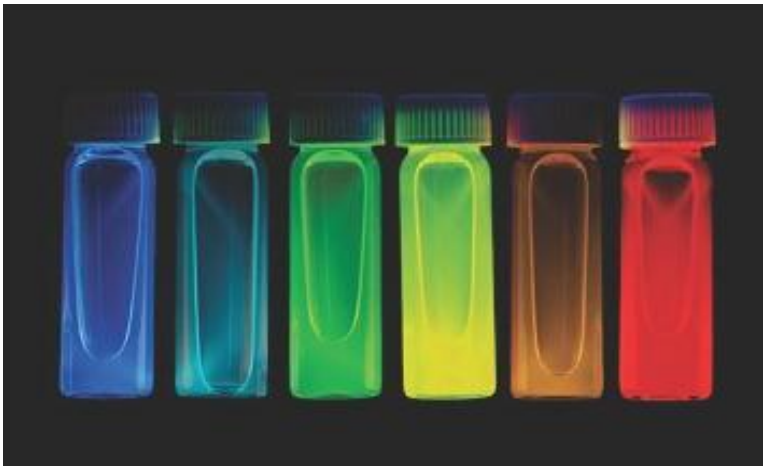

Figure 1. 4: Different colors of quantum dots [8]

1.3 NANOCOMPOSITES

By blending nanomaterials with other material, one can start to customize new materials. The effect is essentially blending the characteristics of the materials to create a composite material that displays characteristics that may not be available in a single material by itself [9]. A common way of making composite materials is to add a nanopowder to a matrix made up of another material [10].

In this study, two ceramic nanopowders, strontium titanate (ST) and barium strontium titanate (BST), were mixed into two different kinds of plastics, Teflon and polyvinylidene fluoride (PVDF) at different loading rates. As these two materials were mixed, the result was a plastic like substance with a dielectric constant that is higher than the normal plastic and was less brittle than ceramic alone and more machinable. The following thesis discusses the results of these tests and the future direction of the research.

1.4 Bibliography for Chapter 1

[1] S. LeVine, "The active denial system: A revolutionary, non-lethal weapon for todays battlefield," National Defense University Center for Technology and National Security Policy, June 2009.

[2] R. Meger, "Railguns materials science," Naval Research Laboratory, 2006.

[3] http://thetension.blogspot.com/2008/02/us-navy-demonstrates-worlds-most.html.

[4] P. S. Anton, R. Silberglitt, and J. Schneider, The Global Technology Revolution: Bio/Nano/Materials Trends and their Synergies with information technology by 2015. RAND, 2001.

[5] P. G. Collins and P. Avouris, "Nanotubes for electronics," Scientific American, December 2000.

[6] http://jnm.snmjournals.org/cgi/content-nw/full/48/7/1039/FIG1.

[7] C. S. Lent and D. P. Tougaw, "A device architecture for computing with quantum dots," Proceedings of the IEEE, vol. 85, no. 4, April 1997.

[8] http://nanoe.ece.drexel.edu/wiki/index.php/Image:Quantum_dots_ glowing.jpg.

[9] J. Gou, S. O'Braint, H. Gu, and G. Song, "Damping augmentation of nanocomposites using carbon nanofiber paper," Journal of nanomaterials, 2006.

[10] F. Hussain, M. Hojjati, M. Okamoto, and R. Gorga, "Review article: Polymer- matrix nanocomposites, processing, manufacturing, and application: An overview," Journal of composite materials, vol. 40, no. 17, 2006.

Chapter 2 – DIELECTRIC THEORY

2.1 DIELECTRIC CONSTANT THEORY

2.1.1 INTRODUCTION TO THE DIELECTRIC CONSTANT

In developing novel capacitor materials, electrical energy density is of preeminent importance. In order to decrease the size of a capacitor while maintaining the same energy within the capacitor, the electrical energy density of the capacitor has to increase. In a parallel plate capacitor, which will be used numerous times in this study, a dielectric material is sandwiched between two metal electrodes. The two electrodes are also connected to a voltage source which applies a voltage across the dielectric, as represented in Figure 2.1.

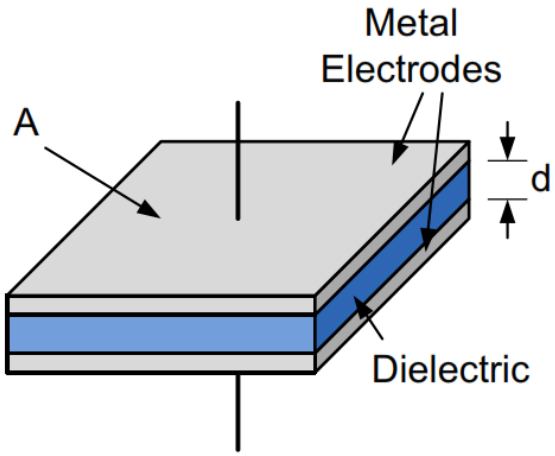

Figure 2. 1: A parallel plate capacitor connected to a voltage source

The electrical energy density is the electrical energy U_E divided by the volume of the material. In DC conditions, the electrical energy in a capacitor is defined as [1].

$$U_E = \frac{1}{2}CV^2 \quad (J) \tag{2.1}$$

The variable V is the static voltage of the voltage source and the variable C is the capacitance of the dielectric material. Excluding the fringe affects of the capacitor, the capacitance comes from the geometry of the capacitor material and a characteristic of the material called the permittivity ϵ. The mathematical relationship of capacitance is defined as [1].

$$C = \frac{\epsilon A}{d} \quad (F) \tag{2.2}$$

A is the surface area of the dielectric and d is the thickness. The permittivity defines how a material will react to an electric field. Dividing the permittivity, which will be defined in more detail later, by the permittivity of free space, ϵ_0 , yields a ratio called the relative permittivity, ϵ_r , which is also called the dielectric constant of the material. This is mathematically defined as [2].

$$\epsilon = \epsilon_r \epsilon_0 \quad (F/m) \tag{2.3}$$

Dividing the electrical energy defined by Equation 2.1 by the volume of the material, which is surface area times the thickness, yields the electrical energy density of the material, u_E.

$$u_E = \frac{U_E}{A\,d} \quad (J/m^3) \tag{2.4}$$

After substituting Equations 2.2 and 2.3 into Equation 2.4, the electrical energy density becomes

$$u_E = \frac{1}{2}\epsilon_r\epsilon_0\left(\frac{V}{d}\right)^2 \quad (J/m^3). \tag{2.5}$$

Therefore, the electric energy density in a dielectric material is directly proportional to the dielectric constant of the material. When developing a new dielectric for use in capacitor applications, the dielectric constant of the material is of paramount importance.

2.1.2 Electric Fields

As shown in Equation 2.5, the voltage and the thickness of the material also contribute significantly to the energy density. Voltage divided by the thickness of the dielectric material, which is also the distance between the electrodes, introduces another term called the electric field intensity, E, which is defined mathematically as [3].

$$\mathbf{E} = \frac{V}{d}\mathbf{a}_x \quad (V/m) \tag{2.6}$$

The term a_x represents the direction of the electric field strength, which is pointing perpendicularly from one electrode to the other and is given as the x direction. Substituting Equation 2.6 into Equation 2.5, yields Equation 2.7.

$$u_E = \frac{1}{2}\epsilon_r \epsilon_0 E^2 \tag{2.7}$$

As this equation shows, the energy density depends on the dielectric constant and the magnitude of the electric field intensity, E. Another way to interpret Equation 2.7 is to state that the energy density depends on the electric field intensity and the reaction of the dielectric material to the electric field, which is essentially the definition of the permittivity of a dielectric. "Dielectrics... are not a narrow class of so-called insulators, but the broad expanse of nonmetals considered from the standpoint of their interaction with electric, magnetic, or electromagnetic fields [4]." Dielectrics are a set of materials that react uniquely to the introduction of an electric field.

In order to define an electric field and a material's response an applied electric field, one must understand the definition of an electric field. "A field is a spatial distribution of scalar or vector quantity, which may or may not be a function of time [2]." The force exerted between two electric charges depends on the sign and magnitude of the charges and the distance between them. Mathematically, the electric force of a charge due to another charge is defined in Coulomb's law, which is [1] [3].

$$F = \frac{q_1 q_2}{4\pi\epsilon_0 r^2} \quad (N) \tag{2.8}$$

This equation assumes that the charges are in free space and they are isolated from all other charges. The term r is the distance between the charges measured, q is the magnitude of the charge, and F is the electric force [3].

The intensity of an electric field is defined as the force per unit of positive charge exerted on a body in the field, which is given by Equation 2.9.

$$E = \frac{F}{q} \quad (N/C) \tag{2.9}$$

A typical example of an electric field is two parallel plates hooked up to a constant voltage supply, as in Figure 2.2. In this case, another way to characterize an electric field is to divide the voltage between the plates V by the distance d between them [2].

$$E = \frac{V}{d} \quad (V/m) \tag{2.10}$$

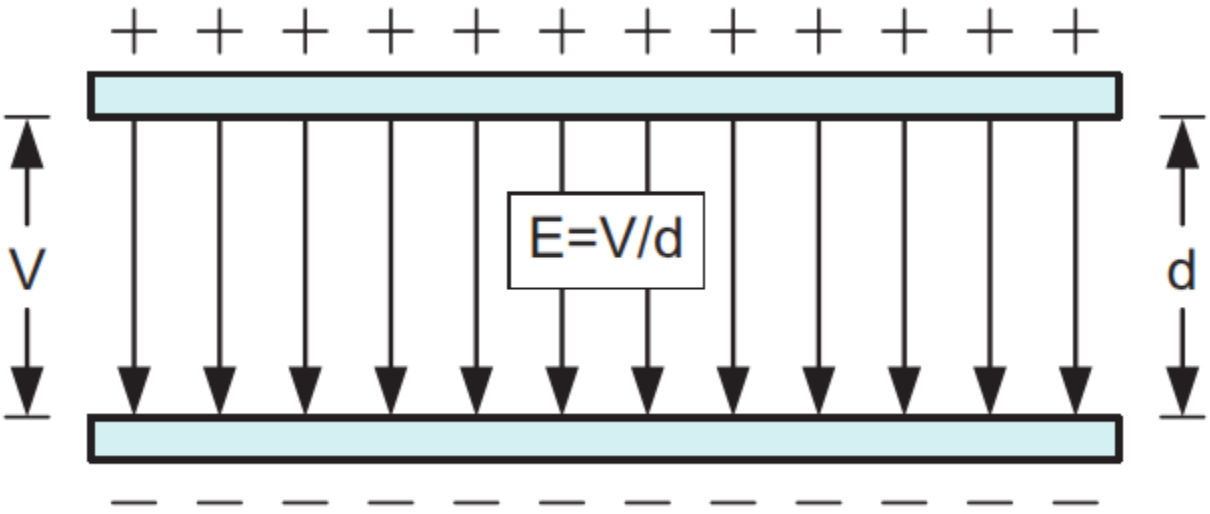

Figure 2. 2: An electric field created by two parallel plates with voltage difference

An application of an electric field is the invention of capacitors. Capacitors make use of electric fields in order to do electrical work. A capacitor can actually store energy within the molecules of the material, which is called a dielectric medium. The material must display certain characteristics in order to function as dielectric medium for a capacitor.

When a molecule is put into an electric field, it will respond in different ways depending on the type of material. Conducting materials have loosely bonded valence electrons that can be excited by thermal energy. When a conductor is acted upon by an electric field, the loosely bonded electrons are free to move between the molecules within the material. In choosing a capacitor material, the electron bonds within the material need to be strong enough to not allow electrons to move between molecules [5].

In an insulating or dielectric, the material has electron bonds that are stronger than that of conducting materials. When an insulating material or a dielectric material is exposed to an electric field, the valence electrons are not allowed to move between molecules of the material. There is a point at which the energy is large enough to break the electronic bonds, which is called intrinsic breakdown and will be discussed in a later section [5].

2.1.3 POLARIZATION

When an electric field is applied to an insulator, the electronic distribution and the nuclear positions are altered and the charges in the molecules are displaced. This displacement creates small electric dipoles within the material, which is represented in Figure 2.3a [6]. Electric dipoles are atomic structures that have a difference in charge

from one end to the other. As opposed to a conductor, the displaced charges, also called bound charges, do not escape the molecules. This displacement can be thought of as two opposite charges, +q and -q, which are separated by a distance a, which is represented in 2.3b. The dipole can be represented by a vector p that points from the negative charge to the positive charge and has a magnitude of the distance (a) between them. This vector is called the electric dipole moment [7] [8]. The direction of the dipole moment is always in the direction of the applied field.

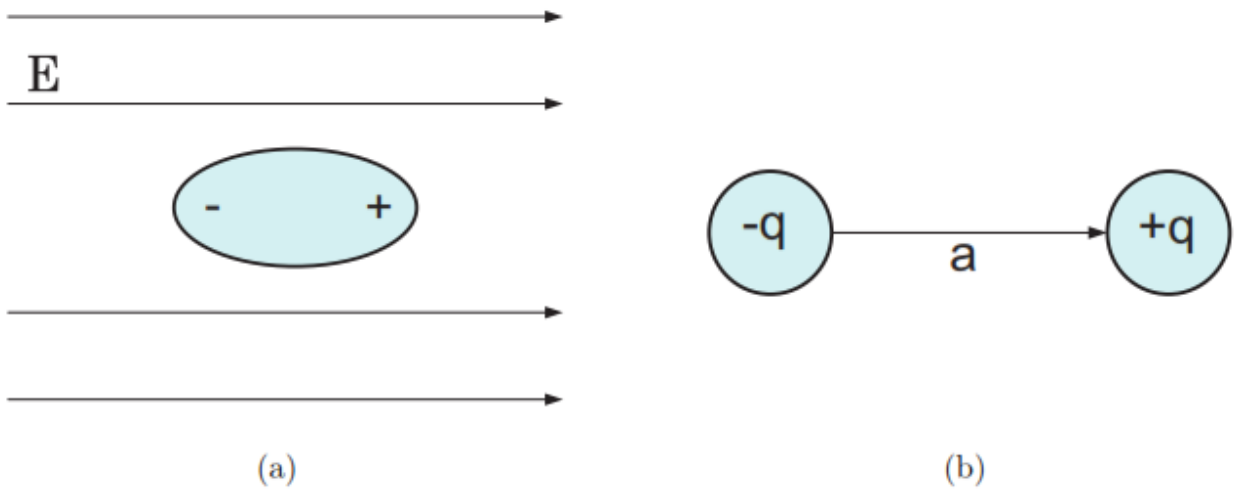

Figure 2. 3: (a) An electric dipole induced in an applied electric field and (b) an electric dipole moment can be represented as a vector which points in the direction of -q to +q and a magnitude of the distance (a) between them.

Another way of illustrating an electric dipole is to use two spheres of charge; one positive and one negative. The two spheres are the same size and are superimposed on top of one another. This superposition helps to show the idea of bound charge. In the absence of an external electric field, the two spheres cancel each other's charge and

are, overall, electrically neutral. When an external electrical field is applied, the negative sphere shifts one direction and the positive sphere shifts the other direction, as illustrated in Figure 2.4. The charges of the two spheres no longer cancel each other. As a result, an electric dipole is created, where one side is slightly positive in charge and the other side is slightly negative in charge [3]. The amount of uncancelled charge is called the bound surface charge σ_b [3]. The two spheres essentially represent the nucleus of an atom, which is positively charged, at the center of an electron cloud, which is negatively charged [1].

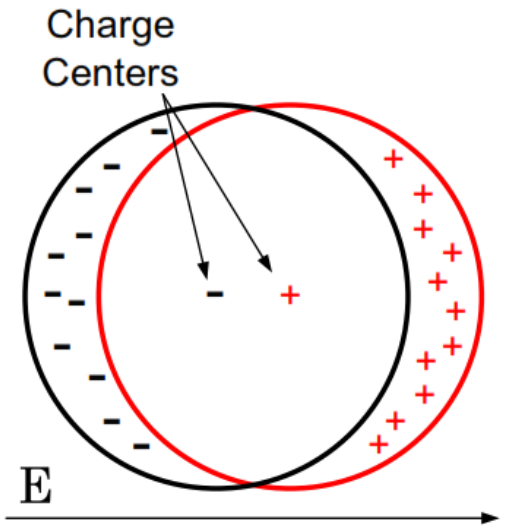

Figure 2. 4: Two displaced charge spheres illustrating an electric dipole [3] Creating electric dipoles within a material through an application of an electric

field is called polarization. Polarization is mathematically defined as P and is the number of induced dipole moments per unit volume. The amount of polarization depends on

the electric field E and the a quantity called the polarizability α, which is shown by [3] [7].

$$\mathbf{P} = \alpha \mathbf{E} \quad (C/m^2) \tag{2.11}$$

To better define charge displacement, a term called the electric displacement, D, is defined as total charge displacement induced in the material. Maxwell defines the electric displacement mathematically as [3].

$$\mathbf{D} = \epsilon_0 \mathbf{E} + \mathbf{P} \quad (C/m^2) \tag{2.12}$$

Electric displacement consists of two parts, the displacement of charge which is a result of the applied electric field and the displacement caused by polarization. The induced dipole from the polarization induces its own electric field which further contributes to the electric displacement.

The polarizability α of a dielectric can be separated into the electric susceptibility χ_e and permittivity of free space ϵ_0 [3]. The electric susceptibility is a dielectric's ability to polarize, and the permittivity of free space is a universal polarizability constant that is defined for all of free space. Incorporating the electronic susceptibility, the number of induced dipoles per unit volume, Equation 2.11, then turns into [3].

$$\mathbf{P} = \chi_e \epsilon_0 \mathbf{E} \quad (C/m^2) \tag{2.13}$$

Substituting Equation 2.13 into Equation 2.12 yields [3].

$$\begin{aligned} \mathbf{D} &= \epsilon_0 \mathbf{E} + \chi_e \epsilon_0 \mathbf{E} \\ &= \epsilon_0 (1 + \chi_e) \mathbf{E} \quad (C/m^2) \end{aligned} \tag{2.14}$$

The permittivity of the material ϵ is defined as [3]

$$\epsilon = \epsilon_0 (1 + \chi_e). \quad (F/m) \tag{2.15}$$

Substituting Equation 2.15 into Equation 2.14 yields

$$\mathbf{D} = \epsilon \mathbf{E}. \quad (C/m^2) \tag{2.16}$$

As defined earlier, ϵ is the permittivity of the material and by dividing the permittivity by the permittivity of free space yields the relative permittivity or the dielectric constant, ϵ_r , and is defined as

$$\epsilon_r = 1 + \chi_e = \frac{\epsilon}{\epsilon_0} \tag{2.17}$$

The dielectric constant is one of the central themes in this study and is a key characteristic in capacitor materials. The equations above illustrate the fact that the dielectric constant defines how the dielectric material reacts to the introduction of an electric field. The higher the dielectric constant in a capacitor material causes a higher electric energy density in the capacitor.

2.1.4 *ELECTRONIC POLARIZATION*

The most basic form of polarization is electronic polarization and is represented in the two displaced charge spheres in Figure 2.4. When an atom is exposed to an electric field, the electron cloud surrounding the nucleus shifts and is no longer centered about the nucleus. The result is called electronic polarization and is denoted as α_e , which is shown in Figure 2.5.

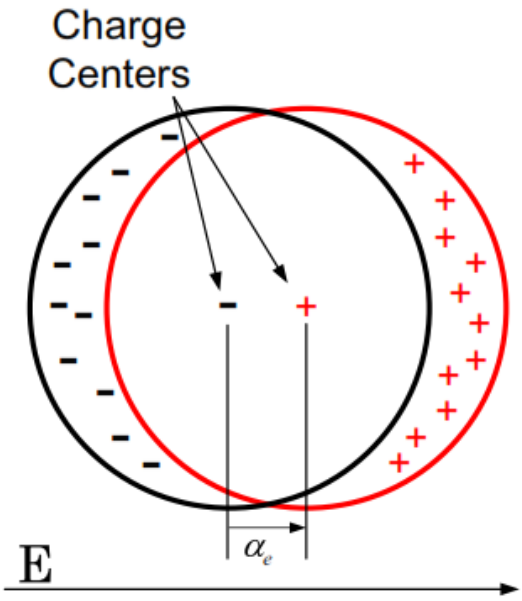

Figure 2. 5: Electronic polarization of a neural atom

After equilibrium is reached, the two forces acting on the electrons are the coulombic attraction called the restoring force and the force due to the electric field that keeps the electron cloud shifted. The average induced polarization per molecule due to electronic polarization is [8] [9]

$$P_e = \alpha_e E \quad (C/m^2) \tag{2.18}$$

As reflected earlier, the induced electronic dipole moment α_e due to electronic polarization is proportional to the electric field E. This equation is valid only under equilibrium or static conditions.

2.1.5 Electronic Polarization in Covalent Solids

A covalent bond is when two or more atoms share one or more valence electrons, which bonds the atom together. In a solid that utilizes a lattice of covalent bonds between atoms, which is represented in Figure 2.6 in a Si lattice, there are many electrons that are shared between the nuclei [8]. Instead of an electron being shared between two atoms, this type of sharing produces a cloud of electrons that can tunnel and switch places with other electrons. These electrons and their resulting wave functions are referred to as delocalized. When an electric field is applied, there are two different types of electronic polarizations that occur. One type of polarization, which is the lesser of the two polarizations, happens when the individual nuclei experiences a shift within its own electron shell which is not shared within the lattice bonds. The electronic polarization that has the dominant affect is the shifting of the atom's valence electrons which contribute to the lattice bonds surrounding the nuclei within the material [8].

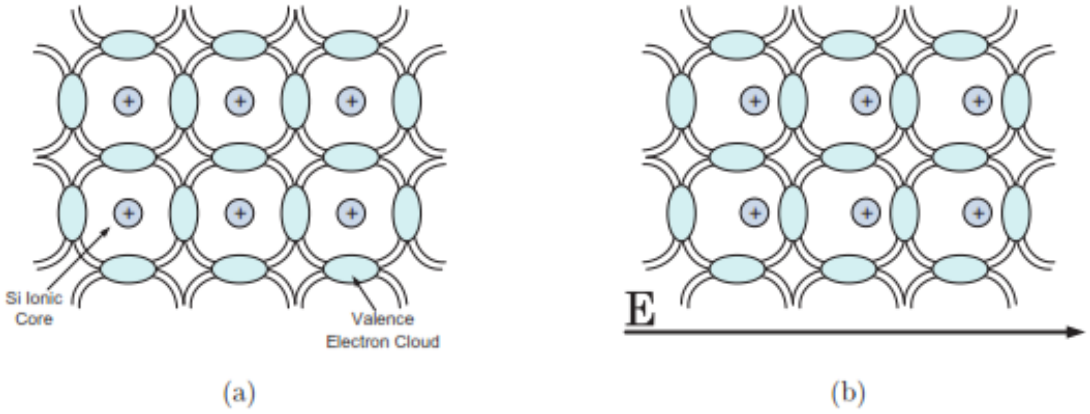

Figure 2. 6: An illustration of electronic polarization in covalent bond of Si (a) before the application on an electric field and (b) after a field is applied [8]

2.1.6 IONIC POLARIZATION

Ionic polarization occurs in crystal lattices that employ ionic molecules such as NaCl. Although the an individual molecule has a dipole moment, the net dipole moment of the material is zero because the individual molecules are lined up head to head and tail to tail, as shown in Figure 2.7. When an electric field is applied, the cations are pushed one direction and the anions are pushed in the other, which creates a net polarization in the material, reflected in Figure 2.7. The average induced polarization per molecule due to ionic polarization is [8] [9]

$$P_i = \alpha_i E \quad (C/m^2) \tag{2.19}$$

where α_i is the ionic polarization of the material, and E is the applied electric field.

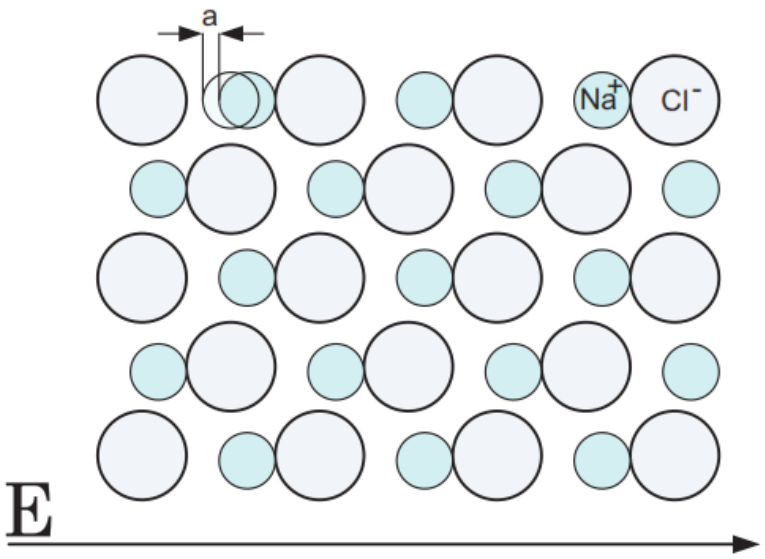

Figure 2. 7: An illustrated example of ionic polarization in NaCl [9]

2.1.7 Orientational Polarization

Some materials have molecules that have permanent dipole moments such as water molecules. Figure 2.8 shows that, in the liquid or gas phase, these dipole molecules can move about and are randomly orientated. When an electric field is applied to a polar material, the dipoles experience a torque which aligns them with the direction of the applied field. This process is called orientational polarization [3] [8] [9].

Some solids are made up of polar molecules which are normally randomly orientated. There are materials such as certain plastics can be softened by heating and exposed to an electric field in order to align the dipoles. The electric field is left on as the material cools which solidifies the direction of the dipole moments. This process is used to produce materials that have a permanent dipole moment. Electrets and have many uses especially in high fidelity microphones [2].

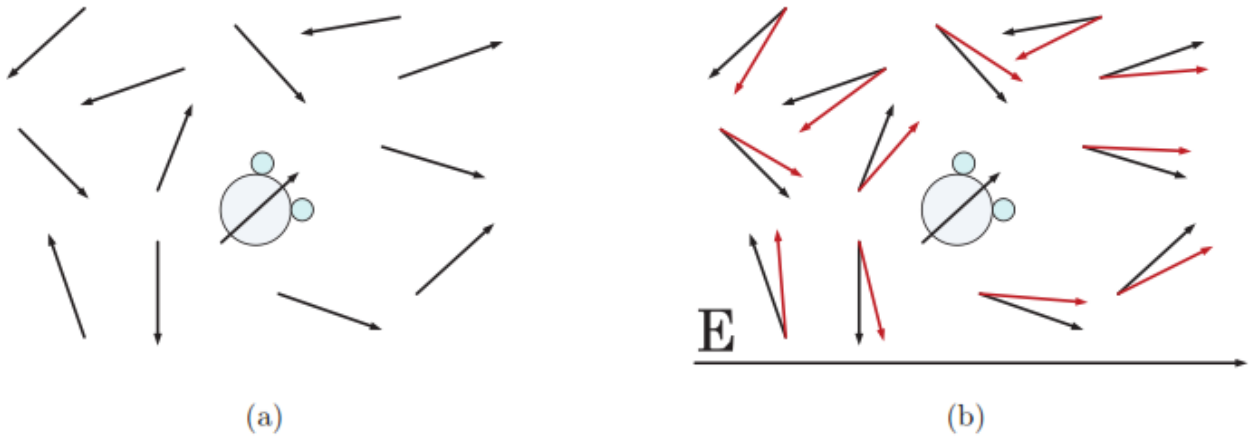

Figure 2. 8: A dielectric medium consisting of polar molecules (a) that are randomly oriented before an electric field is applied and (b) after a field is applied [3] [8] [9]

The average induced polarization per molecule due to orientational polarization is [8] [9]

$$P_o = \alpha_o E \quad (C/m^2) \tag{2.20}$$

where α_o is the orientational polarization of the material, and E is the applied electric field.

2.1.8 Interfacial Polarization

Even in the most pure of crystals and materials, there are impurities and charge carriers such as electrons, holes, and ions. These charge carriers can actually move within the material and build up at different boundaries such as the dielectric-electrode boundary or at grain boundaries within the material itself. This accumulation contributes to the dielectric constant of the material [8].

2.1.9 *Total Polarization*

All of the above mechanics of polarization are additive and define the total polarization of the material. The average induced dipole moment per molecule is [8]

$$P_{av} = \alpha_e E + \alpha_i E + \alpha_o E \quad (C/m^2) \tag{2.21}$$

where α_e is the electronic polarization, α_i is the ionic polarization, α_o is the orientational polarization, and E is the applied electric field. The interfacial polarization is not added to the above equation because it occurs at interfaces and does not correlate to an average polarization in the bulk material. This is again a simplification because the electric field E in the above equation is the local field experienced by the individual molecules and not the applied electric field [6] [8].

2.1.10 *Dielectric constant versus frequency*

The aforementioned polarization assumes a static electric field which does not vary with time. The introduction of a time varying electric field adds a little more complexity to the idea of polarization. The mechanics of polarization depends on the movement of particles with mass. Particles have to be accelerated and shifted back and forth as the electric field changes, which cannot occur instantaneously. Since certain movements of particles involve the movement of different masses and different distances, the different types of polarization will have different rates at which polarization occurs. When a time varying electric field is applied, the dielectric constant depends on the frequency of the field. At low frequencies, all of the polarization types have time to reach their relaxed

state. As the frequency increases, the slower processes do not have time to completely relax before the polarity of the electric field changes. As a result, the slower processes cease to contribute to the dielectric constant [6]. Figure 2.9 illustrates the decrease in the dielectric constant as frequency increases [8].

This is a simplification of the phenomenon. In reality the frequency and the degree at which these occur will vary and will sometimes overlap. The graph also shows resonance that can occur at the boundaries of the different polarization mechanisms. Although this particular study does not deal with experimental measurements of frequency dependent dielectric constants, this concept is an important phenomenon in the field of dielectrics and should be explored further in future studies.

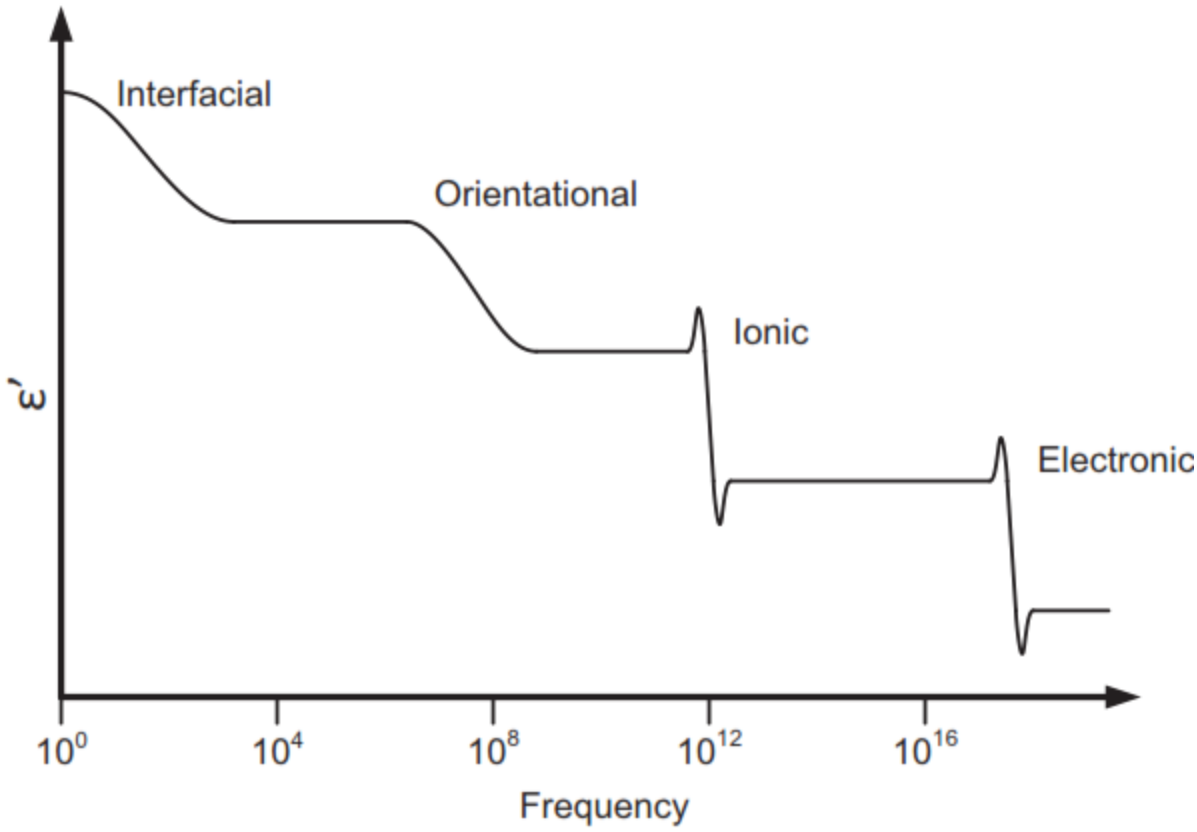

Figure 2. 9: The real part of the dielectric constant versus frequency of an applied electric field with different polarizations [8]

2.2 Dielectric Constant Modeling

2.2.1 Prediction Introduction

In the past few decades, the production of a new dielectric materials based on mixtures of materials have been on the rise [10]. As a result, the need of better mathematical models has also increased. These models are grouped into a larger family of models called Effective Medium Theories (EMT) and Effective Medium Approximations (EMA) [10] [11]. All EMTs start with the assumption that the different phases of the material,

which each have their own dielectric constants, can be combined into a single effective macroscopic dielectric constant [12].

2.2.2 *Maxwell-Garnett Model*

The most common model used to calculate the dielectric constant of a mixture of dielectric materials is James C. Maxwell's model [13]. Maxwell wrote the equation for the dielectric constant of randomly dispersed spheres into a continuous matrix. Once the materials are blended, they essentially become one material with two different phases [14]. Garnett rearranged Maxwell's model into a more convenient format, which is subsequently called the Maxwell-Garnett model which is [15] [16]

$$\epsilon_e = \epsilon_m \frac{\epsilon_f (1 + 2\delta) - \epsilon_m (2\delta - 2)}{\epsilon_m (2 + \delta) + \epsilon_f (1 - \delta)} \tag{2.22}$$

where ϵ_e is the effective dielectric constant of the blended material, ϵ_f is the dielectric constant of the filler, ϵ_m is the dielectric constant of the matrix, and δ is the volume fraction of the filler material.

This relationship assumes that the spheres of the filler have enough distance between them that the flux lines around each sphere do not interfere. This assumption is relevant at low filler volume fraction and therefore limits the applicability of the model to between 10% to 50% [14].

When the difference of the dielectric constants of the matrix and the filler is small, the effective dielectric constant changes almost linearly as the volume fraction of the filler is

increased. When that difference is large, the effective dielectric constant shows some interesting trends.

In this study, Strontium Titanate, $SrTiO_3$, (referred to as ST in this study) and Barium Strontium Titanate, $BaSrTiO_3$ (referred to as BST in this study) powders are being used as the filler material. The BST material was primarily used because of its higher dielectric constant of 6000. The matrix material is polyvinylidene fluoride (PVDF) and Teflon, which have dielectric constants of 8 and 2, respectively [17] [18].

Using the Maxwell-Garnett model with Barium Strontium Titanate and PVDF, the relationship between the dielectric constant and the volume of filler material is plotted in Figure 2.10.

The plot shows that the dielectric constant of the matrix has a large effect on the effective dielectric constant at low filler volumes than the dielectric constant of the filler material. It is not until larger volumes of filler are added that the effective dielectric constant starts to reflect the dielectric constant of the filler.

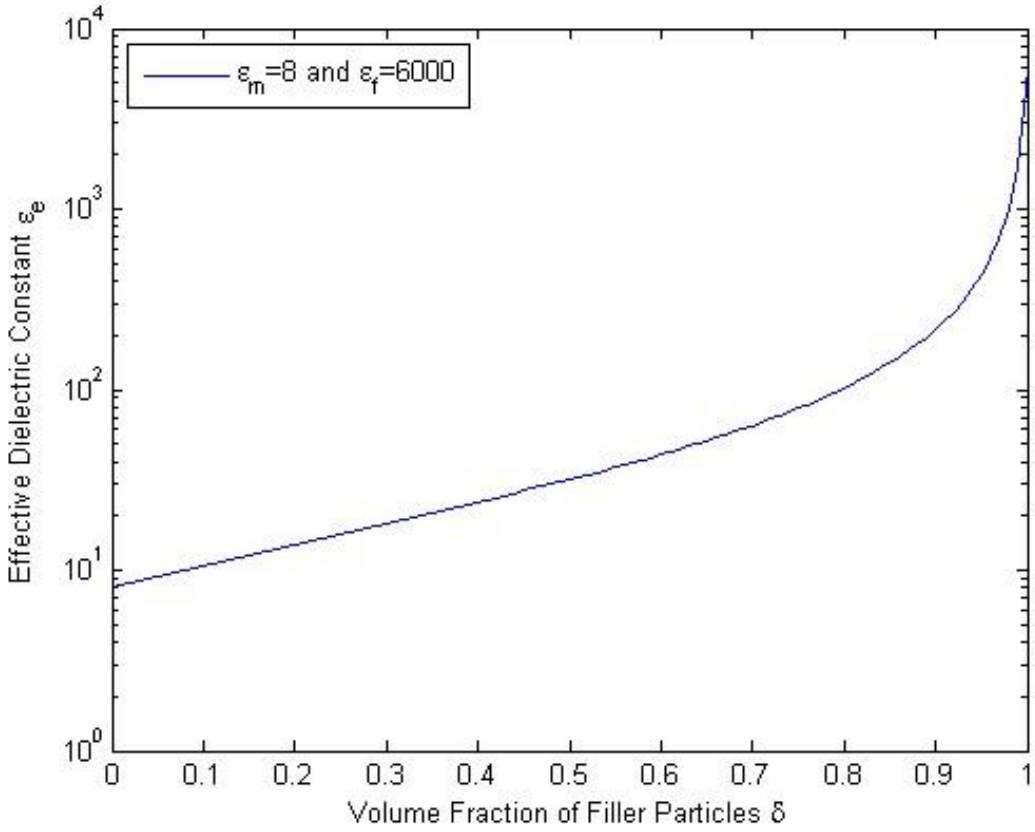

Figure 2. 10: A plot of the effective dielectric constant, ϵ_e, using the Maxwell-Garnett model versus the volume of added filler material, δ, in a two phase system consisting of a matrix material and added spherical filler particles. The dielectric constant of the PVDF matrix ϵ_m =8 and the BST filler ϵ_f =6000.

2.2.3 LICHTENECKER MODEL

Another model that is used often is a simple empirical model called the Lichtenecker model. It seems to give similar results as the Maxwell-Garnett model when the difference in the dielectric constant of the filler and the matrix is small but differs

significantly when the difference between the dielectric constant is large. This model is defined mathematically as [19]

$$\log \epsilon_e = \delta_f \log \epsilon_f + \delta_m \log \epsilon_m \tag{2.23}$$

where δ_f is the volume fraction of the filler phase and δ_m is the volume fraction of the matrix phase of the medium. Figure 2.11 shows the Lichtenecker model compared to the Maxwell-Garnett model when ϵ_f =6000 and ϵ_m =8.

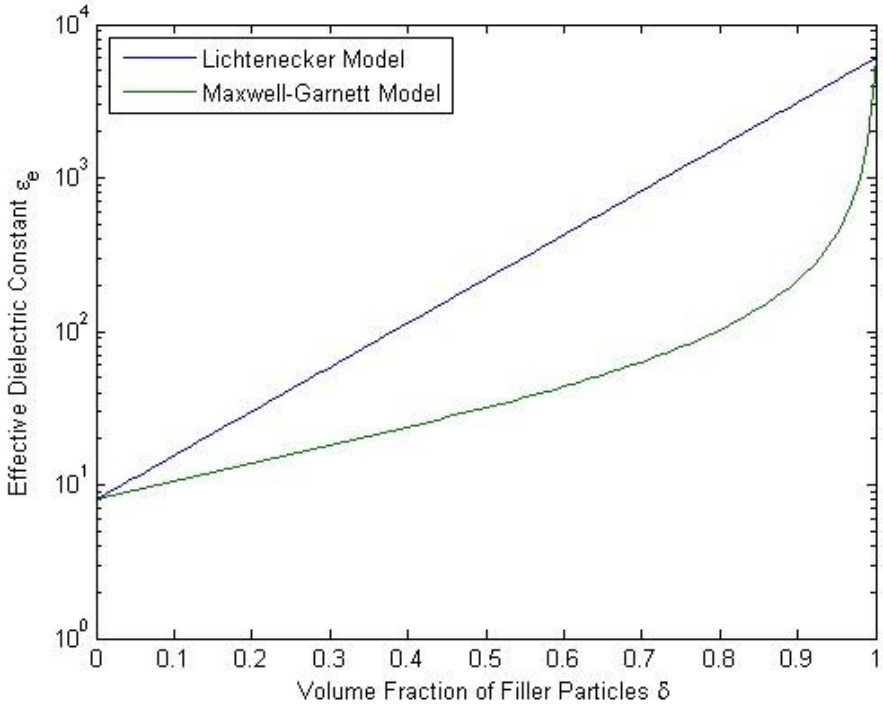

Figure 2. 11: A plot of the effective dielectric constant, ϵ_e , versus the volume of added filler material, δ, in a two phase system consisting of a matrix material and added spherical filler particles where ϵ_m =8 and ϵ_f =6000. The ϵ_e using the Maxwell-Garnett equation is also graphed for comparison.

2.2.4 *INTERPHASE MODEL*

A common failure of effective medium theories is their inability to predict the effective dielectric constant of two phase materials with a high volume loading of inclusions. The EMTs are similar at low volume levels but start to diverge, drastically in some cases, as the volume increases. One explanation is the possible existence of an "interphase" region that exists between the inclusion and the matrix. This interphase region is where the matrix material becomes bonded or fixed in a specific orientation resulting in a region that has its own electrical properties [12] [20] [21] [22]. An example of the interphase region is in Figure 2.12, where the filler material is spherical. The interphase model is expressed mathematically as [20]

$$\epsilon_c = \frac{h + 2l}{h - l}, \tag{2.24}$$

where

$$\begin{aligned} h = \; & 1 + 2\frac{(\epsilon_3 - \epsilon_2)(\epsilon_2 - \epsilon_1)}{(2\epsilon_3 + \epsilon_2)(2\epsilon_2 + \epsilon_1)}\left(\frac{a^3}{b^3}\right) \\ & -2\frac{(\epsilon_3 - 1)(\epsilon_3 - \epsilon_2)}{(\epsilon_3 + 2)(2\epsilon_3 + \epsilon_2)}\left(\frac{b^3}{c^3}\right) \\ & -2\frac{(\epsilon_3 - 1)(\epsilon_3 + 2\epsilon_2)(\epsilon_2 - \epsilon_1)}{(\epsilon_3 + 2)(2\epsilon_3 + \epsilon_2)(2\epsilon_2 + \epsilon_1)}\left(\frac{a^3}{c^3}\right), \end{aligned} \tag{2.25}$$

$$l = \frac{(\epsilon_3 - 1)}{(\epsilon_3 + 2)} j - \frac{(2\epsilon_3 + 1)\, m}{(\epsilon_3 + 2)(2\epsilon_3 + \epsilon_2)}\left(\frac{b^3}{c^3}\right), \tag{2.26}$$

$$j = 1 + 2\frac{(\epsilon_3 - \epsilon_2)(\epsilon_2 - \epsilon_1)}{(2\epsilon_3 + \epsilon_2)(2\epsilon_2 + \epsilon_1)}\left(\frac{a^3}{b^3}\right), \tag{2.27}$$

$$m = (\epsilon_3 - \epsilon_2) + \frac{(\epsilon_3 + 2\epsilon_2)(\epsilon_2 - \epsilon_1)}{(2\epsilon_2 + \epsilon_1)} \left(\frac{a^3}{b^3}\right), \tag{2.28}$$

$$\frac{a^3}{b^3} = \frac{(1 + k\delta_F)}{(1 + k)}, \tag{2.29}$$

$$\frac{a^3}{c^3} = \delta_F, \tag{2.30}$$

$$\frac{b^3}{c^3} = \delta_F \left[1 + k\frac{(1 - \delta_F)}{(1 + k\delta_F)}\right]. \tag{2.31}$$

The dielectric constants ϵ_1, ϵ_2, and ϵ_3 are defined as in Figure 2.12 as the dielectric constants of the filler, the interphase, and the matrix. The variable δ_F is the volume fraction of the filler material and k is the matrix and filler interaction strength, where a k of zero represents the case where there is no interaction.

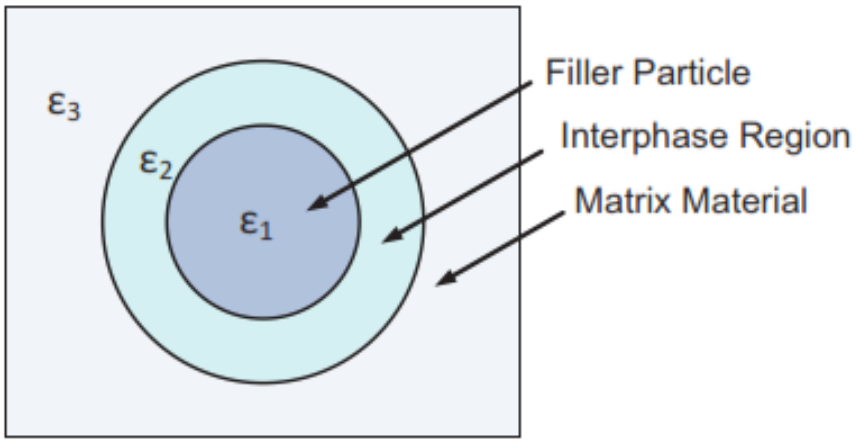

Figure 2. 12: An illustration of the interphase region between the spherical filler phase and the matrix phase in a dielectric material

Figure 2.13 shows a plot of the dielectric constant verses the volume fraction of the filler at different values of k. When the volume fraction of the filler is one, the effective dielectric constant is that of the filler and when the volume fraction is zero, the effective dielectric constant is that of the matrix.

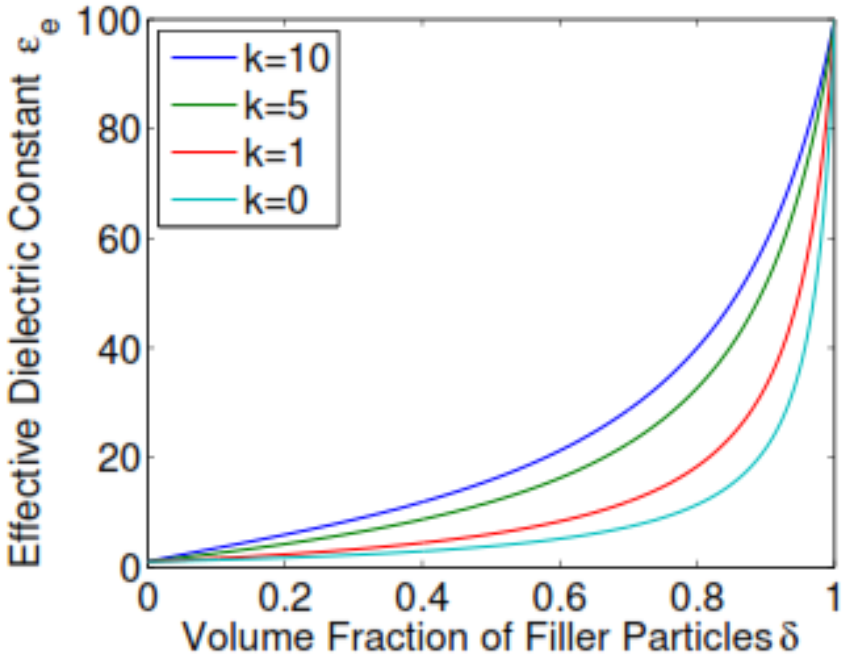

Figure 2. 13: The effective dielectric constant ϵe versus the filler material volume fraction δ with different interaction strengths k using the interphase model, where the dielectric constant of the filler, interphase, and matrix is 100, 10, and 1; respectively

Figure 2.14 shows a plot of the dielectric constant versus the volume fraction of the filler at different interphase dielectric constant values. Figure 2.13 and Figure 2.14 show that the effective dielectric constant of the composite material increases as the interaction strength or the interphase dielectric constant increase.

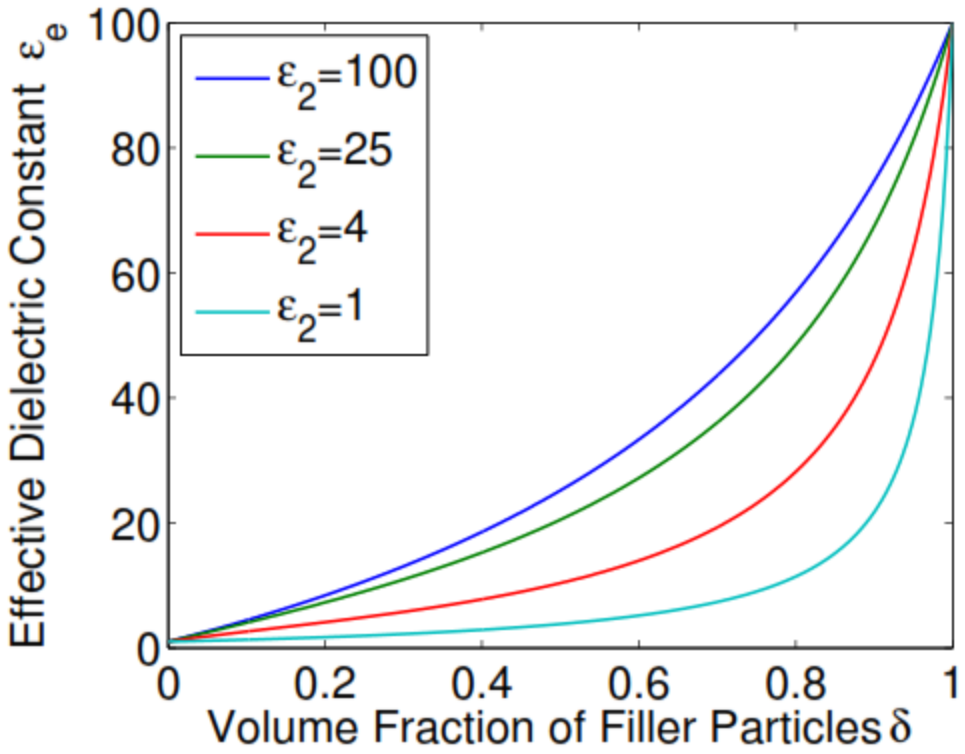

Figure 2. 14: The effective dielectric constant ϵ_e versus the filler material volume fraction δ with different interphase dielectric constants using the interphase model, where the dielectric constant of the filler and matrix is 100 and 1, respectively, and the interactions strength k is 10

A criticism of the interphase theory is its difficulty in explicitly solving for the k value and the dielectric constant of the interphase region. For example, Vo and Shi, Lombardo, Todd and Shi, and Murugaraj et al. make reference to k values and dielectric constants for different material but do not specifically show how they solved for their constants [20] [23] [21] [22] [24]. Lombardo does state that a certain k value gives the best fit for the experimental data, which infers that he used a best fit algorithm to solve for k [23]. When solving for two parameters in this way, one parameter is dependent on the other

and therefore does not give a definitive solution to the parameters. Lombardo [23] also comments on the fact that his interphase parameters did not match the determined interphase parameters in the Vo and Shi [20] study even though they were using the same materials.

2.3 Dielectric Breakdown Theory

2.3.1 Introduction to Dielectric Breakdown

When using a dielectric material in a particular design, an engineer has to also take into account properties other than the dielectric constant. The environment or the specifications of the design itself can dictate other material properties of the material.

The dielectric strength of the material has to be taken into consideration when developing new materials for high voltage applications. The different causes of breakdown and the definition of dielectric strength will be defined.

2.3.2 Intrinsic Breakdown

The dielectric strength of a material comes from its ability to prevent intrinsic breakdown [2], which is also called dielectric or electronic breakdown [25]. When the magnitude of a field across a dielectric material increases, the resulting polarization causes a strain or electric displacement in the atoms [5]. This strain cannot increase without limit. When an atom is placed in an electric field, the atom develops a coulombic force in the opposite direction of the force to keep the charges bound to the atom. When that energy that the atom can withstand is exceeded, an electron breaks

free of the atom [26]. Now free from the atom, the electron is accelerated in the presence of the electric field. If the magnitude of the electric field is large, the electron will have enough energy to ionize other atoms in the lattice, which generates new electrons. These newly produced electrons are now free to generate more electrons by ionization. The result is an avalanche of electrons that result in a large amount of current between the electrodes. Figure 2.15 shows an electron avalanche.

In a gas or a liquid, the dielectric will probably not be permanently damaged. In a solid dielectric, however, the resulting heating will melt and carbonize the dielectric, which will form permanent conduction paths and cause irreparable damage. Figure 2.16 shows what happens when a voltage is applied across dielectric material. At first the voltage increases and a displacement current is manifested in the material. As the voltage continues to increase, the current plateaus. Once the voltage is raised above a certain value, the current increases exponentially and results in an intrinsic breakdown.

The magnitude of the electric field at which the dielectric material undergoes intrinsic breakdown is called the dielectric strength [8]. There are many factors that contribute to the dielectric strength of a material such as density, impurities, geometry of the molecular structure, temperature, humidity, the frequency of the applied voltage, rise time of the voltage, and many other factors like whether the applied voltage is ac or dc [14]. Because of the numerous factors that can affect intrinsic breakdown, a microscopic theory is as yet unavailable [28].

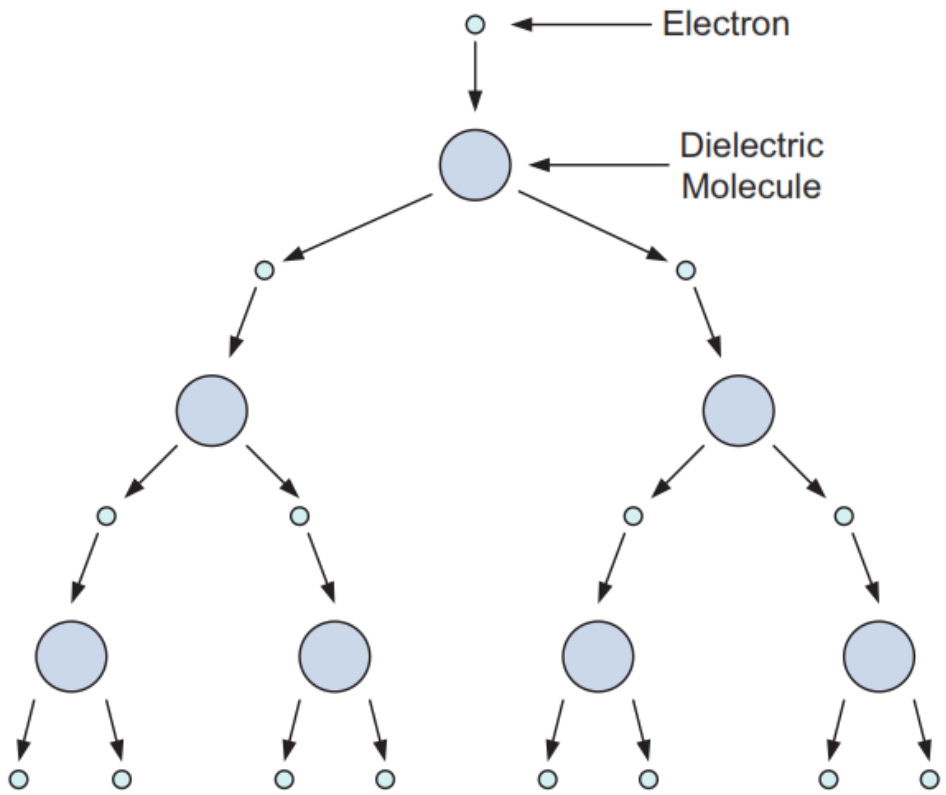

Figure 2. 15: An electron, accelerated by the applied electric field, collides with a dielectric molecule which ionizes it and generates secondary electrons thereby forming a chain reaction. This chain reaction is called dielectric breakdown [25].

2.3.3 Intrinsic Breakdown in Composites

In the case of a composite material, the process becomes more complicated. As the different phases of the material are mixed together, different shapes form within the composite. When there is an interface between two materials which have different permittivities, field enhancement occurs which is where the electric field lines become closer together when there are irregularities on one surfaces [29]. An example of field

enhancement is represented in Figure 2.17. The field enhancement factor is mathematically represented as

$$\eta = \frac{E_{max}}{E_{mean}} \tag{2.32}$$

where E_{max} is the maximum peak field and E_{mean} is the mean field [30].

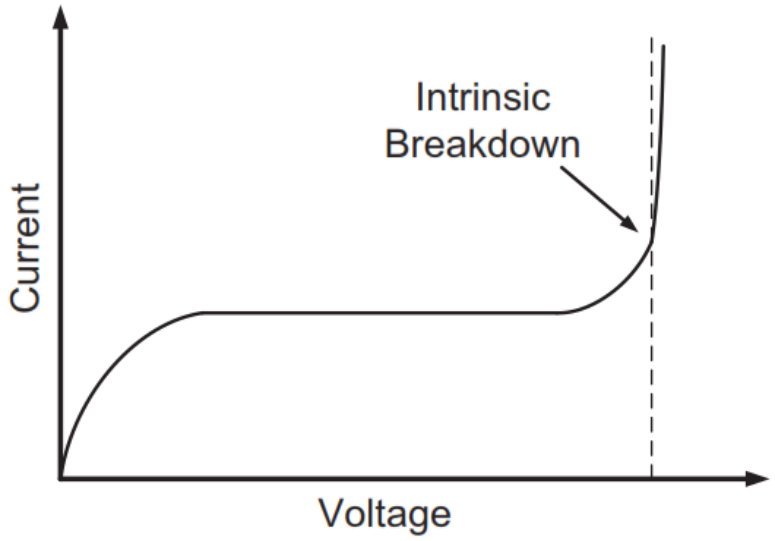

Figure 2. 16: A typical plot of current versus voltage of a dielectric material. Once the voltage exceeds the breakdown threshold, the current increases exponentially and causes irreparable damage in the case a solid dielectric [27].

Intrinsic breakdown in composites takes place in steps with each step strongly dependent on the last [31]. This step process leads to the formation of breakdown trees such as the one represented in Figure 2.18. Because of this step process, breakdowns are heavily affected by the many different kinds of interfaces within the phases of a

composite. Considering the superposition of those processes, it is much more difficult to generate a mathematical model for composites than in normal homogeneous dielectrics.

2.3.4 THERMAL BREAKDOWN

There are other types of breakdown that can permanently damage a solid dielectric material. Thermal breakdown [13] occurs when a current is conducted across a dielectric at low voltages, Joule heating occurs as a rate of I^2R [14]. If the heat cannot dissipate fast enough, the temperature of the material increases. The increased temperature increases the conductivity, which generates more current. The result is called thermal runaway [8]. The current increases exponentially, which results is a discharge through the material, thereby permanently damaging it.

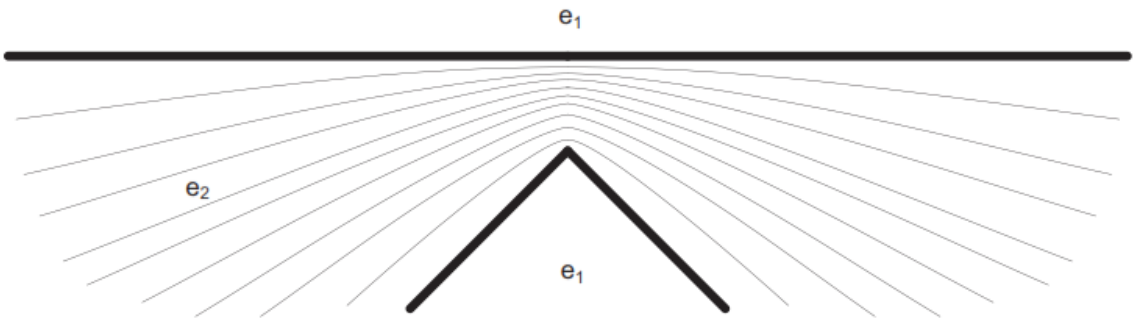

Figure 2. 17: An example of field enhancement on a sharp corner in a composite system

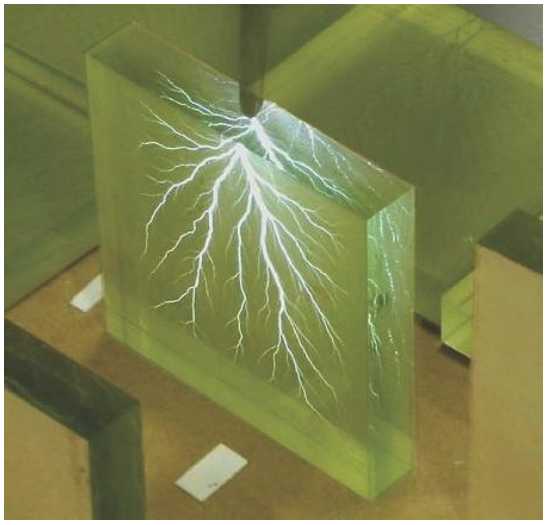

Figure 2. 18: An example of an intrinsic breakdown tree [32]

2.3.5 DISCHARGE BREAKDOWN

Another type of breakdown is called discharge breakdown [26], which occurs when there is a void in the material or the surface of the material is porous and contains voids. The resulting fields in the voids can be much higher than in the surrounding material, which can cause a small discharge that occurs locally in the void. This small discharge does not cause permanent damage but this type of discharge can happen many times in the same place, which can result in cracking and damage to the material over a long period of time [13] [8].

2.4 Bibliography for Chapter 2

[1] F. T. Ulaby, Fundamentals of Applied Electromagnetics. Pearson Prentice Hall, 2004.

[2] D. K. Cheng, Field and Wave Electromagnetics, 2nd Ed. Addison-Wesley Publishing Company, 1992.

[3] D. J. Griffiths, Introduction to Electrodynamics, 2nd Ed. Prentice Hall, 1989. [4] A. Von Hippel, Dielectric Materials and Applications. Technology Press of MIT and John Wiley, 1954.

[5] V. A. Suydam, Fundamentals of Electricity and Electromagnetism. D. Van Nostrand Company, Inc., 1940.

[6] L. V. Azaroff and J. J. Brophy, Electronic Processes in Materials. McGraw Hill, 1963.

[7] P. W. Atkins, Physical Chemistry, 4th Ed. W.H. Freeman and Company, 1990. [8] S. O. Kasap, Principles of electrical engineering materials and devices. McGraw Hill, 2000.

[9] W. D. J. Callister, Materials Science and Engineering, 3rd Ed. John Wiley and Sons, Inc., 1994.

[10] C. Brosseau, "Modeling and simulation of dielectric heterostructures: a physical survey from an historical perspective," Journal of Applied Physics D: Applied Physics, vol. 39, pp. 1277–1294, 2006.

[11] L. Jylha and A. Sihvola, "Differential equation for the effective permittivity of random mixture of spheres," Electromagnetic Theory Symposium, July 2007.

[12] W. Tinga, W. Voss, and D. Blossey, "Generalized approach to multiphase dielectric mixture theory," Journal of Applied Physics, vol. 44, no. 9, pp. 3897–3902, 1973.

[13] A. Moulson and J. Herbert, Electroceramics, 2nd Ed. John Wiley and Sons Ltd, 2003.

[14] R. C. Buchanan, Ceramic Materials for Electronics. Marcel Dekker, Inc., 1986. [15] S. B. Jones and S. P. Friedman, "Particle shape effects on the effective permittivity of anisotropic or isotropic media consisting of aligned or randomly oriented ellipsoidal particles," Water Resources Research, vol. 36, no. 10, pp. 2821–2833, October 2000.

[16] W. Merrill, R. Diaz, M. LoRe, M. Squires, and N. Alexopoulos, "Effective medium theories for artificial materials composed of multiple sizes of spherical inclusions in a host continuum," IEEE Transactions on Antennas and Propagation, vol. 47, no. 1, pp. 142–148, 1999.

[17] G. Rashmi and P. Narula, "Dielectric properties of solution-cast poly(vinylidene fluoride) films," Journal of materials science, vol. 22, 1987.

[18] B. Chung, "Dielectric constant measurement for thin material at microwave frequencies," Progress In Electromagnetics Research, PIER, vol. 75, 2007.

[19] P. Neelakantaswamy, R. Turkman, and T. Sarkar, "Complex permittivity of a dielectric mixture: corrected version of Lichtenecker's logarithmic law of mixing," Electronic Letters, vol. 21, no. 7, pp. 270–271, 1985.

[20] H. T. Vo and F. G. Shi, "Towards model-based engineering of optoelectronic packaging materials: dielectric constant modeling," Microelectronics Journal, vol. 33, pp. 409–415, 2002.

[21] M. Todd and F. Shi, "Complex permittivity of composite systems: a comprehensive interphase approach," IEEE Transactions on Dielectrics and Electrical Insulations, vol. 12, no. 3, pp. 601–611, 2005.

[22] M. G. Todd and F. G. Shi, "Characterizing the interphase dielectric constant of polymer composite materials: effect of chemical coupling agents," Journal of Applied Physics, vol. 94, no. 7, pp. 4551–4557, 2003.

[23] N. Lombardo, "A two-way particle mapping for calculation of the effective dielectric response of graded spherical composites," Composites Science and Technology, vol. 67, 2007.

[24] P. Murugaraj, D. Mainwaring, and N. Mora-Huertas, "Dielectric enhancement in polymer-nanoparticle composites through interphase polarizability," Journal of Applied Physics, vol. 98, 2005.

[25] R. G. Lerner and G. L. Trigg, Encyclopedia of Physics, 2nd Ed. VCH Publishers, Inc., 1991.

[26] M. W. Barsoum, Fundamentals of Ceramics. Institute of Physics Publishing, 2003.

[27] R. F. Pierret, Advanced Semiconductor Fundamentals. Pearson Education, Inc., 2003, vol. 4.

[28] D. Hong-Zhi, X. Xiu-San, and Z. He-Sun, "Dynamic aspects of linear elastic fracture mechanics applied to dielectric breakdown," Journal of applied physics, vol. 26, pp. 829–835, 1993.

[29] E. Le Ru and P. Etchegoin, "Rigorous justification of the E^4 enhancement factor in surface enhanced Raman spectroscopy," Chemical Physics Letters, vol. 423, pp. 63–66, 2006.

[30] E. Kuffel and W. Zaengl, High Voltage Engineering Fundamentals. Pergamon Press, 1984.

[31] N. Barreaud, L. Vouyovitch, L. Flandin, J. Bessede, A. Beroual, and N. Alberola, "A meso-macro approach of the dielectric breakdown in heterogeneous systems: experimental results and comparison to numerical simulation," Inter- national conference on solid dielectrics, July 2004.

[32] http://bored-night.com/index.php/Amazing/Lichtenberg-Figures-Electric-Discharges.html.

Chapter 3 – EXPERIMENTAL TEST SETUP

3.1 MATERIAL SELECTION

An investigation was undertaken to study a commercially fabricated nanocomposite material made from a composite of a ceramic nanopowder and a thermoplastic which was used as a matrix material to contain the nanopowder. The ceramic nanopowders, strontium titanate, $SrTiO_3$, (referred to as ST in this study) and barium strontium titanate, $BaSrTiO_3$ (referred to as BST in this study), were chosen because of their high dielectric constant and the stability of their dielectric constant over different temperatures and frequencies. These two materials were also chosen because of new innovations in making smaller grain sized particles that has made these nanopowders more cost efficient. As the grain size of the nanopowder gets smaller, the surface area increases, which can increase the dielectric constant of the nanopowder. The nanopowder that was used for this study has a grain size distribution that is centered at 100 nanometers.

The two plastic materials, Teflon, which is polytetrafluoroethylene (PTFE), and polyvinylidene fluoride (PVDF), were each chosen for a different reason. Teflon was chosen for its relatively high dielectric strength. PVDF was chosen for its high dielectric constant when compared to other materials. The thing that they have in common

though is they are both thermoplastics, which means that they melt very well at reasonable temperatures. This attribute helps in the mixing process.

3.2 Nanocomposite Sample Preparation

A commercial company was given the task of mixing the composite materials. Since both the plastics matrices are thermoplastics, the plastics were heated above their respective melting points and mixed in a mixer while in their liquid phases. The filler material was then added at different volume fractions as the composite was being mixed. The liquid composite material was then extruded and formed into disks approximately 4” in diameter and 0.5” thick.

After receiving these samples, the faces of the disks were machined with a lathe in order to produce a smoother surface. The disks were then wet sanded on a flat surface to produce a smooth finish. A smooth surface minimizes voids or air pockets between the dielectric material and the electrodes, which diminishes the accuracy of your measurement. Figure 3.1 shows a BST/PVDF disk after machining and sanding.

3.3 Dielectric Constant Test Setup

These disks were then used to measure the dielectric constant of each composite material. Two aluminum disks, used as electrodes, were machined to match the diameter of the composite disks. The composite disk was then placed between the two aluminum electrodes and lightly clamped together. A Sencore LC103 Capacitor/Inductor Analyzer was attached to the electrodes and used to measure the capacitance of the

disk. The dielectric constant was calculated from the measured capacitance using the disk capacitor equation and solving for the dielectric constant, ϵ_r , which is [1]

$$C = \frac{\epsilon_r \epsilon_0 A}{d} \quad (F) \tag{3.1}$$

where A is the surface area of the composite disk, d is the disk thickness, ϵ_0 is the permittivity of free space, and C is the measured capacitance.

Figure 3. 1: An example of a mixed dielectric disk after machining and sanding. This disk has a matrix of PVDF polymer with 65% BST by volume

The Sencore meter charges the dielectric material using a constant current and measures the change in voltage versus time to calculate the capacitance [2]. By

measuring the capacitance in this way, the frequency of the charging depends on the capacitance of the dielectric material. As covered in Chapter 2, the dielectric constant is dependent on the frequency of charging of the dielectric material.

Since this study does not concentrate on the dielectric constant versus frequency and since the frequency of charging does not vary significantly between all of the composites, a charging frequency of 1 MHz was assumed for the data.

3.4 Dielectric Strength Test Setup

After the dielectric constant was measured using the composite disks, the samples were then cut into 0.762 mm (30 mil) thick samples using a lapidary saw, represented in Figure 3.2. The samples were then wet sanded down to a thickness of 0.508 mm (20 mil). The samples are represented in Figure 3.3.

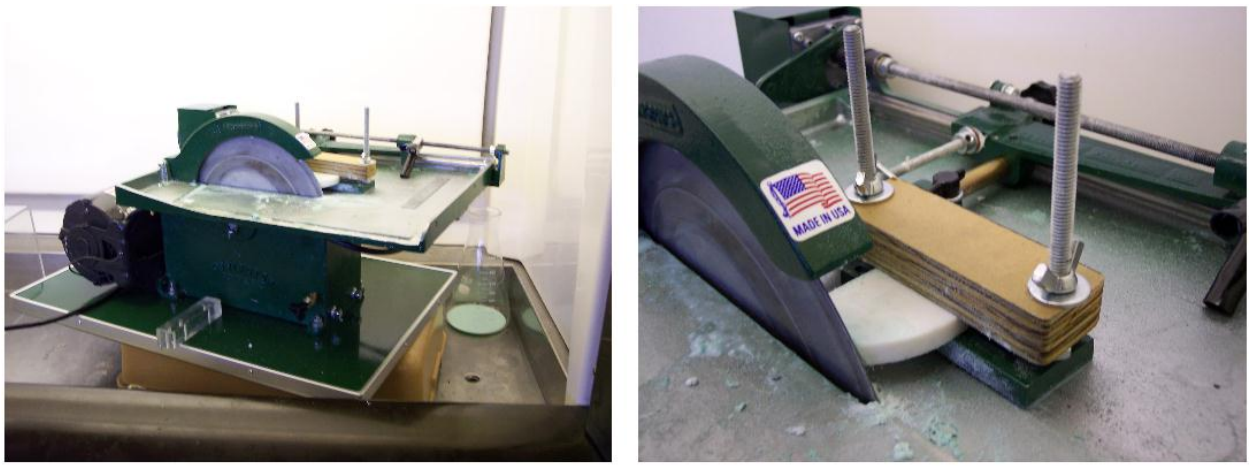

(a) (b)

Figure 3. 2: The lapidary saw used in cutting thin slices of dielectric material. (a) shows the saw inside the fume hood and (b) shows the saw with a piece of the dielectric material that it was cutting

In order to test the dielectric strength of the sample dielectric nanocomposites, a voltage pulse was applied to the sample composites. To accomplish this, a test cell was utilized in which the sample was submerged in mineral oil and held between two stainless steel electrodes with a tapered profile and blunted ends. An illustration of the test cell is represented in Figure 3.4 and pictures of the test stand are represented in Figures 3.5 through 3.8.

The high voltage pulse was generated using a PA-80 pulse generator from L-3 Communications in conjunction with a Glassman high voltage power supply. The capacitor could be charged to as high as 80 kV. A RG 218/U cable, which has an impedance of 50 Ω was used to connect the PA-80 to the test cell. On the other side of the test cell, the electrode was connected to a high impedance load. The schematic of the test stand is shown in Figure 3.9 [3].

3.4.1 Field Enhancement Factor (FEF)

As described in Chapter 2, the field enhancement factor (FEF) can increase the electric field flux density around certain geometries. In order to compute the FEF of the electrode configuration, ANSYS Maxwell 2D Electromagnetic Simulation software was used. The electrode and dielectric sample configuration described in Figure 3.4 was incorporated into the electric field solver. Figure 3.10 is an illustration of the electric field magnitudes generated by the field solver.

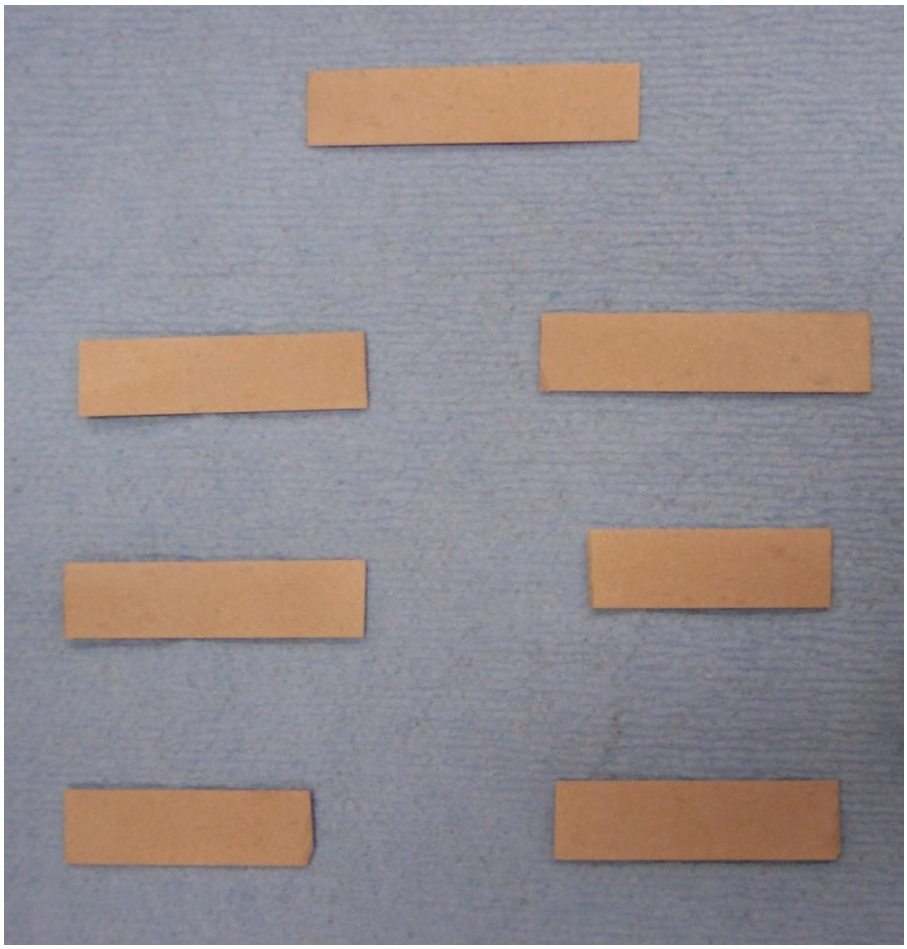

Figure 3. 3: Dielectric samples after being cut and sanded to 0.02 inches with a lapidary saw

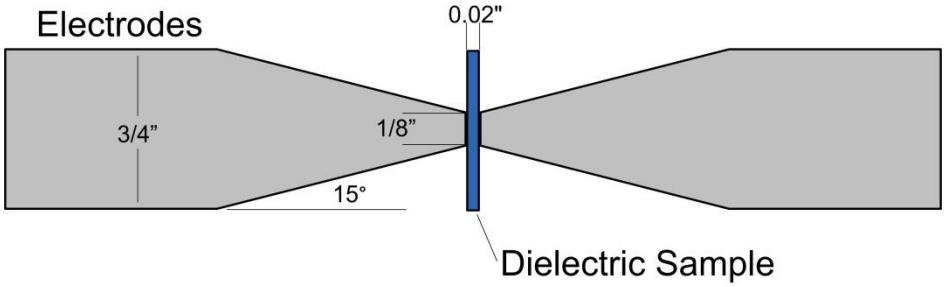

Figure 3. 4: An illustration of the dielectric strength test cell and its physical dimensions. The electrodes are made of stainless steel rod that machined with a conical end and a blunted tip. The edge on the blunted tip is rounded to a radius of 0.127 mm (5 mil)

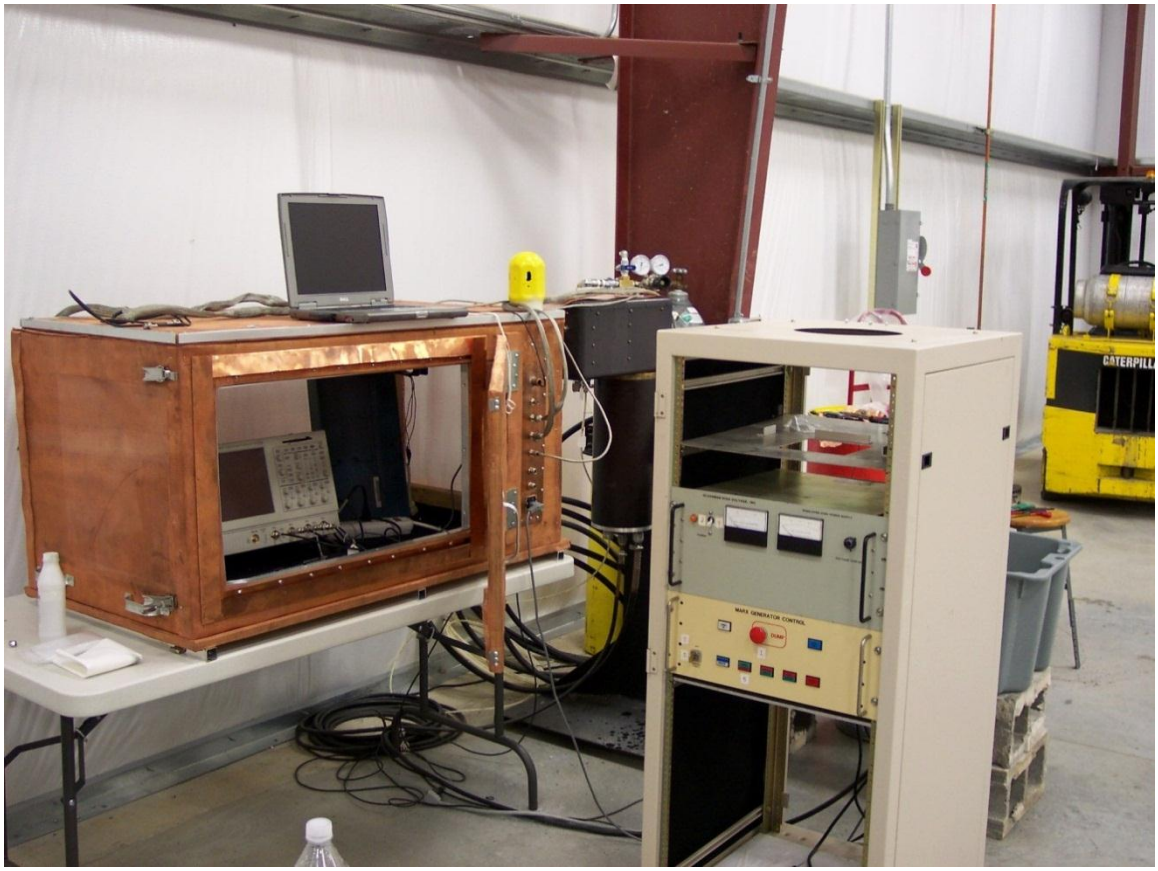

Figure 3. 5: A Picture of the control station, the Faraday cage, and the oscilloscope of the voltage breakdown test stand

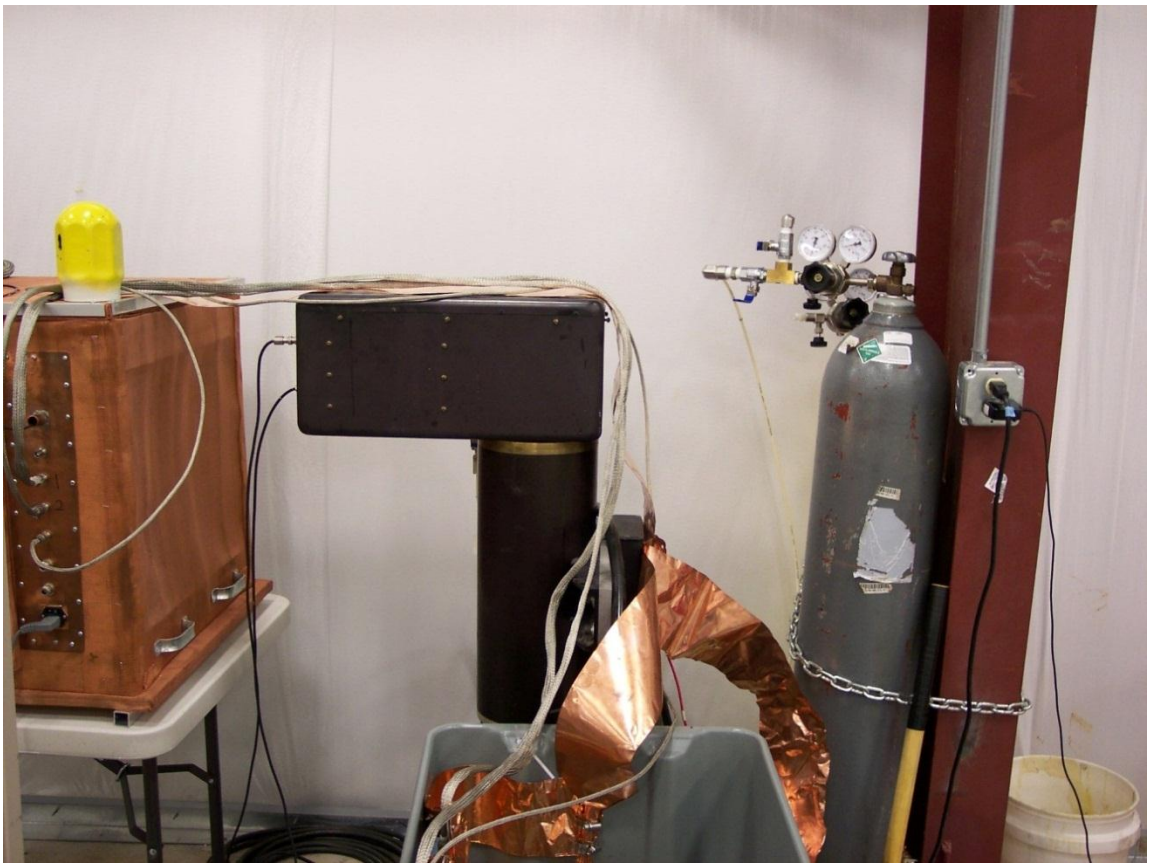

Figure 3. 6: A Picture of the oil tank and the pulse generator of the voltage breakdown

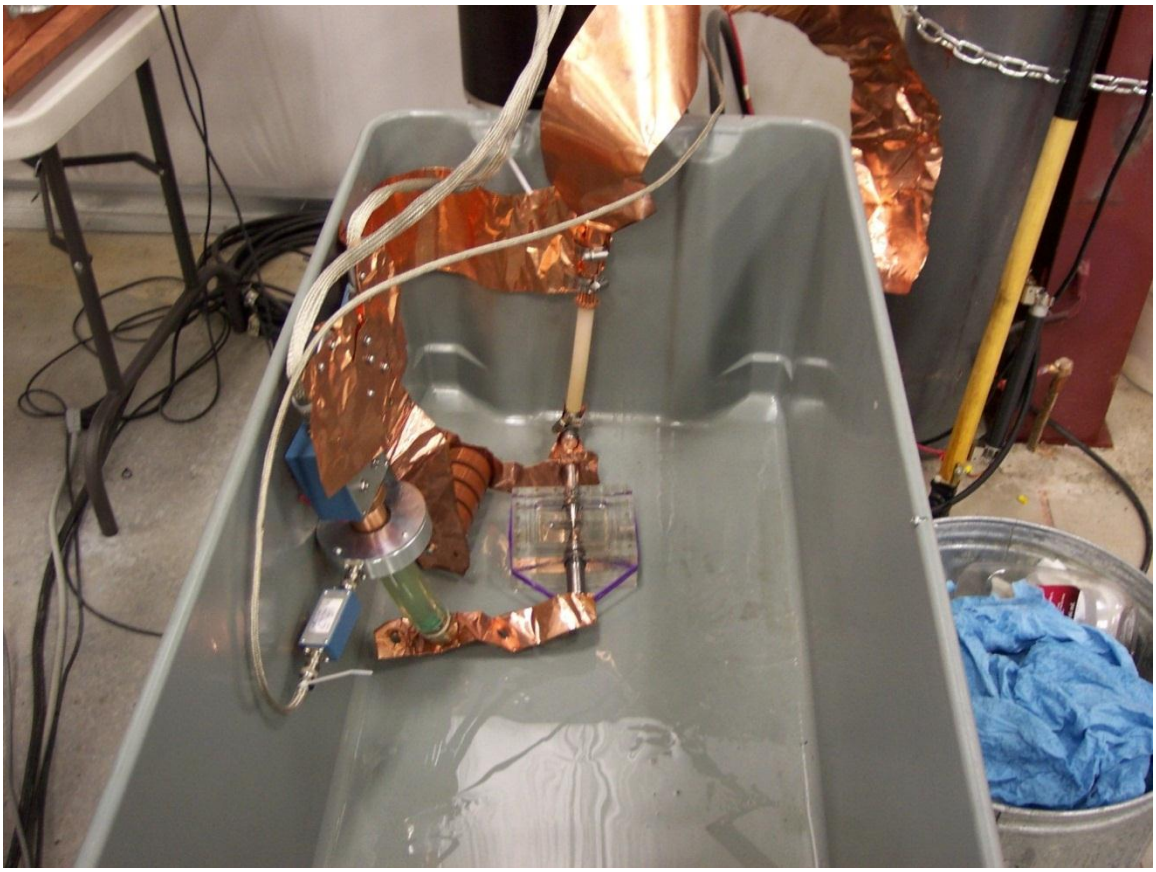

Figure 3. 7: A picture of inside the dielectric strength test stand oil tank. The picture shows the test cell and the voltage probes

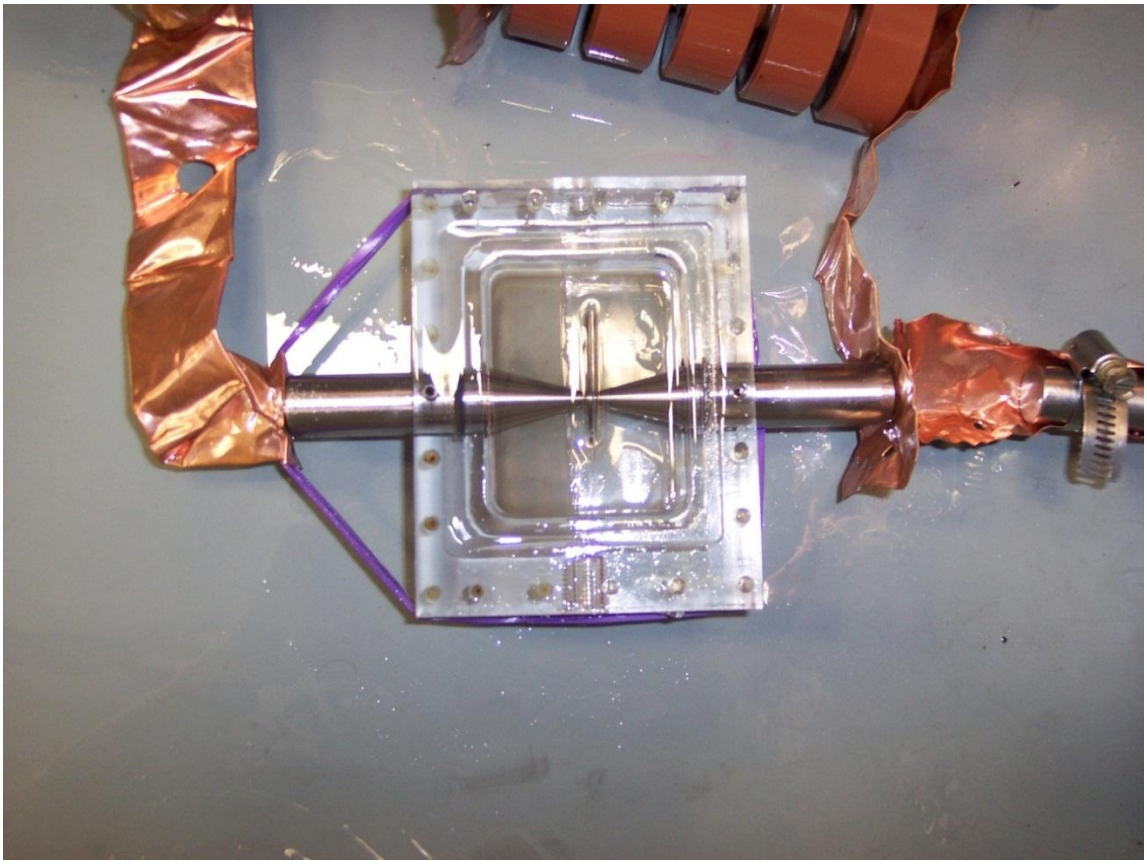

Figure 3. 8: A picture of the test cell, the electrodes, and a dielectric sample contained within the voltage breakdown test stand

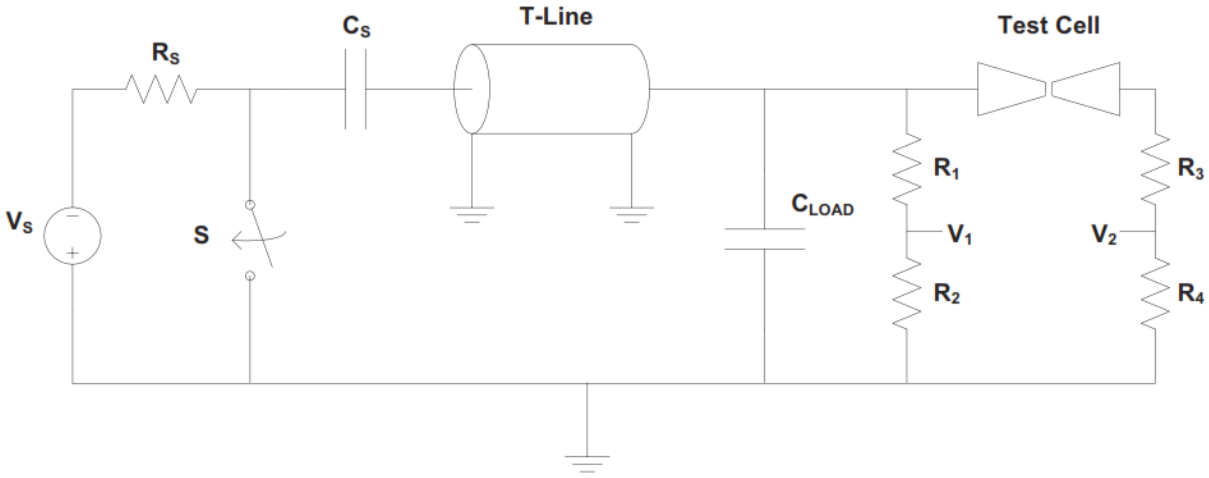

Figure 3. 9: The schematic layout of the dielectric strength test stand [3]

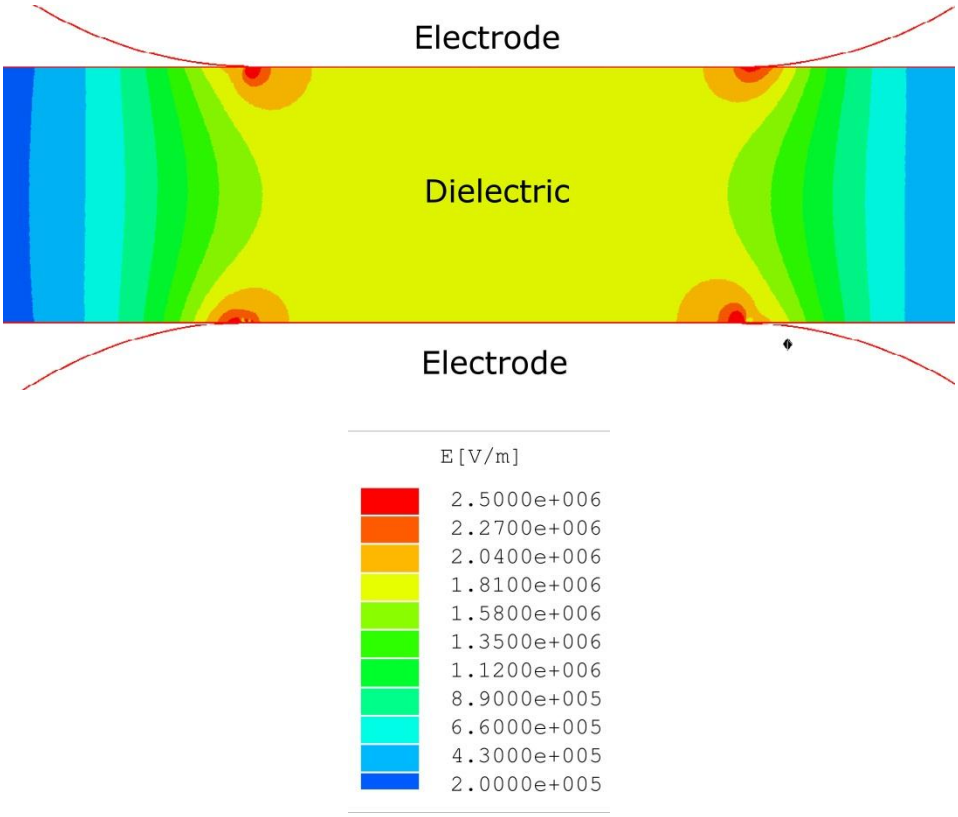

Figure 3. 10: An illustration from the ANSYS Maxwell 2D field simulation between the blunted conical electrodes, which shows the magnitude of the electric field. The blunted edges of the electrodes are rounded to a radius of 0.127 mm (5 mil), there is a 1 kV potential difference between the electrodes, and an electrode spacing of 0.508 mm (20 mil).

The mean field was calculated by

$$E = \frac{V_{diff}}{d} \quad (V/m), \tag{3.2}$$

where V_{diff} is the potential difference of the electrodes and d is the electrode separation. In the model, a potential of 1 kV and an electrode separation of 0.508 mm (20 mil) was used, which yielded a mean field of 1.97 MV/m. The peak field was calculated by the electric field simulation to be 14.9 MV/m. As described in Chapter 2, the FEF is the peak field divided by the mean field, which yields a FEF of 7.57. Even though the peak field is located at the corner of the blunted electrode, the breakdowns actually occur just outside the center of the electrode where there is no FEF. The breakdown locations can be seen by examining the electrodes after a set of breakdowns, which is evidence that the FEF was not a contributing factor to the breakdown. Therefore, this study uses the average electric field instead of the peak field when calculating the dielectric strength of the material.

There can also be a field enhancement within the material itself caused by the difference in the dielectric constant of the matrix and the nanoparticles. To calculate the FEF within the material, complex simulation codes would have to be incorporated, which is not a part of this particular investigation.

3.4.2 DIAGNOSTICS

A few different diagnostics were used to measure dielectric strength. When the switch was closed, the voltage across the test cell increased. When the voltage reached the breakdown point of the dielectric material, the voltage difference between the electrodes was measured. There were three different measurements that were utilized to obtain the voltage at the point of breakdown; the voltage on the anode, the voltage on the cathode, and the current in the circuit. Resistor dividers that made use of large water resistor cells were used to measure the voltages on the electrodes. The resistor dividers were made of water and copper sulfate.

The current in the circuit through the test cell was used to determine when the sample underwent dielectric breakdown. The current measurement shows a sharp knee at the point when the breakdown occurs. This current spike was used to trigger the oscilloscope to take the voltage measurements. The current was observed by utilizing a Pearson coil, which generates a voltage proportional to the current in the coil. A load capacitance was also used to slow down the rise time of the voltage in order to increase the resolution of the voltage measurements.

The voltage measurements taken by the oscilloscope consisted of 500 data points that were taken over 200 nanoseconds. In order to show the statistical analysis that was used, a sample of the oscilloscope view and the raw collected voltage data are displayed in Figure 3.11 for a sample of 75% BST by volume in a PVDF matrix. The data was then smoothed, as shown in Figure 3.12 using a moving average filter in MATLAB.

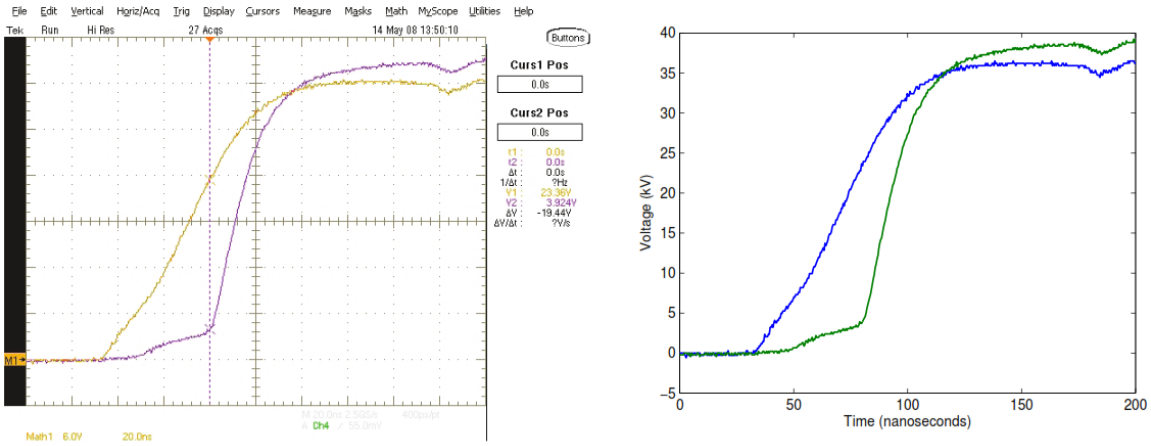

(a) (b)

Figure 3. 11: An example of (a) oscilloscope image and (b) the raw voltage data before and after the dielectric sample in the voltage breakdown testing. The dielectric material used in this particular graph is 75% BST by volume added to a PVDF matrix. The blue or the leftmost waveform is the voltage on the electrode on the same side of the test cell as the pulser. The green or rightmost waveform is the voltage on the electrode on the opposite side of the test cell.

Figure 3.11b also shows a few things that are worth noting. The most pertinent piece of data to this study is the voltage difference between the two electrodes when the oscilloscope is triggered by the sharp rise in the current. This is recorded as the voltage breakdown of the particle sample, after which the voltage difference quickly drops back to approximately zero.

Just before the breakdown, there is a small rise in voltage on the opposite electrode, which can be seen in Figure 3.12. This small rise is due to the polarization of the dielectric material, which causes a displacement current in the material. The dielectric material begins to act like a capacitor and begins slightly charging the dielectric material.

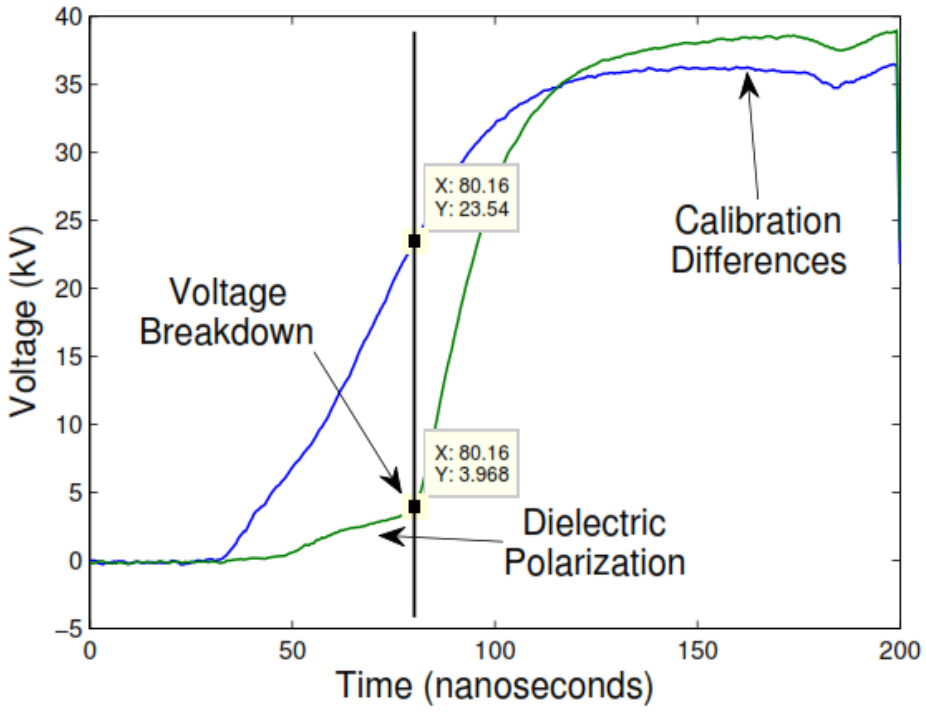

Figure 3. 12: The smoothed breakdown voltage data which shows a slight polarization of the dielectric before breakdown, the voltage difference of the two electrodes at breakdown, and the calibration difference well after breakdown.

The difference in voltage after the breakdown is a result of calibration differences. These differences are a result of a mismatch between the division ratios if the voltage dividers. The calibration of the voltage dividers, which is the specific used to measure

the true voltages on the two electrodes, were adjusted so that they were most accurate at the time of breakdown. Once the voltage that caused the breakdown was measured, Equation 3.2 was used to calculate the mean breakdown.

This voltage breakdown test was repeated on 20 different samples in order to obtain a statistical analysis of the voltage breakdown. Table 3.13 shows an example of the sample breakdown data from 75% BST/PVDF.

Shot#	Vbreak (kV)	Ebreak (kV/mil)	Ebreak (MV/m)
1.00	19.44	0.97	38.27
2.00	19.65	0.98	38.68
3.00	19.87	0.99	39.11
4.00	19.21	0.96	37.81
5.00	21.11	1.06	41.56
6.00	19.29	0.96	37.97
7.00	18.41	0.92	36.24
8.00	17.83	0.89	35.10
9.00	16.73	0.84	32.93
10.00	16.88	0.84	33.23
11.00	16.80	0.84	33.07
12.00	16.37	0.82	32.22
13.00	18.49	0.92	36.40
14.00	17.32	0.87	34.09
15.00	19.00	0.95	37.40
16.00	20.46	1.02	40.28
17.00	17.24	0.86	33.94
18.00	19.65	0.98	38.68
19.00	19.87	0.99	39.11
20.00	19.58	0.98	38.54
AVRG	18.66	0.93	36.73
STDEV	1.39	0.07	2.73
MED	19.11	0.96	37.61

Figure 3. 13: The electric field values at which breakdown occurred in 75% BST/PVDF with a thickness of 0.508 mm (20 mil)

The Weibull distribution is commonly used to analyze the statistics of failure in materials. The MATLAB computer program was used to create a cumulative probability distribution graph utilizing the Weibull distribution. Figure 3.14 shows the classic cumulative Weibull distribution with the individual peak field breakdown points. The dashed line is the approximated Weibull distribution curve for the breakdown data. Figure 3.15 shows a Weibull distribution curve and the electric field at which there is a 63% probability of breakdown. The same plot using MV/m is also represented in Figure 3.17.

The voltage at which the material has a 63% probability of breakdown is how the dielectric strength is commonly compared between materials in the open literature [4] [5], but as long as the same percent breakdown value is used with each material, any number could be chosen for the comparison. This process was then repeated for several conventional plastics and for the other nanocomposites that were made in this investigation.

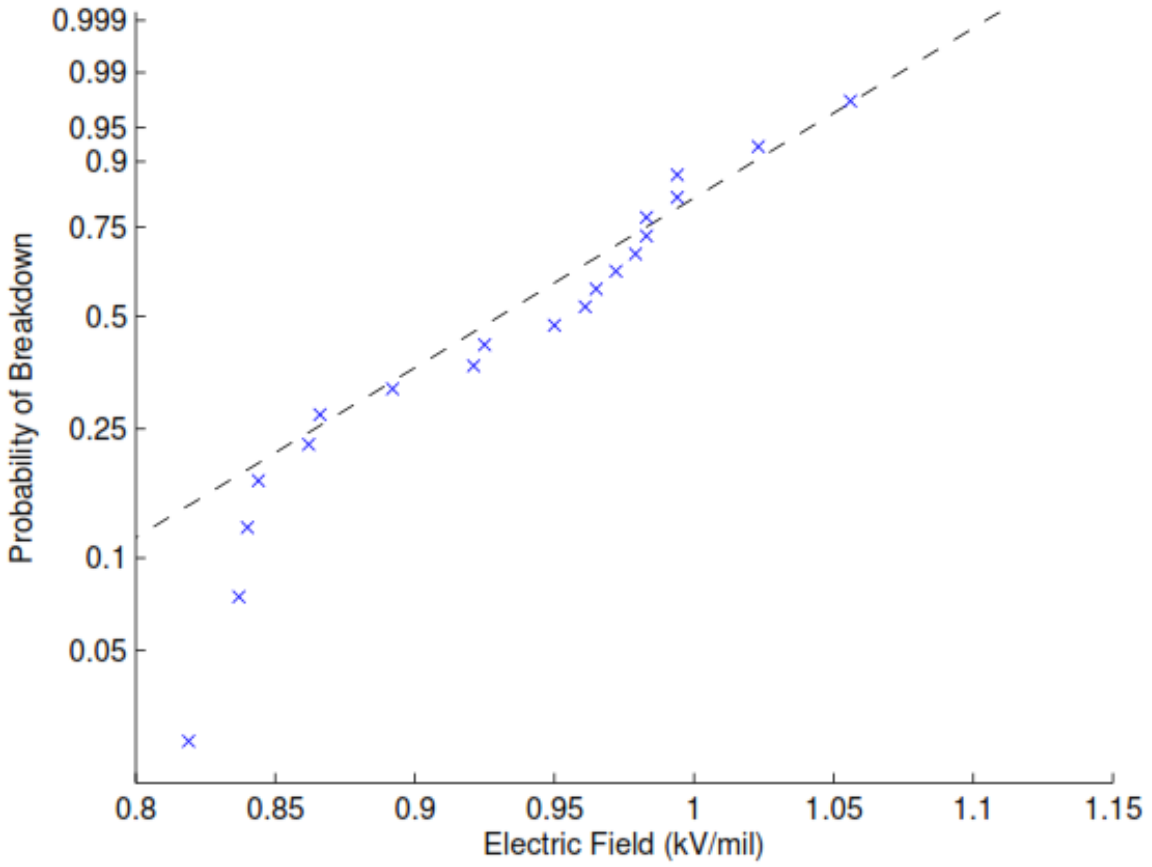

Figure 3. 14: The cumulative Weibull probability distribution in kV/mil with the breakdown points of a 0.508 mm (20 mil) thick sample of 75% BST by volume added to a PVDF matrix

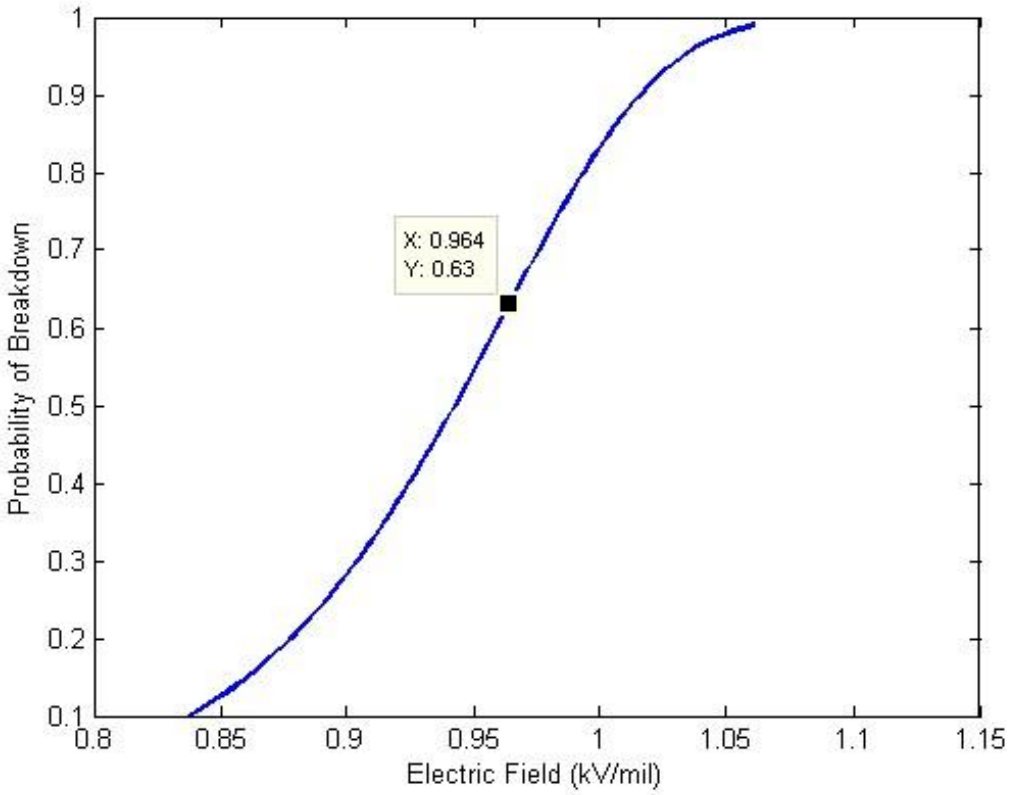

Figure 3. 15: The approximated cumulative Weibull probability distribution plot in kV/mil based on the breakdown data with the 63% breakdown probability shown. The dielectric material is a 0.508 mm (20 mil) thick sample of 75% BST by volume added to a PVDF matrix.

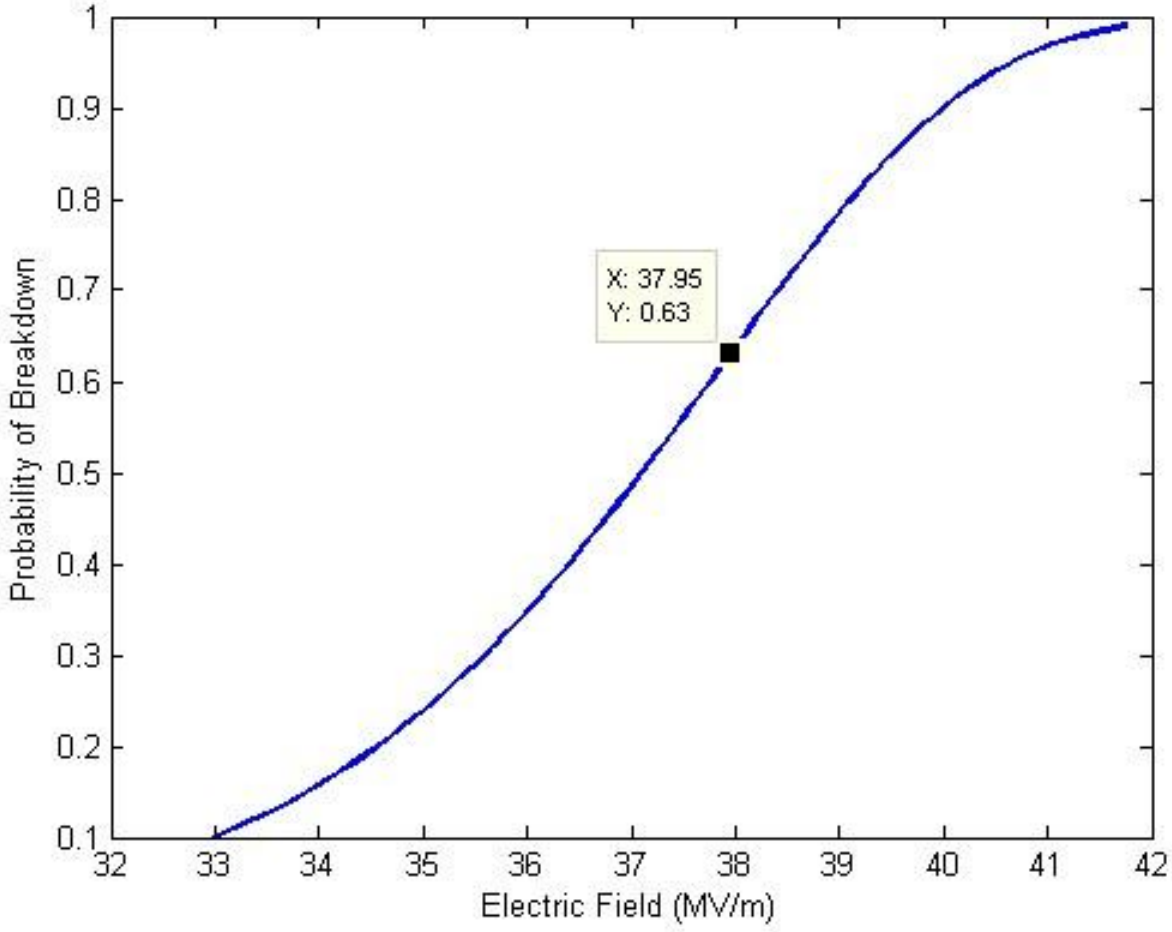

Figure 3. 166: The approximated cumulative Weibull probability distribution plot in MV/m based on the breakdown data with the 63% breakdown probability shown. The dielectric material is a 0.508 mm (20 mil) thick sample of 75% BST by volume added to a PVDF matrix.

3.5 BIBLIOGRAPHY FOR CHAPTER 3

[1] F. T. Ulaby, Fundamentals of Applied Electromagnetics. Pearson Prentice Hall, 2004.

[2] LC103 ReZolver Capacitor and Inductor Analyzer Operation and Application Manual, Sencore, Sioux Falls, South Dakota.

[3] K. O'Connor, J. Smith, and R. Curry, "Dielectric characterization of polymer- ceramic nanocomposites," 17th IEEE International Pulsed Power Conference, July 2009.

[4] H.-J. Winter, J. Lambrecht, and R. Barsch, "On the measurement of the dielectric strength of silicone elastomers," Universities Power Engineering Conference (UPEC), 2010.

[5] S. Zelmat, S. Diaham, M. Decup, M.-L. Locatelli, and T. Lebey, "Weibull statistical dielectric breakdown in polymide up to 400," Annual Report Conference on Electrical Insulation and Dielectric Phenomena (CEIDP), 2008.

Chapter 4 – EXPERIMENTAL RESULTS

4.1 INTRODUCTION

As described in Chapter 1, the goal of this investigation was to create a new dielectric material for use in pulsed power applications. This new material would possess a higher dielectric constant and have a high dielectric strength while still being machinable and durable. To accomplish this goal, a composite material was pursued, which was a mixture of a commercially available ceramic nanopowder mixed in a plastic as a matrix material, thereby mixing the characteristics of a ceramic and a plastic. A commercial company was utilized to fabricate the samples.

The choice of the ceramic and the plastic materials for this study was explained in Chapter 3. The ceramics that were chosen were Barium Strontium Titanate, $BaSrTiO_3$, (called BST in this study) and Strontium Titanate, $SrTiO_3$, (called ST in this study) with a median grain size of 100 nanometers. The plastic that was chosen was polyvinylidene fluoride (PVDF) and Teflon, which is polytetrafluoroethylene (PTFE) [1]. After the first round of mixing was completed, the BST/PVDF composites displayed a higher dielectric constant then the other composites. Because of this, the primary focus of this study concentrated on the BST/PVDF composite.

4.2 Dielectric Constant Experimental Results

The dielectric constants of the composites were measured using the procedure in Chapter 3. The ST/Teflon and the BST/Teflon composites were first to be mixed at volume fractions of filler material to the plastic matrix of 50%, 70%, and 90%. There were two problems with these samples. Both the 90% mixtures did not have enough plastic to keep it together and resembled loosely pressed powder. These mixtures fell apart during handling, which rendered them unusable.

The 50% ST/Teflon and the 50% BST/Teflon composites had other problems. The samples looked normal from the outside but when they were cut using the lapidary saw described in Chapter 3, the samples resembled a reverse Oreo cookie with the white plastic on the outside and the dark ceramic in the middle. A picture of this is represented in Figure 4.1.

Of the Teflon batch, the only usable sample was the 70% filled samples. The same dielectric constant was again measured with the BST and ST filler material with Teflon and was found to be 38.7 and 16.92, respectively, which is represented in Figure 4.2.

Because of the results of the Teflon composites, the ST was not used in the PVDF composites. The volume fractions of filler material versus matrix material used in the BST/PVDF mixtures was 60%, 65%, 70%, 75%, and 80%. Higher loadings were not mixed because of the how brittle the 90% Teflon mixes were. The samples were prepared and the dielectric constant was measured using the procedure in Chapter 3. The dielectric constant versus volume fraction is represented in Figure 4.3. The dielectric constant of

the material rose as the fraction of ceramic filler material increased. The increase in dielectric constant was expected but the numbers were lower than calculated.

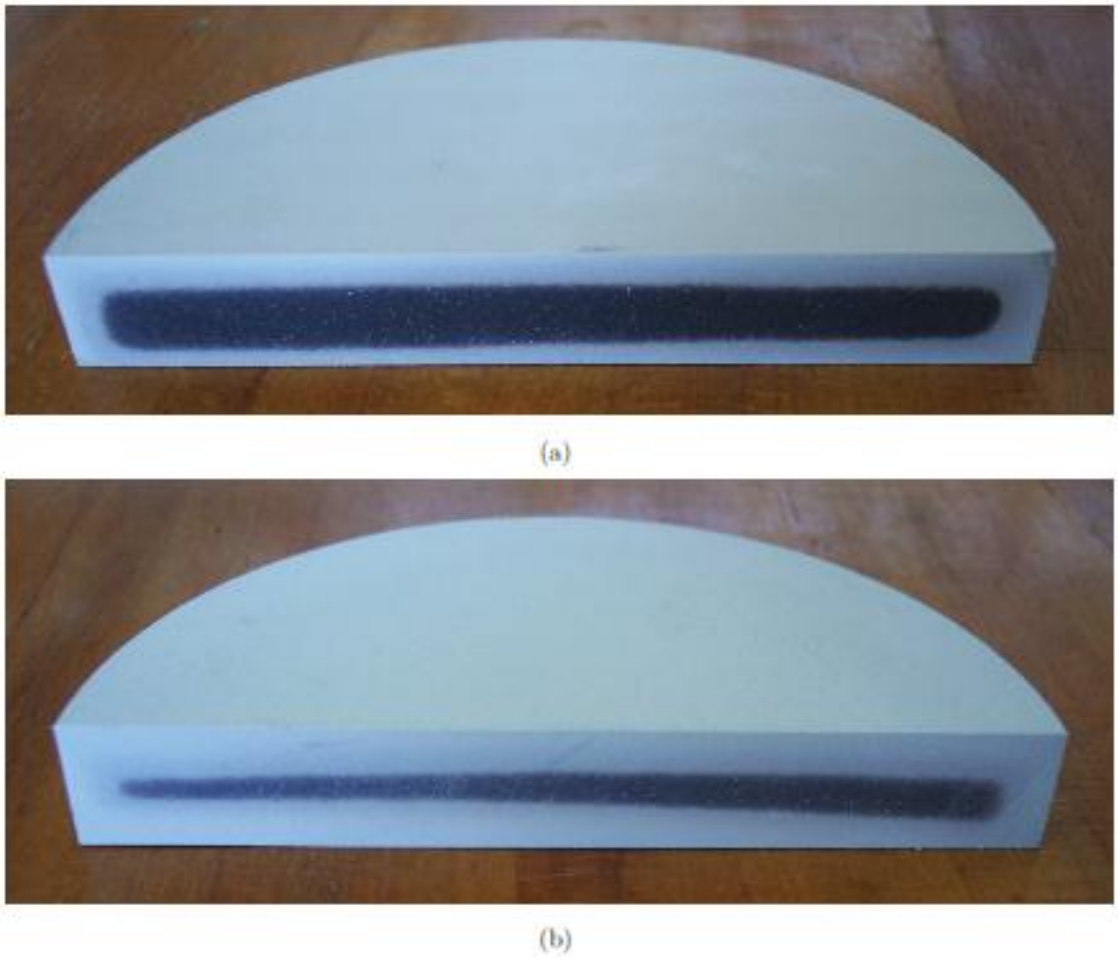

Figure 4. 1: Pictures of the commercially mixed composites of 50% by volume of (a) ST and (b) BST powders mixed in Teflon. The pictures show the poor result of the mixing process for this composite.

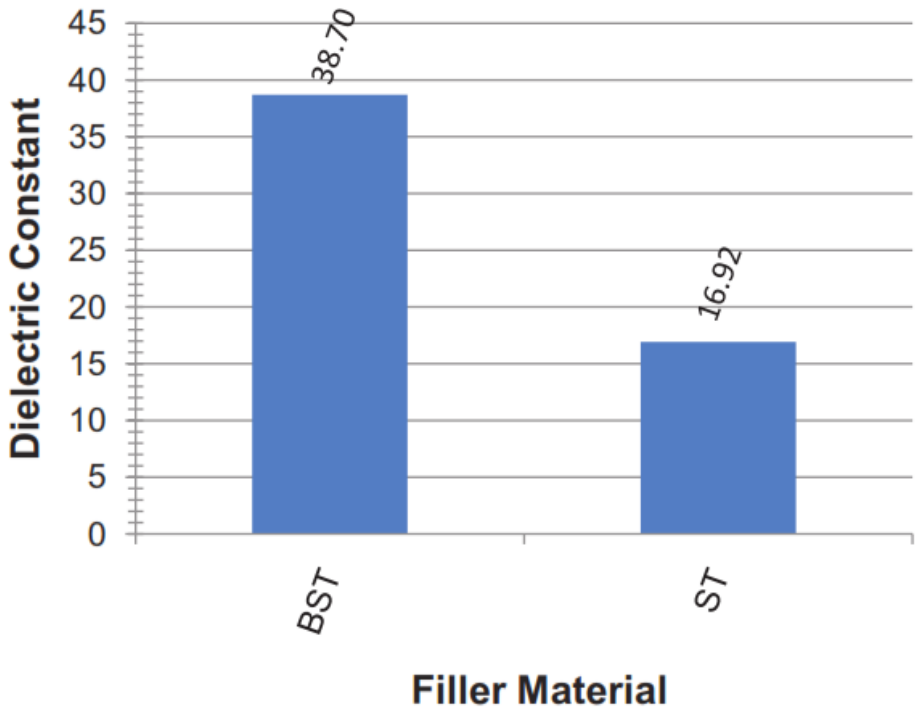

Figure 4. 2: The dielectric constant of ST and BST composites in a Teflon matrix with 70% fill by volume

4.3 Dielectric Constant Experimental Results and Theory Comparison

The Lichtenecker Model and the Maxwell-Garnett Model described in Chapter 2 are fairly straightforward to graph, but the Interphase Model contains two values, k and the dielectric constant of the interphase region ϵ_2 , which have to be solved for before it can be graphed. In keeping with the way Vo and Shi, Lombardo, Todd and Shi, and Murugaraj et al. seemed to solve for these interphase values; a sum of squares approach was used in determining the relationship between k and ϵ_2. The fminsearch function was utilized in MATLAB in order to find the interphase values which gave the

minimum least sums difference between the experimental and expected values [2] [3] [4] [5] [6].

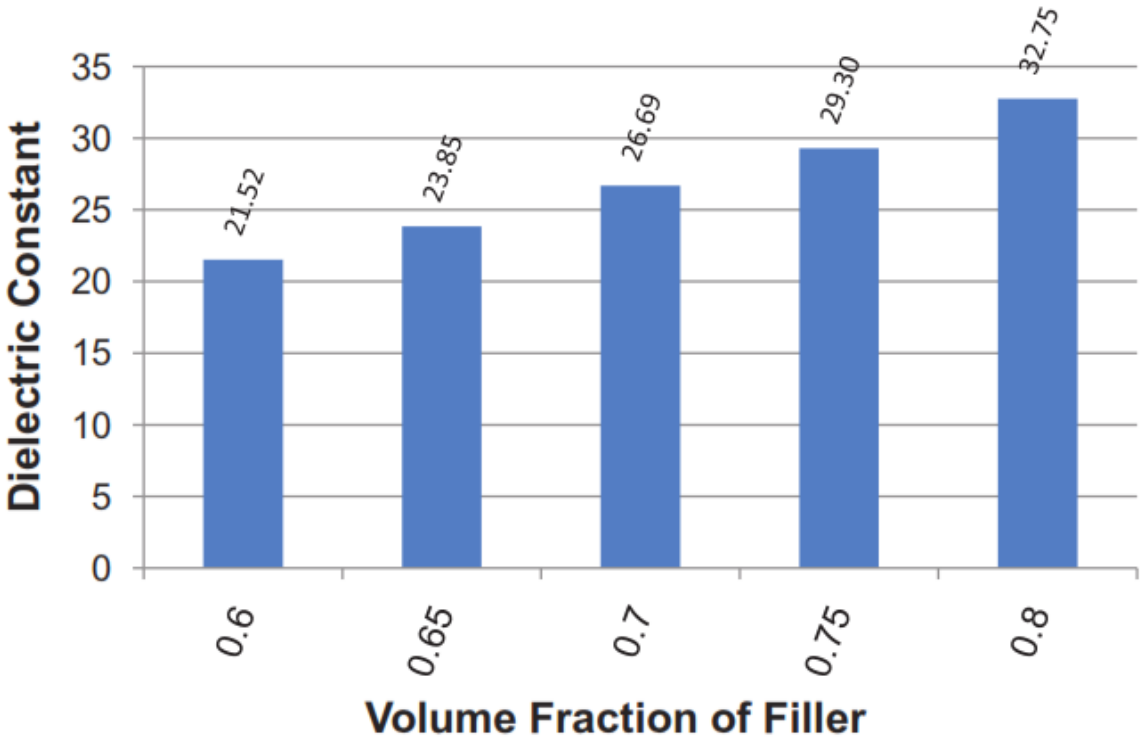

Figure 4. 3: The dielectric constant of BST powder in a PVDF matrix versus volume fraction of filler

The problem with this approach, as described in Chapter 2, is there is difficulty in independently solving for the two values. If fminsearch is allowed to search for minimum values for both k and ϵ_2, they both approach zero, but the search algorithm does come up with some reasonable values when the values are bounded to a realistic range. Figure 4.4 shows a three dimensional graph of the sum of squares of the difference between the theoretical values and the measured values of the dielectric constant at different volume fractions of filler material. This graph shows an interesting

trend. There is a trough with fairly consistent values of ϵ_2. Figure 4.5 shows the trough as a two dimensional graph of k versus ϵ_2.

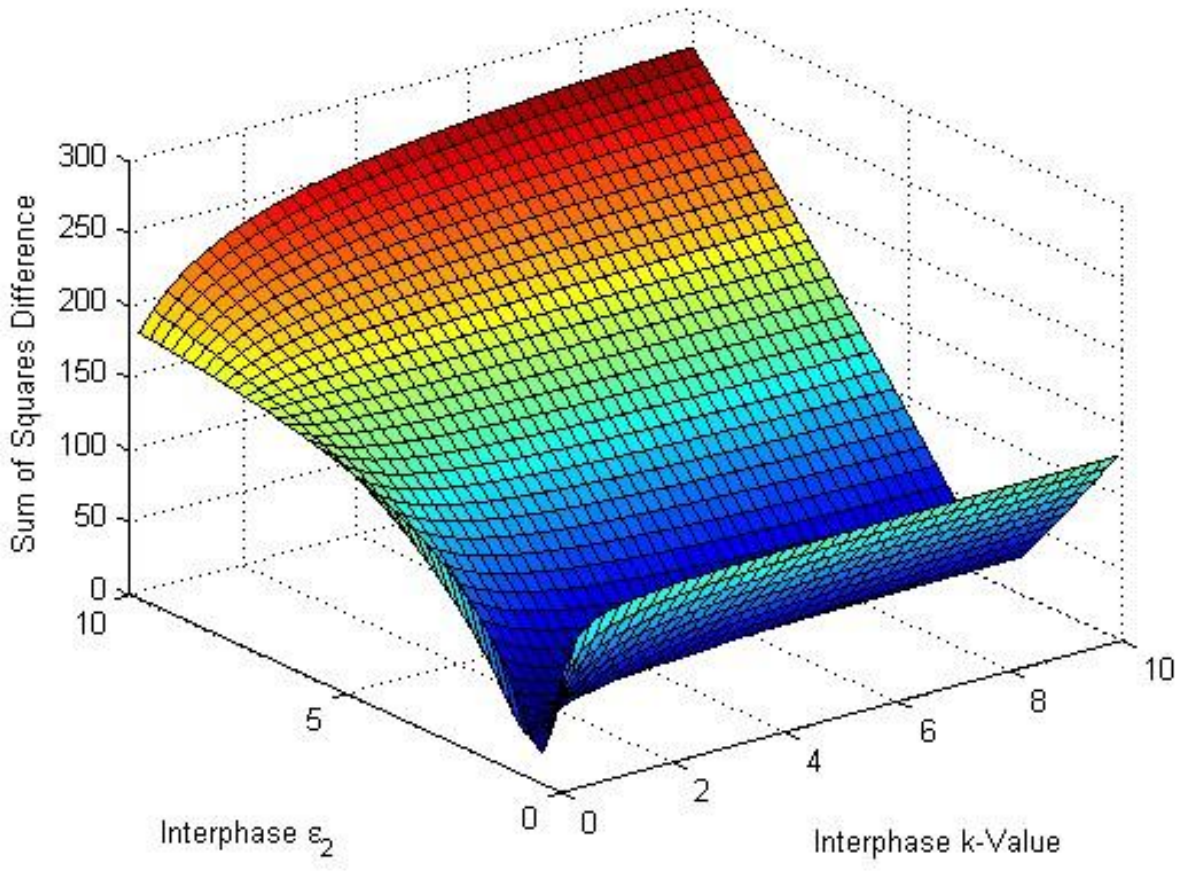

Figure 4. 4: A 3-D graph of k, ϵ_2, and the sum of squares difference between the theoretical values and the measured values of the dielectric constant at different volume fractions of filler material

According to Figure 4.5, the dielectric of the interphase region tends toward approximately 2.92 at high k values. Even though this study does not solve explicitly for k and ϵ_2, Figures 4.4 and 4.5 show trends that can be investigated in the future.

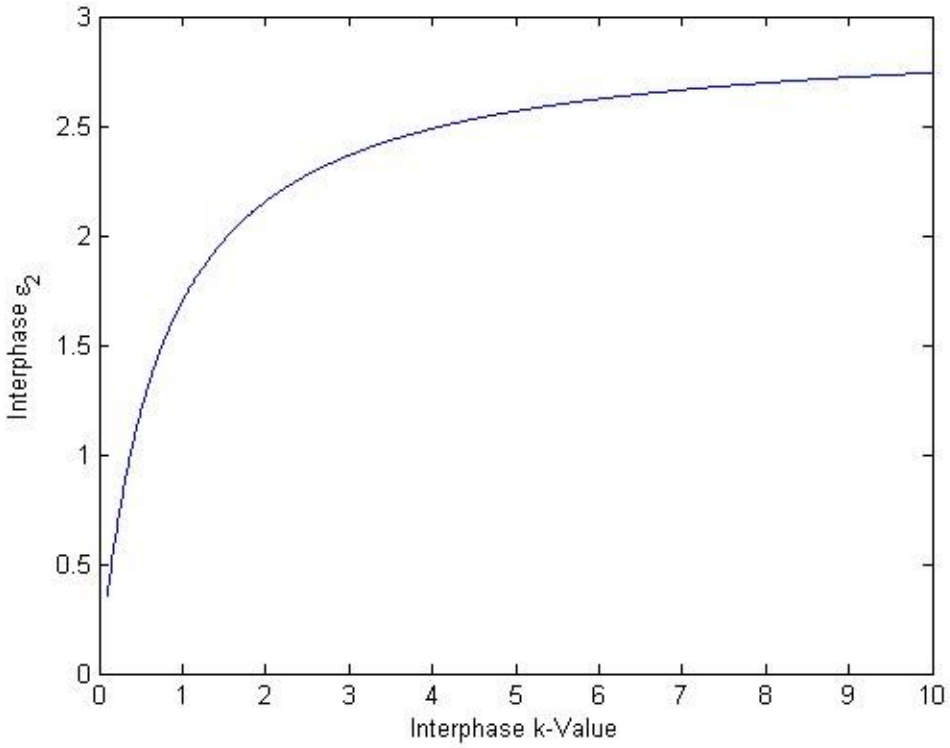

Figure 4. 5: A 2-D graph of ϵ_2 versus k where the minimum sum of squares difference occurs between the theoretical values of the dielectric constant at different volume fractions of filler material

In Lombardo's paper, they obtain a k value of 2.05 [3]. In this study a k value of 2.05 yields a theoretical ϵ2 value of 2.17 using the least sum of squares method. Using 2.05 as the k value and 2.17 as the dielectric constant of the interphase region and comparing it graphically with the measured values yields Figure 4.6 which also show the Lichtenecker and the Maxwell-Garnett models.

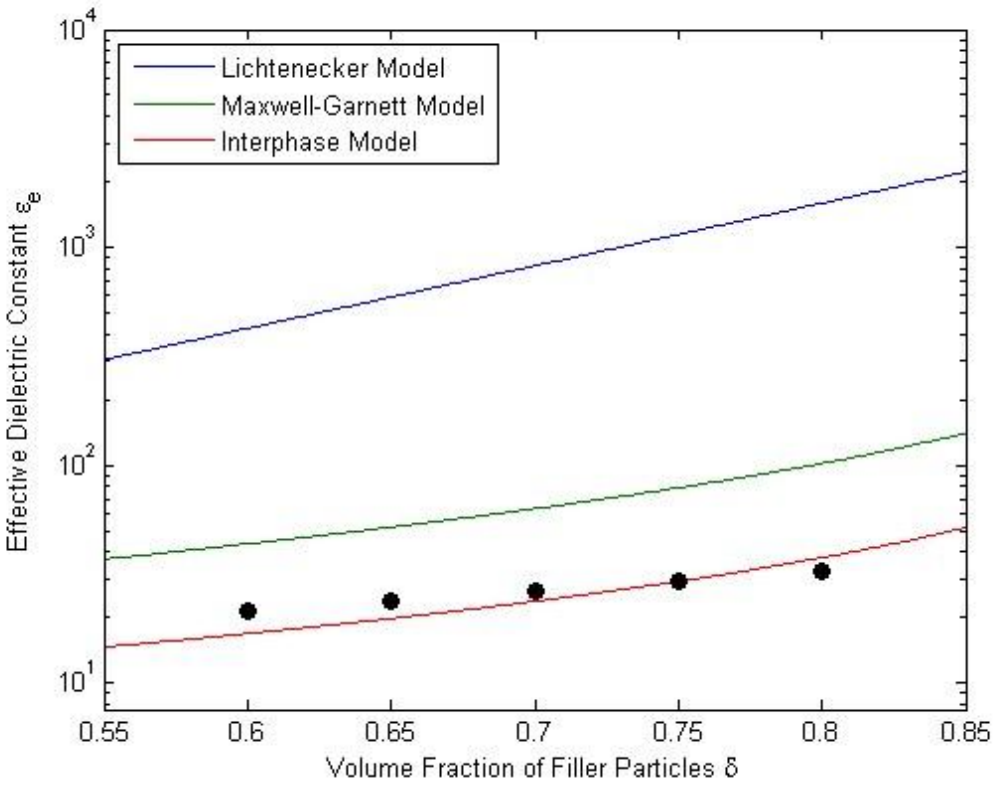

Figure 4. 6: A graphical comparison of the measured values of the dielectric constant versus volume of filler material and the Lichtenecker, Maxwell-Garnett, and Inter-phase Models for BST-PVDF

4.4 Dielectric Breakdown Experimental Results

4.4.1 Dielectric Breakdown of Composites

The dielectric strength was measured using the procedure and test apparatus described in Chapter 3. Each dielectric was subjected to 20 breakdown tests to obtain a statistical variation. The 20 different breakdown values and a Weibull distribution of the breakdown values are recorded in Figures 4.7 through 4.34. Figures 4.35 and 4.36 show Weibull probability distributions for all the custom nanocomposites in kV/mil and MV/m.

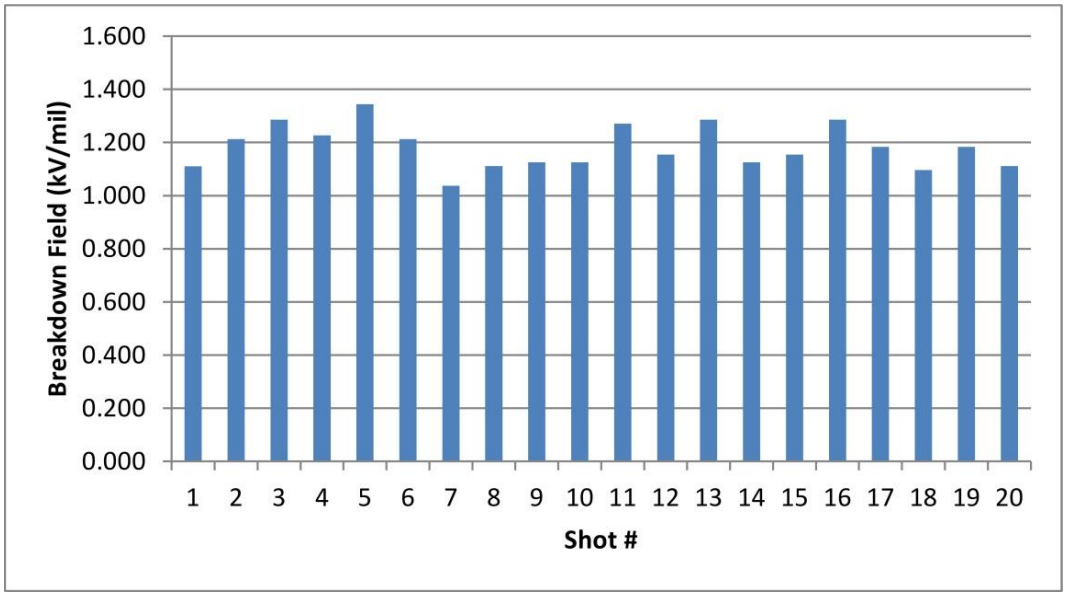

Figure 4. 7: Breakdown table of 0.508 mm (20 mil) 60% by volume BST added to a PVDF matrix in kV/mil

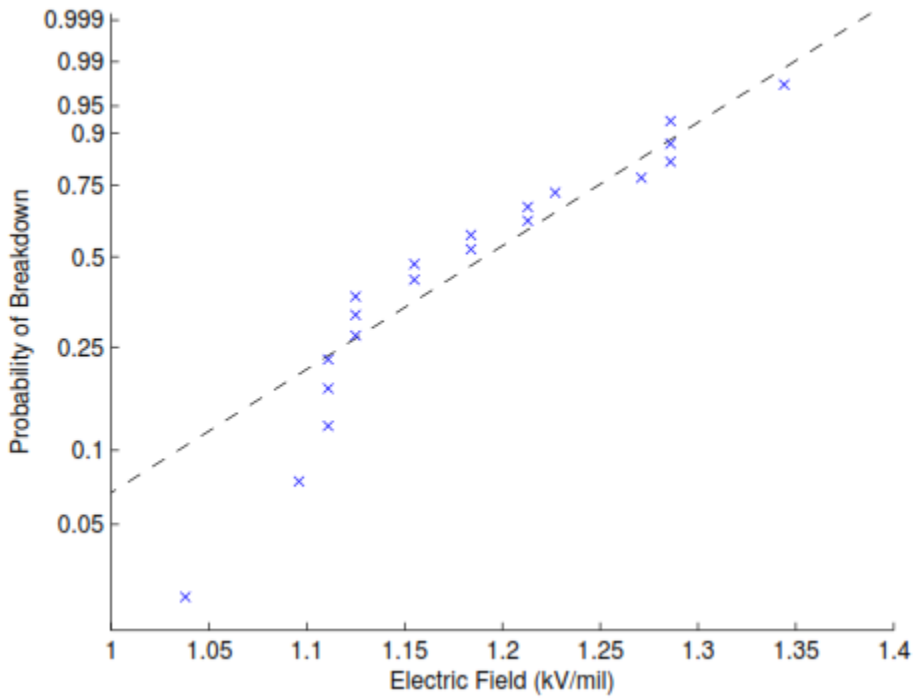

Figure 4. 8: Weibull probability breakdown plot of 0.508 mm (20 mil) 60% by volume BST added to a PVDF matrix in kV/mil

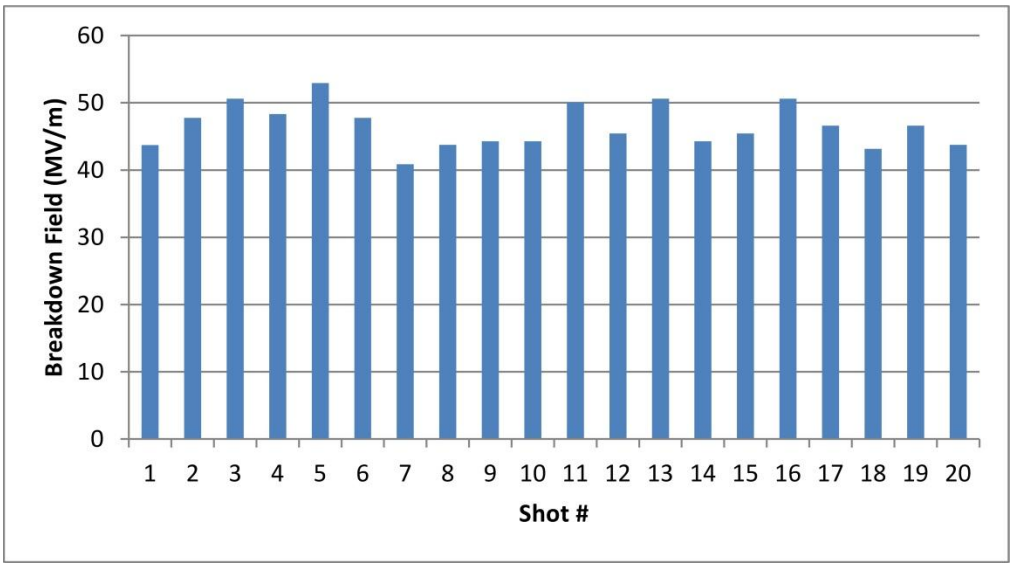

Figure 4. 9: Breakdown table of 0.508 mm (20 mil) 60% by volume BST added to a PVDF matrix in MV/m

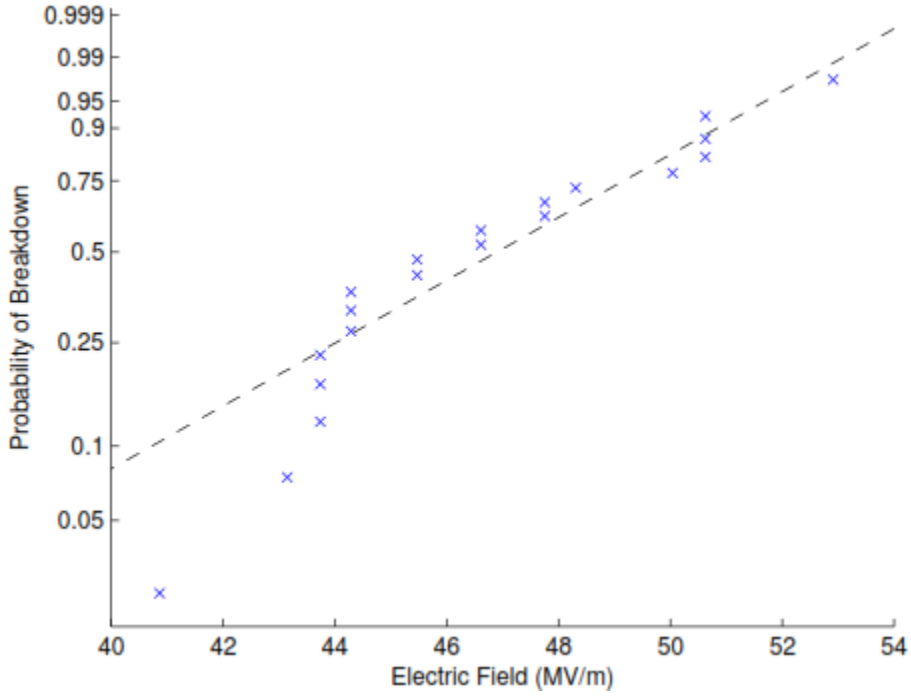

Figure 4. 10: Weibull probability breakdown plot of 0.508 mm (20 mil) 60% by volume BST added to a PVDF matrix in MV/m

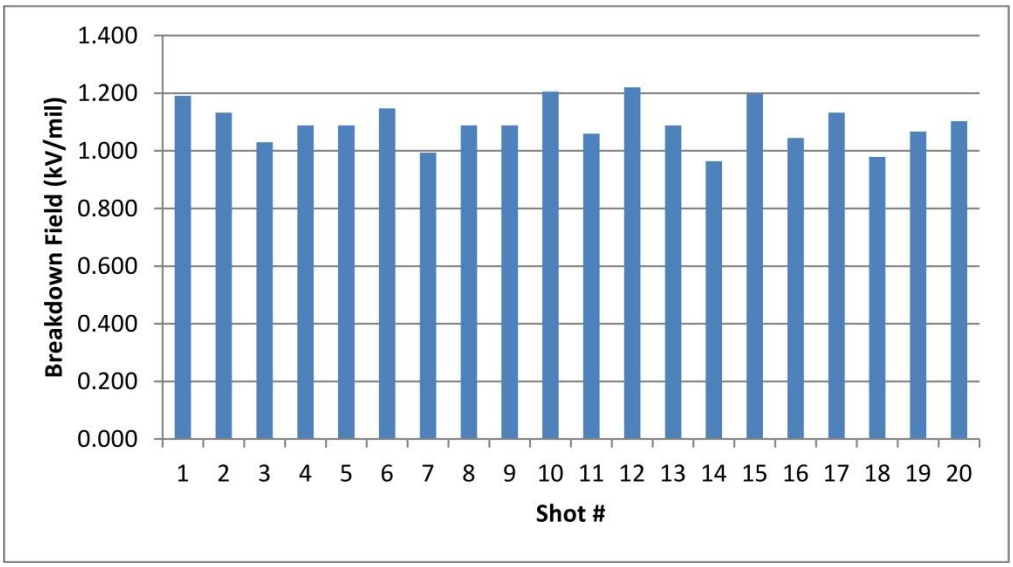

Figure 4. 11: Breakdown table of 0.508 mm (20 mil) 65% by volume BST added to a PVDF matrix in kV/mil

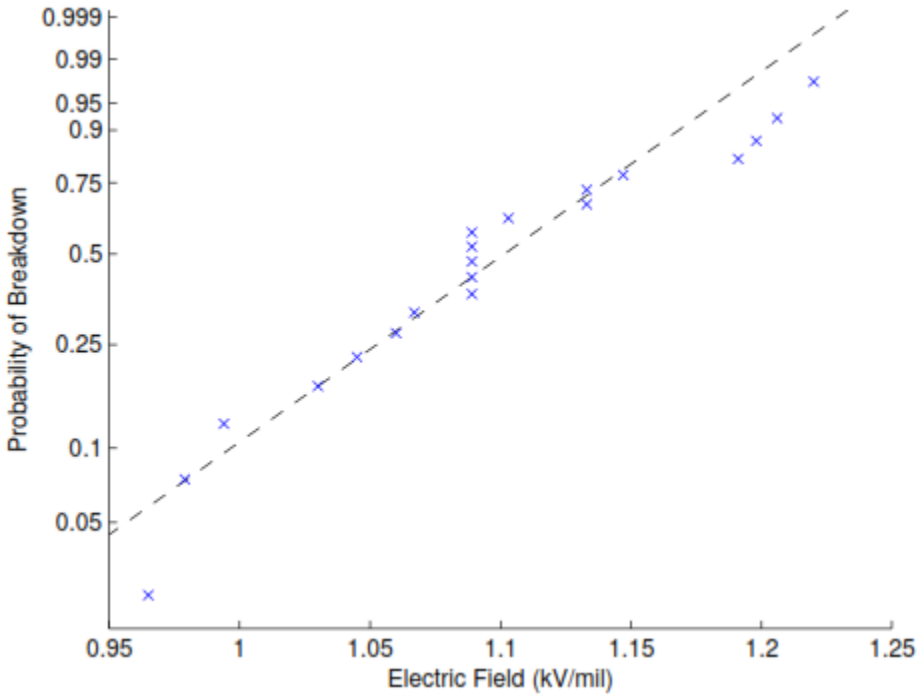

Figure 4. 12: Weibull probability breakdown plot of 0.508 mm (20 mil) 65% by volume BST added to a PVDF matrix in kV/mil

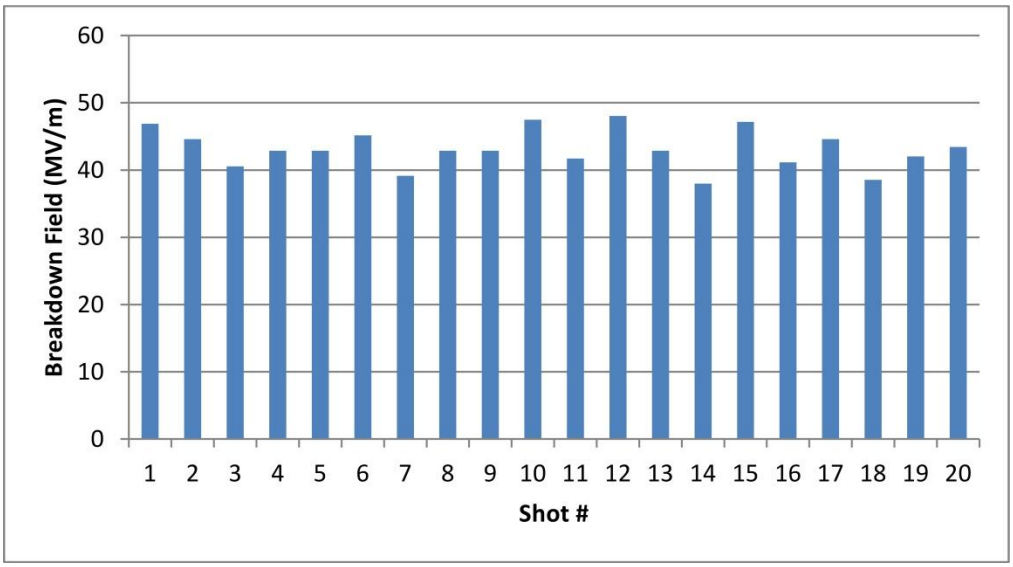

Figure 4. 13: Breakdown table of 0.508 mm (20 mil) 65% by volume BST added to a PVDF matrix in MV/m

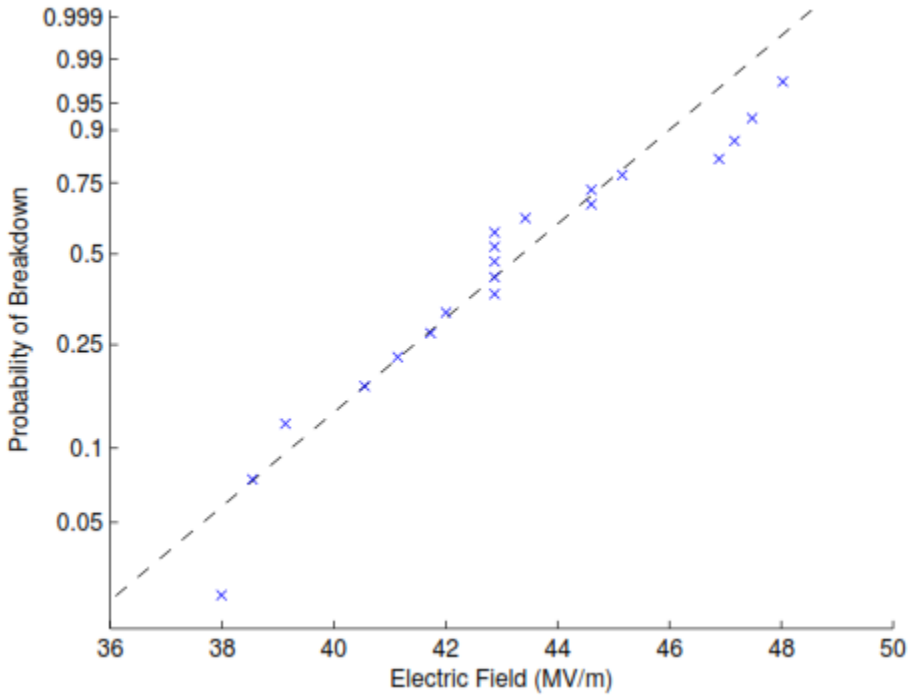

Figure 4. 14: Weibull probability breakdown plot of 0.508 mm (20 mil) 65% by volume BST added to a PVDF matrix in MV/m

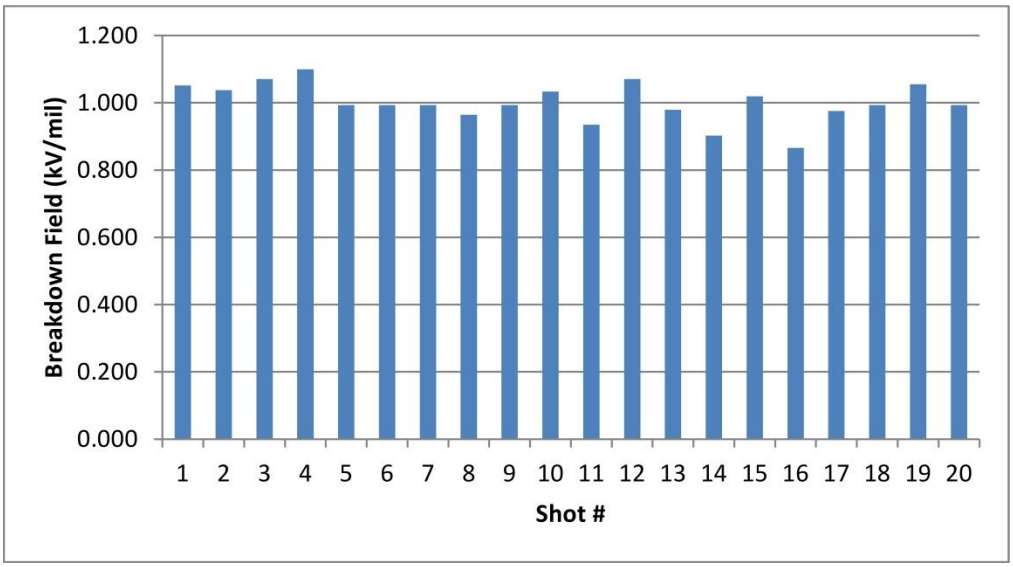

Figure 4. 15: Breakdown table of 0.508 mm (20 mil) 70% by volume BST added to a PVDF matrix in kV/mil

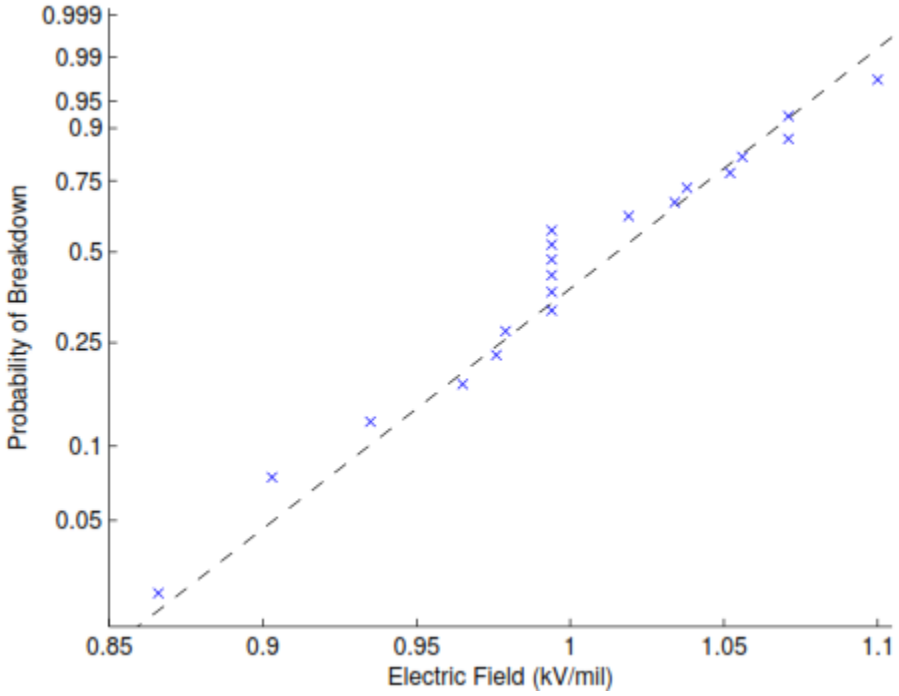

Figure 4. 16: Weibull probability breakdown plot of 0.508 mm (20 mil) 70% by volume BST added to a PVDF matrix in kV/mil

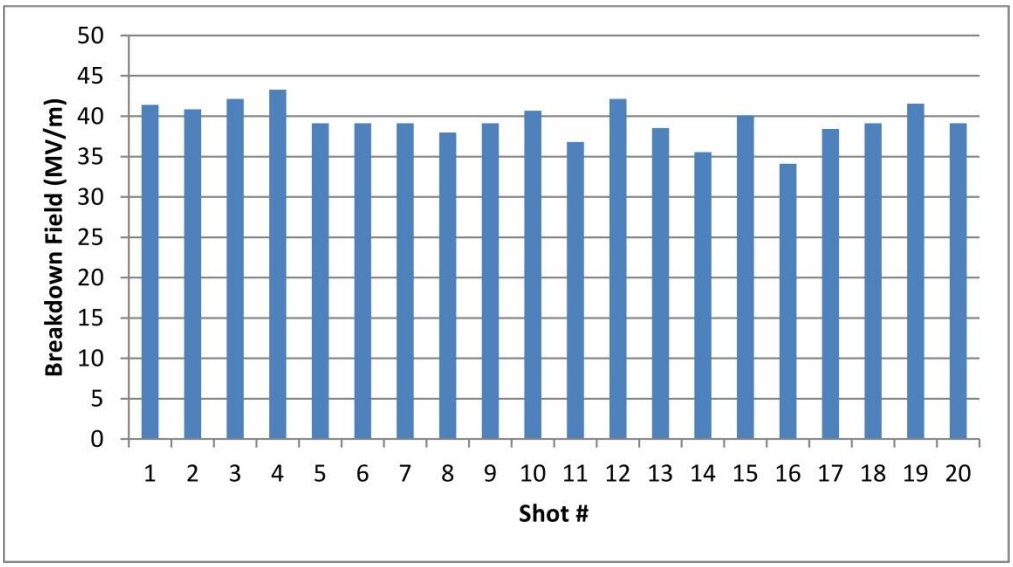

Figure 4. 17: Breakdown table of 0.508 mm (20 mil) 70% by volume BST added to a PVDF matrix in MV/m

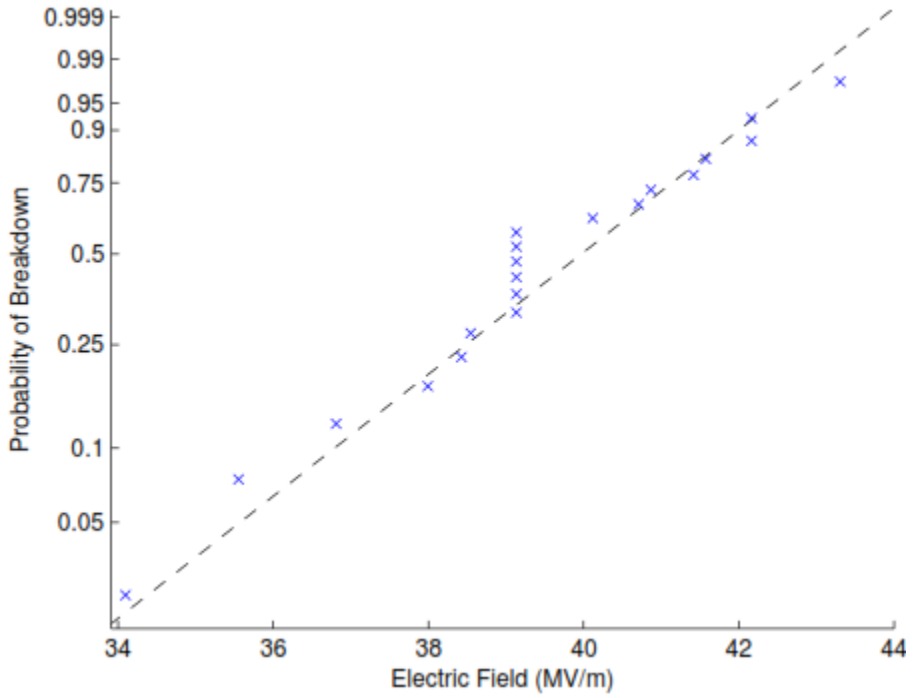

Figure 4. 18: Weibull probability breakdown plot of 0.508 mm (20 mil) 70% by volume BST added to a PVDF matrix in MV/m

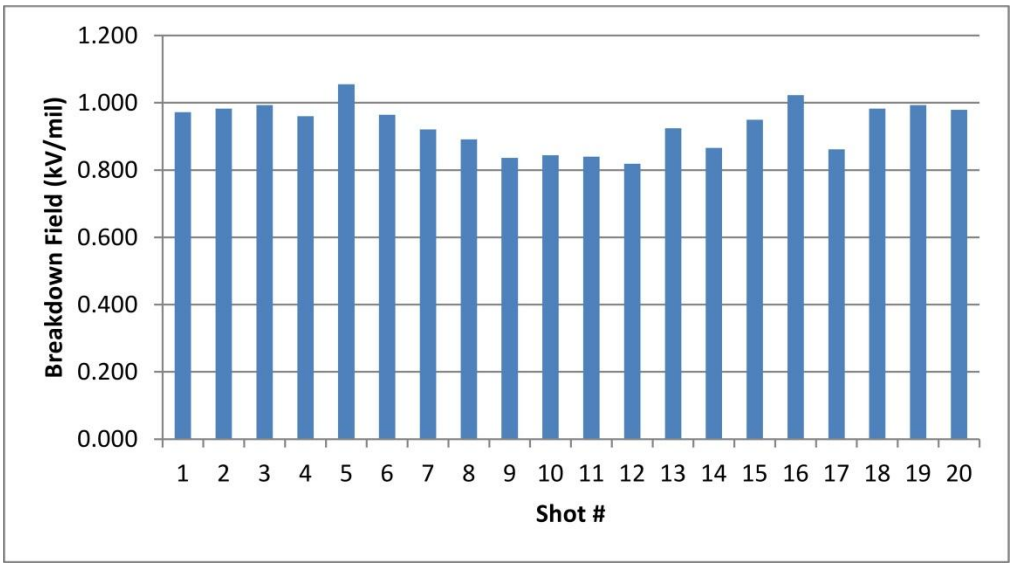

Figure 4. 19: Breakdown table of 0.508 mm (20 mil) 75% by volume BST added to a PVDF matrix in kV/mil

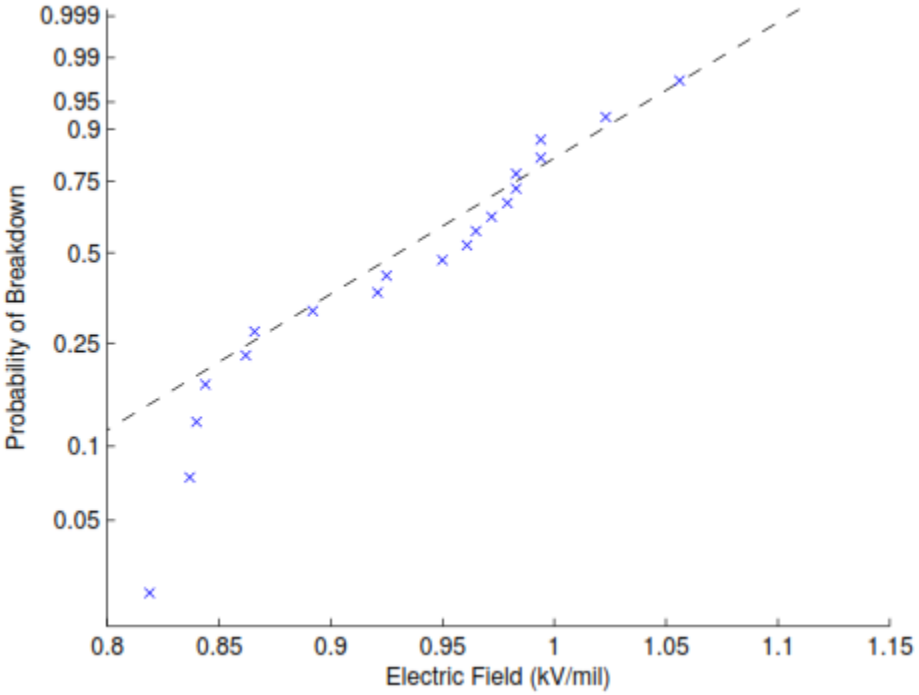

Figure 4. 20: Weibull probability breakdown plot of 0.508 mm (20 mil) 75% by volume BST added to a PVDF matrix in kV/mil

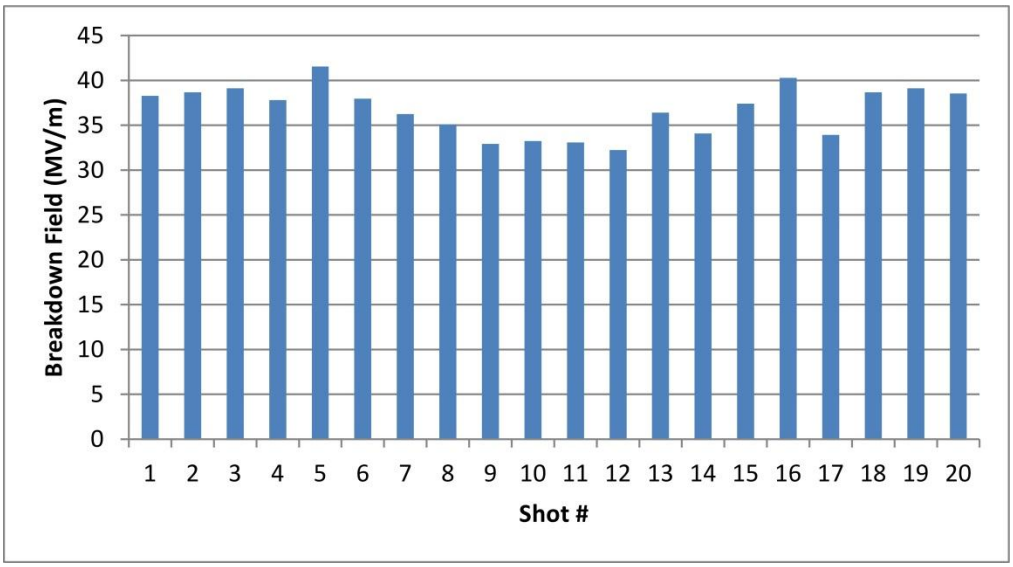

Figure 4. 21: Breakdown table of 0.508 mm (20 mil) 75% by volume BST added to a PVDF matrix in MV/m

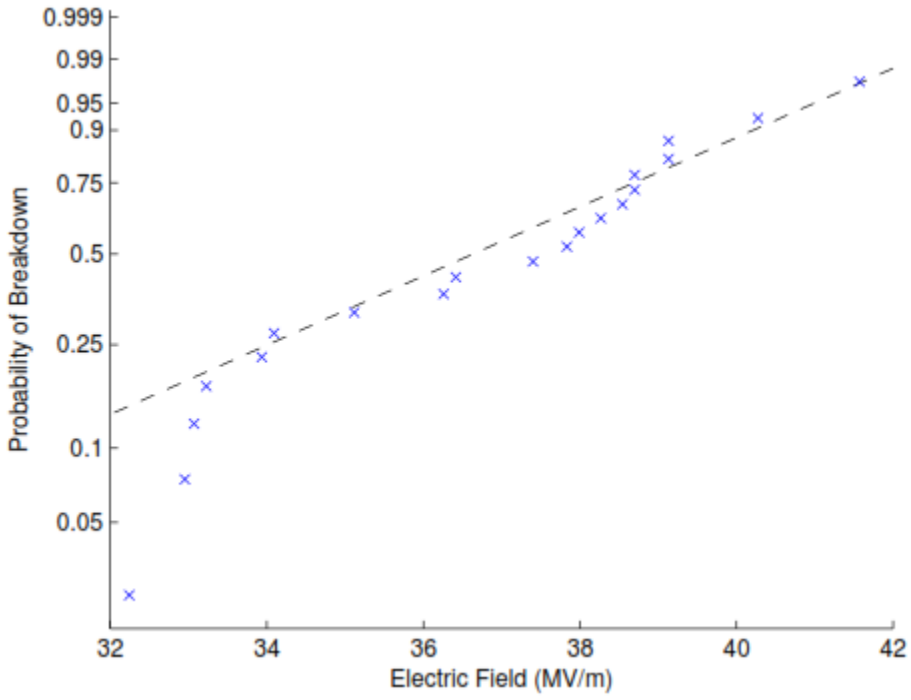

Figure 4. 22: Weibull probability breakdown plot of 0.508 mm (20 mil) 75% by volume BST added to a PVDF matrix in MV/m

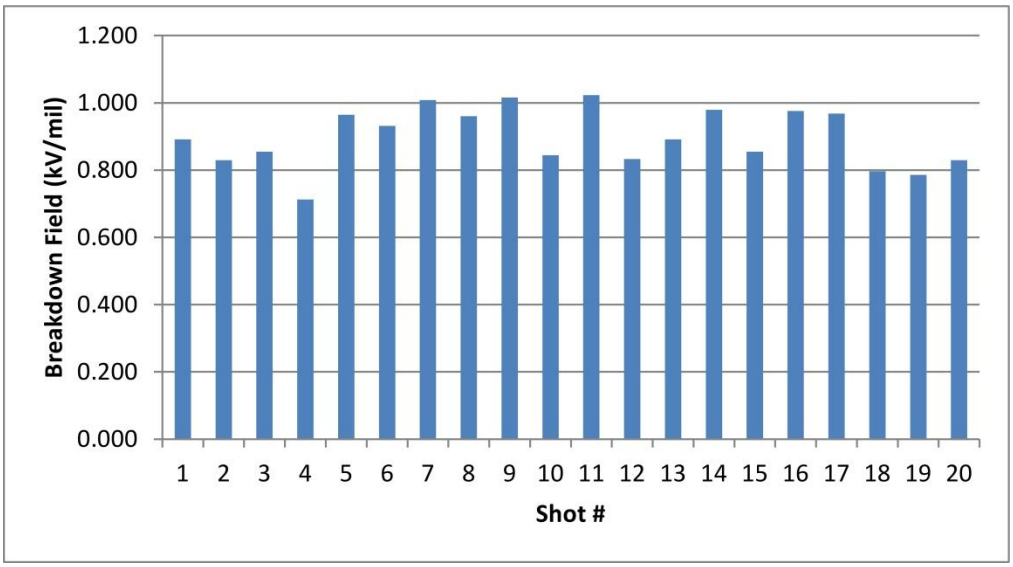

Figure 4. 23: Breakdown table of 0.508 mm (20 mil) 80% by volume BST added to a PVDF matrix in kV/mil

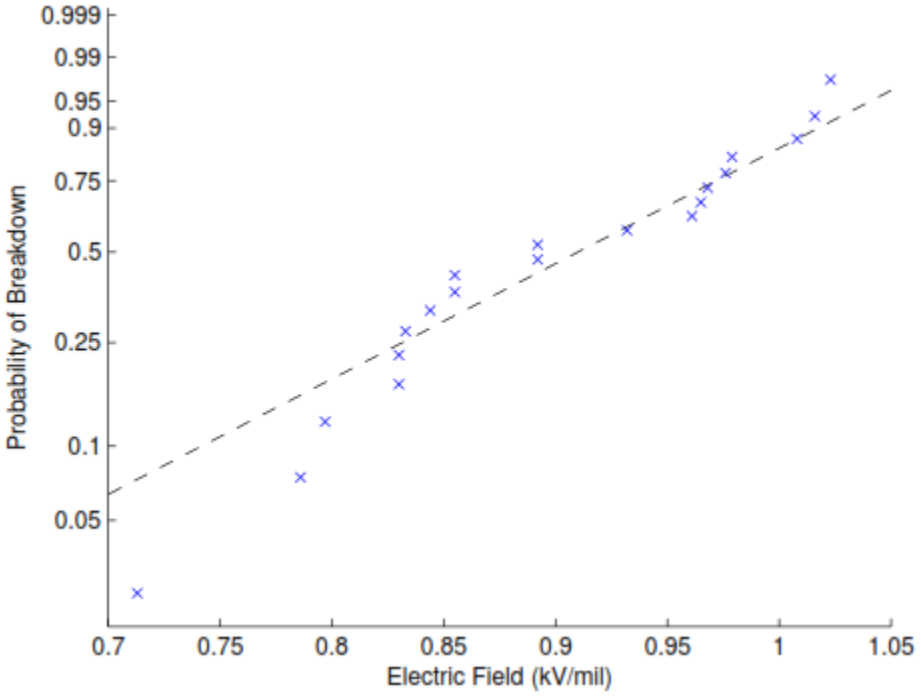

Figure 4. 24: Weibull probability breakdown plot of 0.508 mm (20 mil) 80% by volume ST added to a PVDF matrix in kV/mil

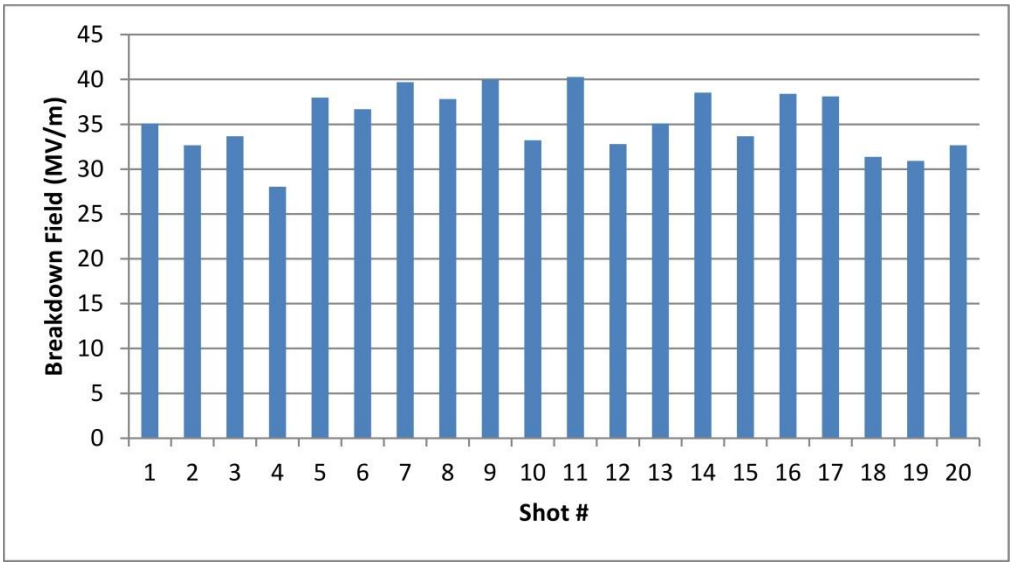

Figure 4. 25: Breakdown table of 0.508 mm (20 mil) 80% by volume BST added to a PVDF matrix in MV/m

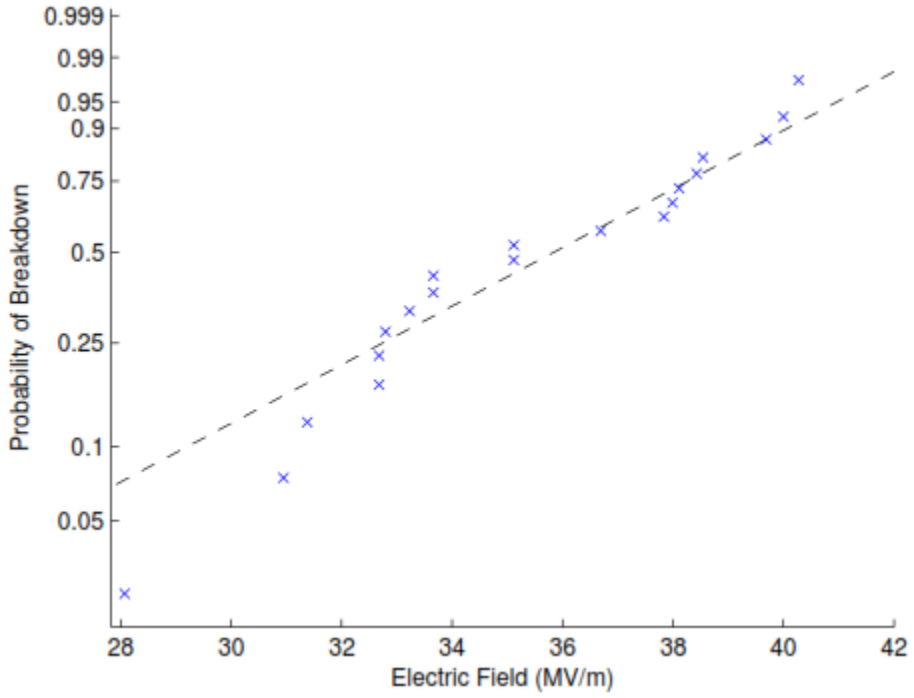

Figure 4. 26: Weibull probability breakdown plot of 0.508 mm (20 mil) 80% by volume BST added to a PVDF matrix in MV/m

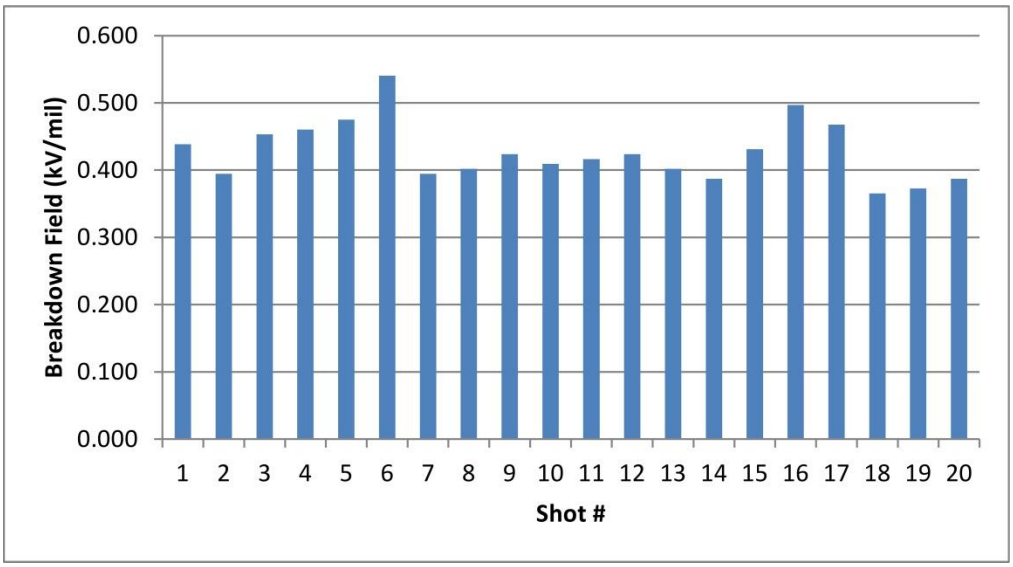

Figure 4. 27: Breakdown table of 0.508 mm (20 mil) 70% by volume BST added to a Teflon matrix in kV/mil

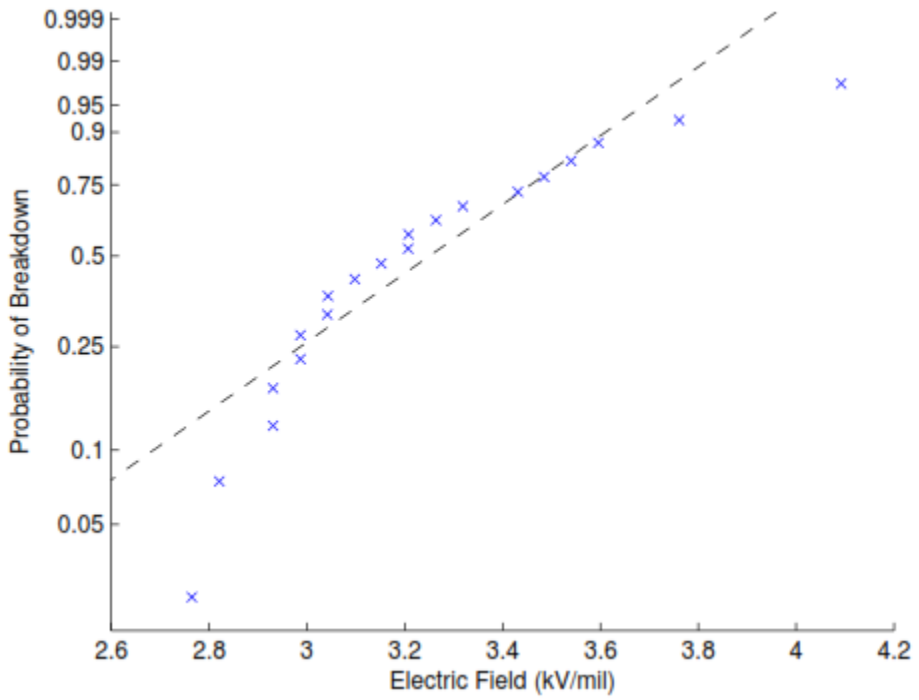

Figure 4. 28: Weibull probability breakdown plot of 0.508 mm (20 mil) 70% by volume BST added to a Teflon matrix in kV/mil

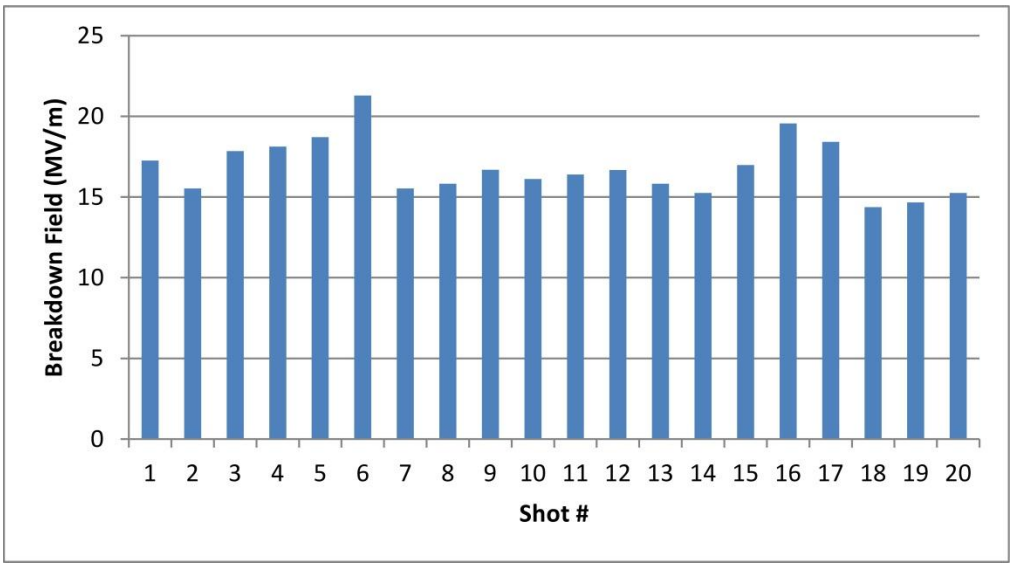

Figure 4. 29: Breakdown table of 0.508 mm (20 mil) 70% by volume BST added to a Teflon matrix in MV/m

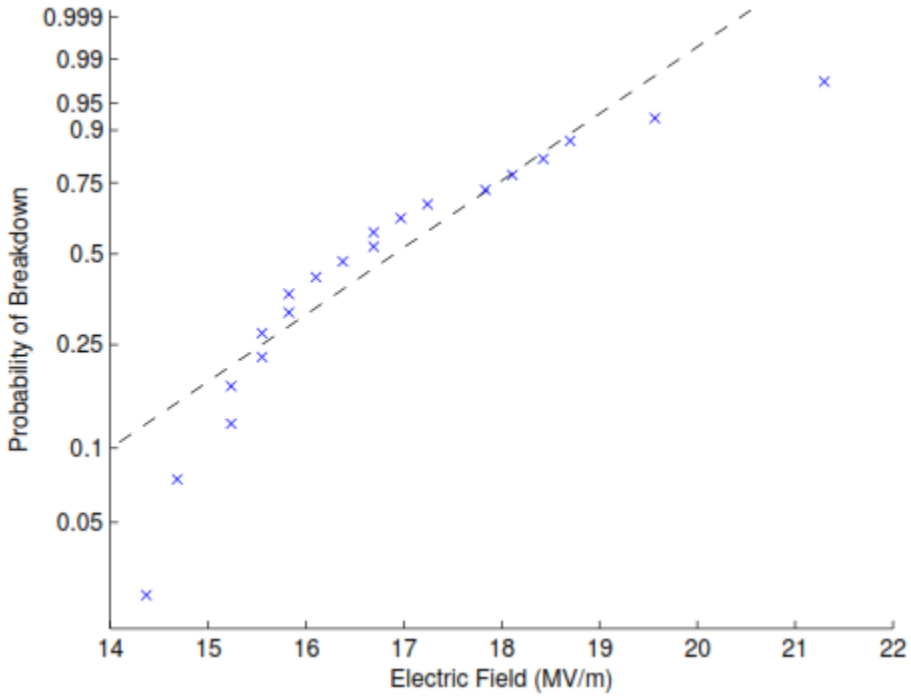

Figure 4. 30: Weibull probability breakdown plot of 0.508 mm (20 mil) 70% by volume BST added to a Teflon matrix in MV/m

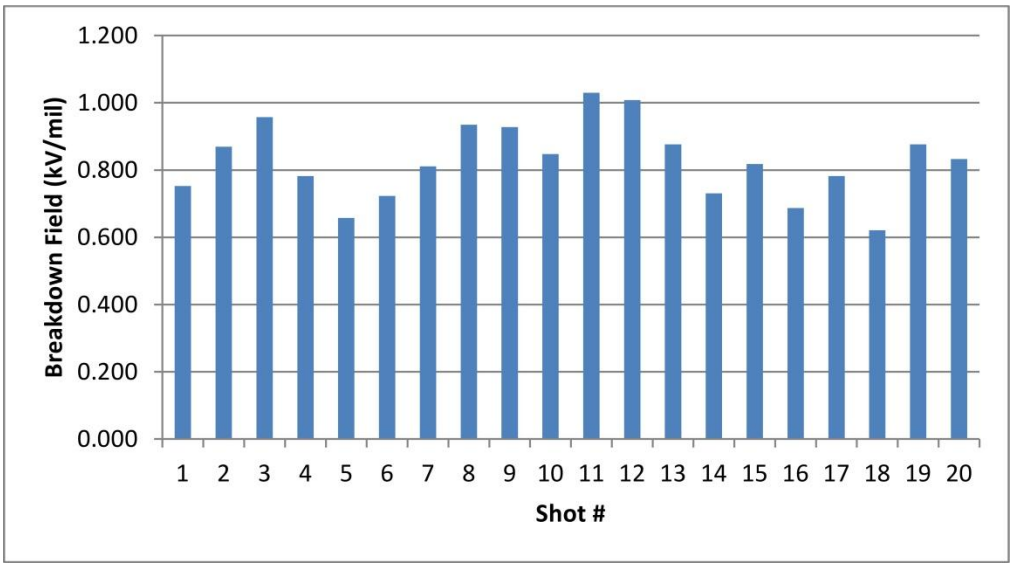

Figure 4. 31: Breakdown table of 0.508 mm (20 mil) 70% by volume ST added to a Teflon matrix in kV/mil

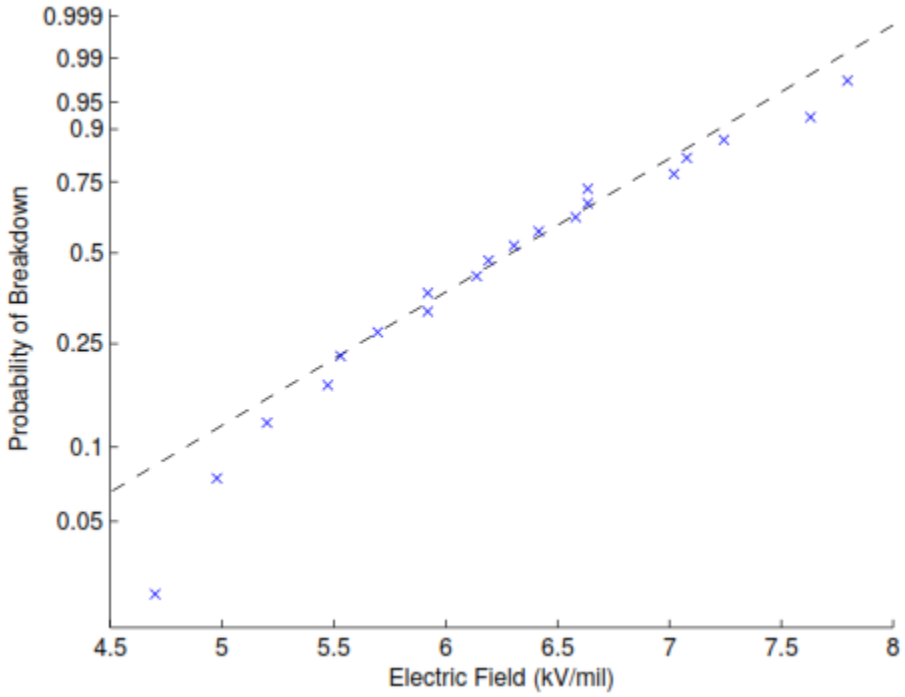

Figure 4. 32: Weibull probability breakdown plot of 0.508 mm (20 mil) 70% by volume ST added to a Teflon matrix in kV/mil

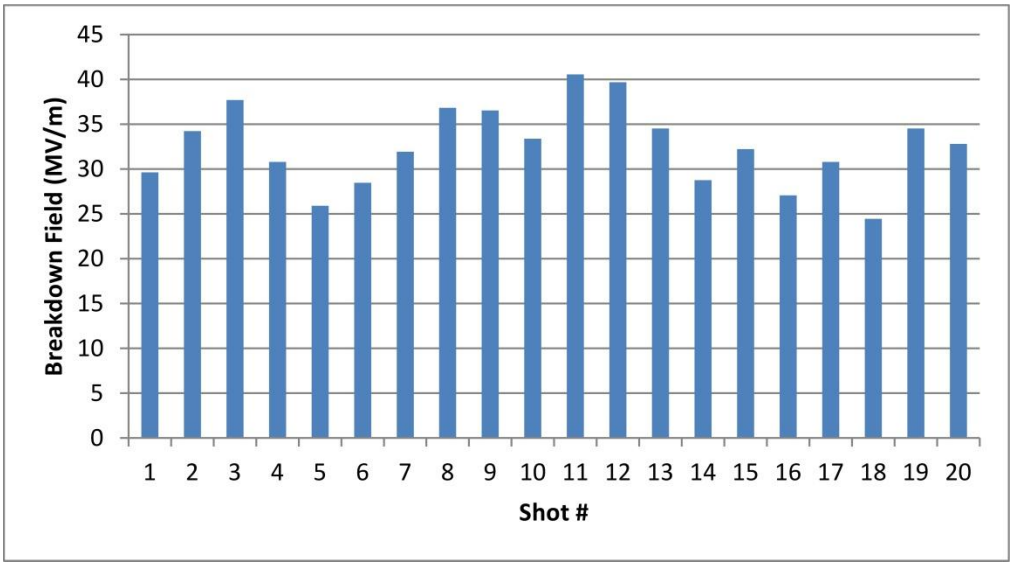

Figure 4.33: Breakdown table of 0.508 mm (20 mil) 70% by volume ST added to a Teflon matrix in MV/m

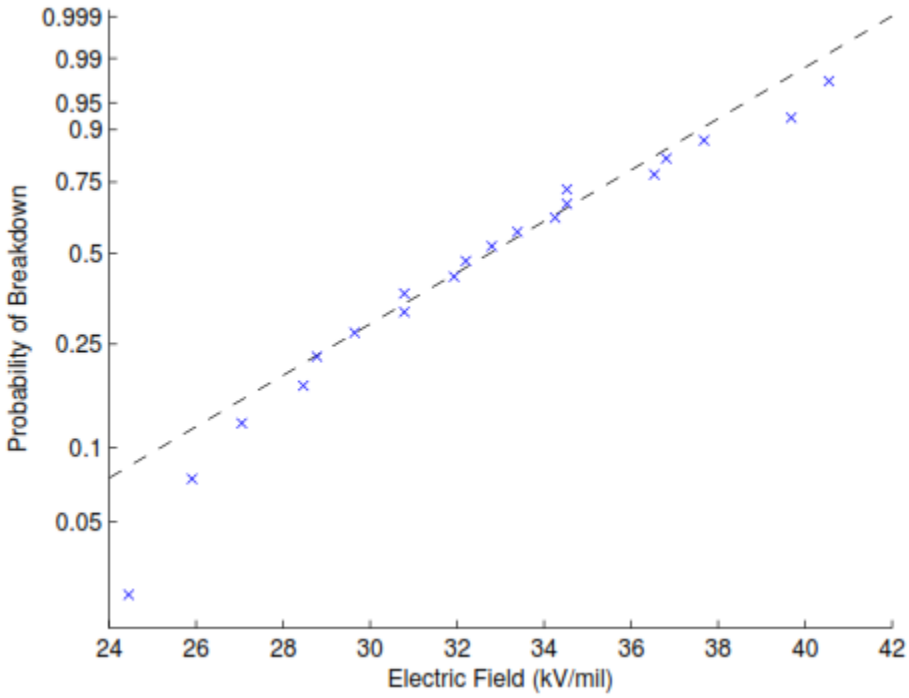

Figure 4.34: Weibull probability breakdown plot of 0.508 mm (20 mil) 70% by volume ST added to a Teflon matrix in MV/m

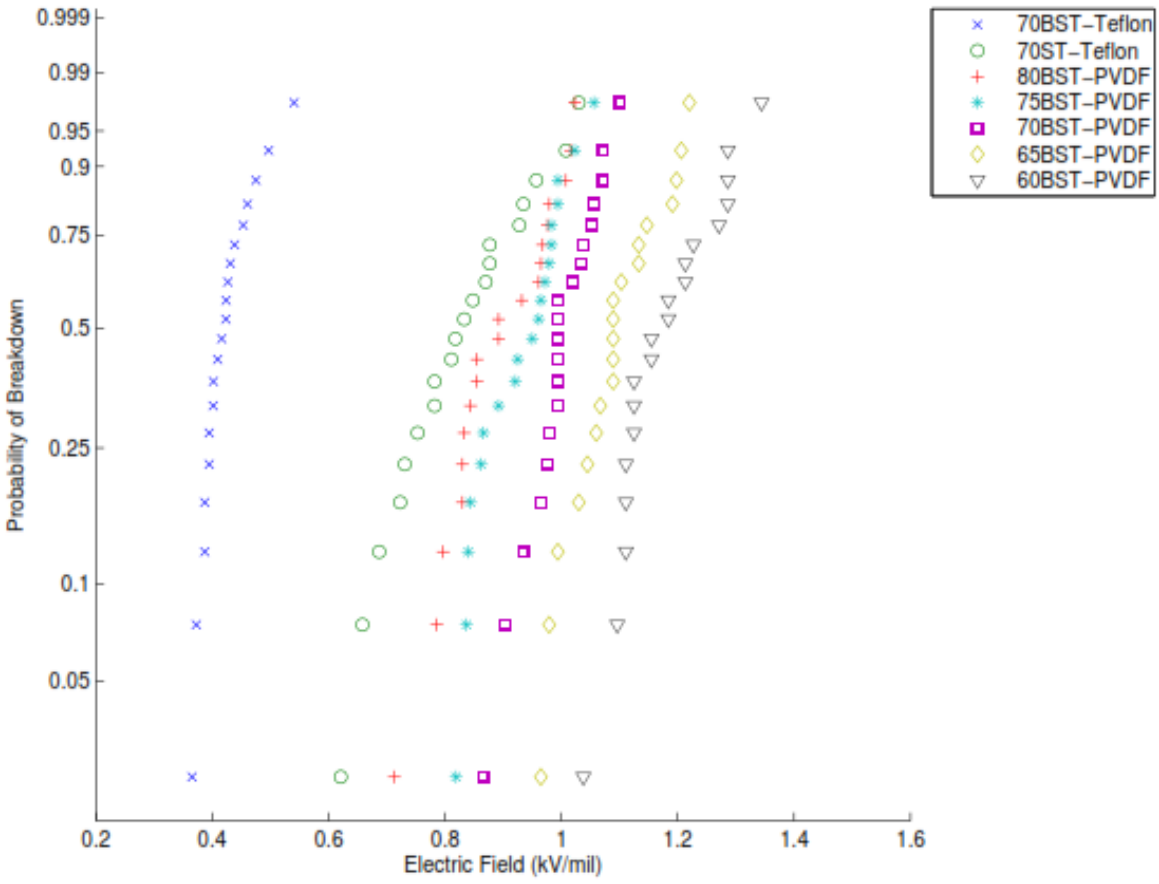

Figure 4.35: A Weibull plot if the custom dielectrics in kV/mil

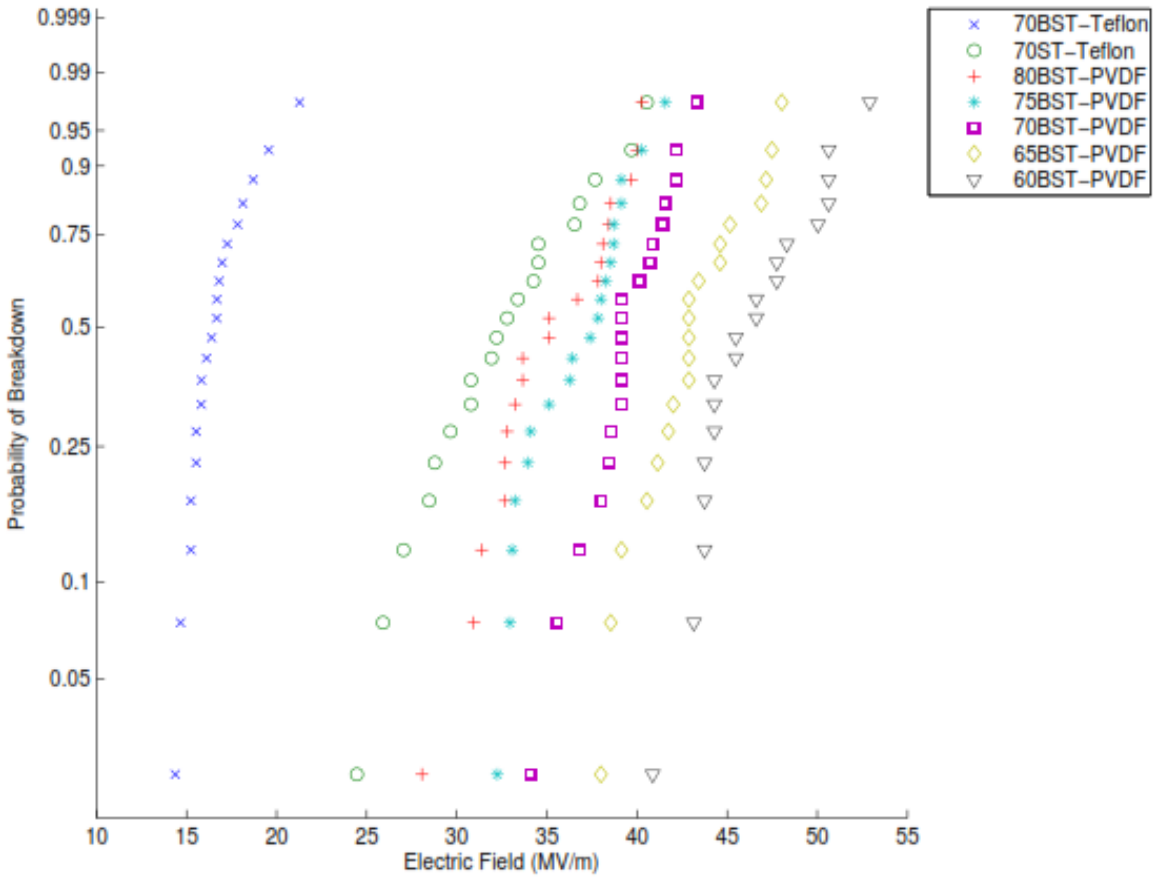

Figure 4.36: A Weibull plot if the custom dielectrics in MV/m

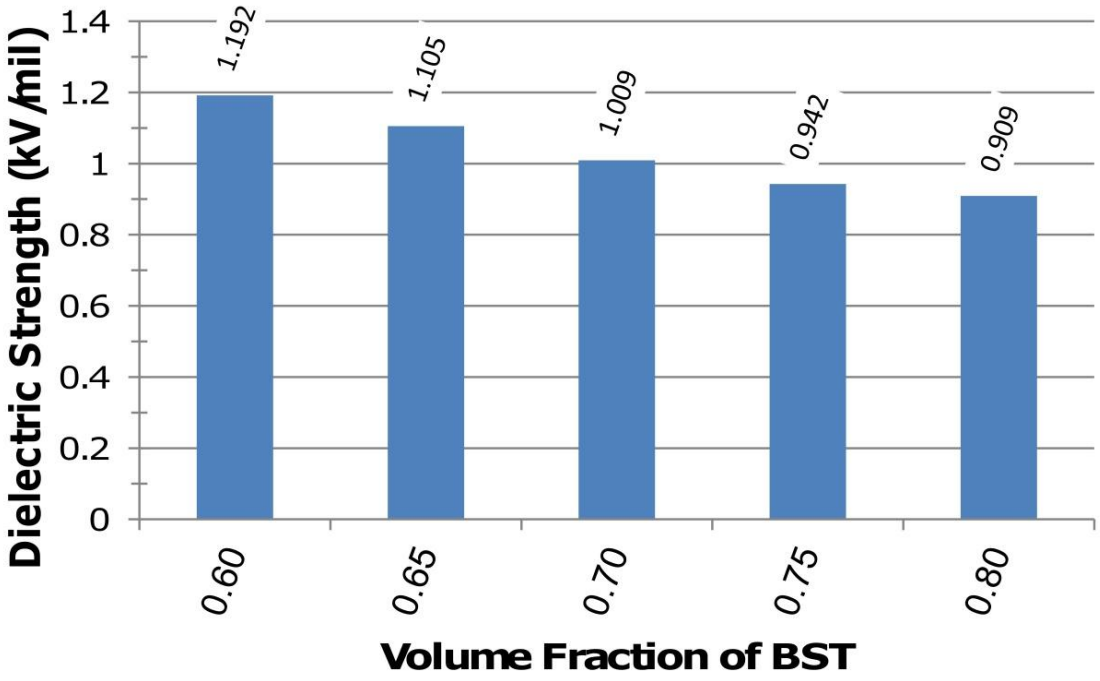

Figure 4.37: The dielectric strength versus volume fraction of added BST in a PVDF matrix

As defined in Chapter 2, the dielectric strength of a material is the electric field at which the material has a 63% probability of experiencing breakdown. The dielectric strength of the different PVDF composites are represented in Figures 4.37 and 4.38 in kV/mil and MV/m.

As the volume fraction of the filler material increases, the experimental results show an approximately linear decrease in the dielectric strength. This occurs because the dielectric strength of the filler material is inherently not as high as the PVDF. This decrease is also compounded by the fact that the dielectric constant of the filler material is different than the PVDF, which essentially increases the dielectric field at the interfaces of the materials because of the field effect as described in Chapter 2.

The dielectric strength of the Teflon composites are represented in Figure 4.39 and 4.40 in kV/mil and MV/m. The data shows that the BST composite has a higher dielectric strength than the ST composite. This may be a result of the intrinsically higher dielectric strength of the bare BST ceramic than that of the ST ceramic. The BST filler material does have a higher dielectric constant which suggests that the BST composite would also have a higher dielectric constant. The large difference could also be because of the differences in the material interactions. Such differences could include the material's ability to bond to itself, and therefore exclude the particles, or the material's ability to bond to the particles themselves.

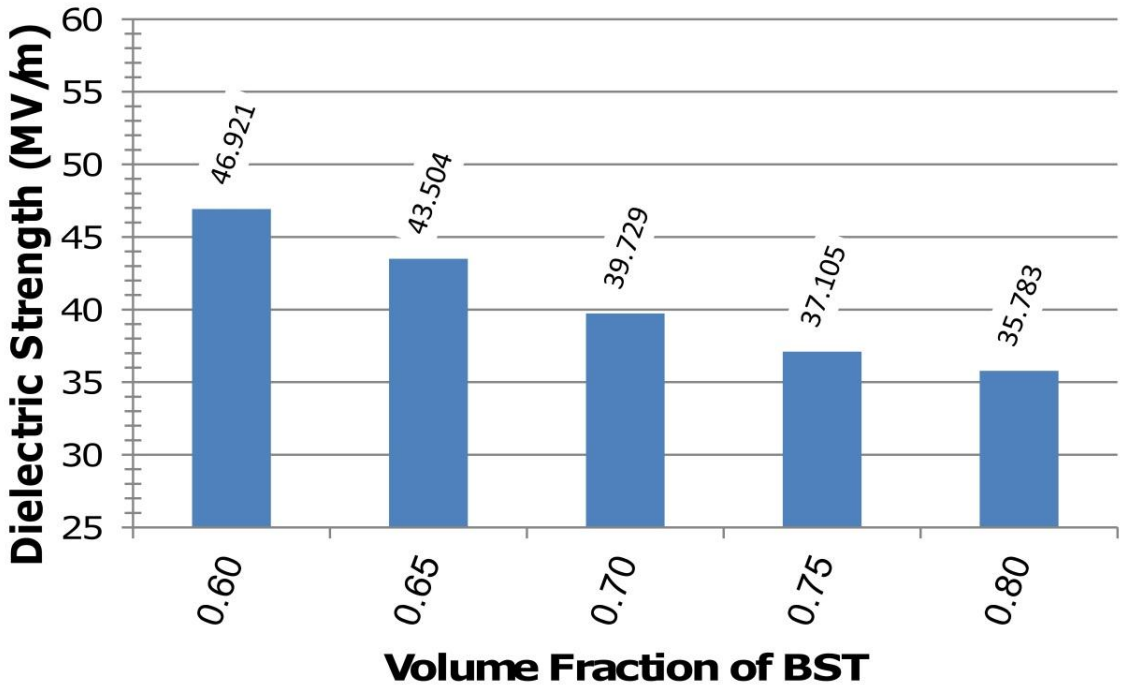

Figure 4.38: The dielectric strength versus volume fraction of added BST in a PVDF matrix.

4.4.2 *Dielectric Strength of Conventional Plastics and Composites*

The breakdown tests were also completed for Nylon, Mylar, Teflon, PVDF, and HDPE to generate a comparison for the new composites. The breakdown values and Weibull plots were generated for all the different commercial dielectrics, which are represented in Figures 4.41 through 4.88.

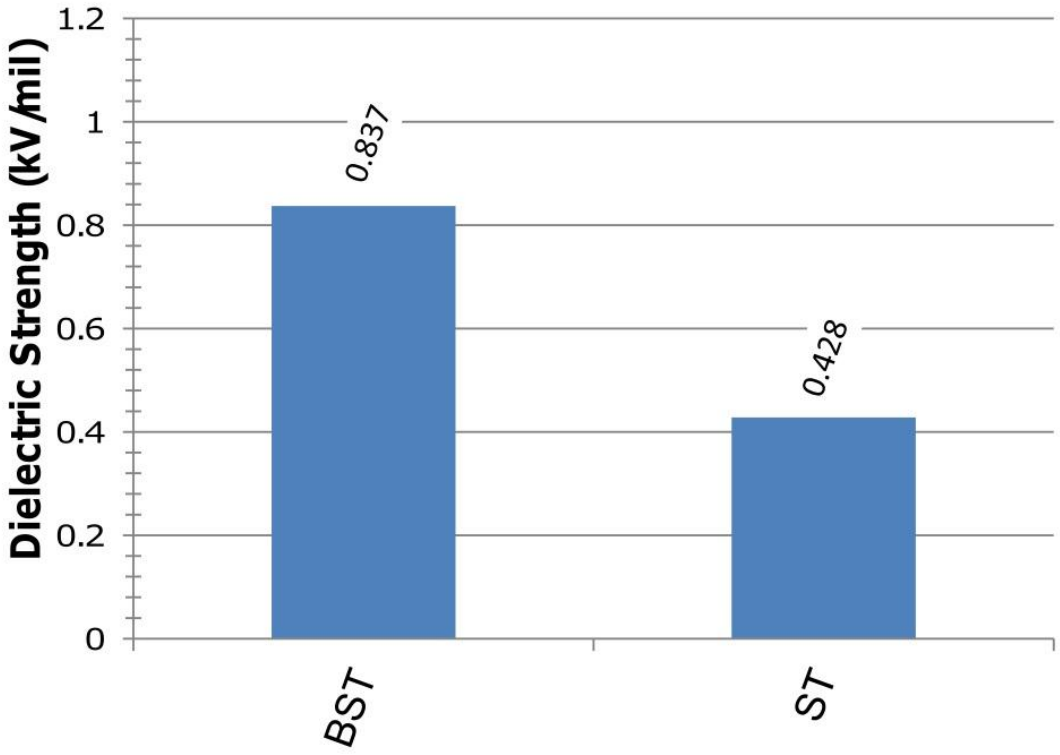

Figure 4.39: The dielectric strength, 63% probability of breakdown, of ST and BST composites in a Teflon matrix will 70% by volume in MV/m

All of the commercial material used consisted of the bare material and did not have an adhesive or any other backing material. The thicknesses that were chosen for this study

were based on availability. There were thicker Kapton samples available but the breakdown test setup used in this study could not generate a voltage high enough to consistently breakdown the material. Samples were cut out of the sheet material and cleaned with Isopropyl alcohol. This comparison shows that the composite materials have a lower dielectric strength than the tested conventional plastics. A comparison of the dielectric strengths of the custom dielectrics generated in this study to commercial dielectrics is represented the graph in kV/mil in Figure 4.95 and in MV/m in Figure 4.96. A Weibull breakdown plot of the custom and commercial dielectric used in this study was generated in kV/mil in Figure 4.35 and in MV/m in Figure 4.36. A Weibull breakdown plot comparing the custom Teflon composites to commercial Teflon in kV/mil is represented in Figure 4.91 and is represented in MV/m in Figure 4.92. A Weibull breakdown plot comparing the PVDF composites to commercial Teflon in kV/mil is represented in Figure 4.93 and is represented and is represented in MV/m is Figure 4.94.

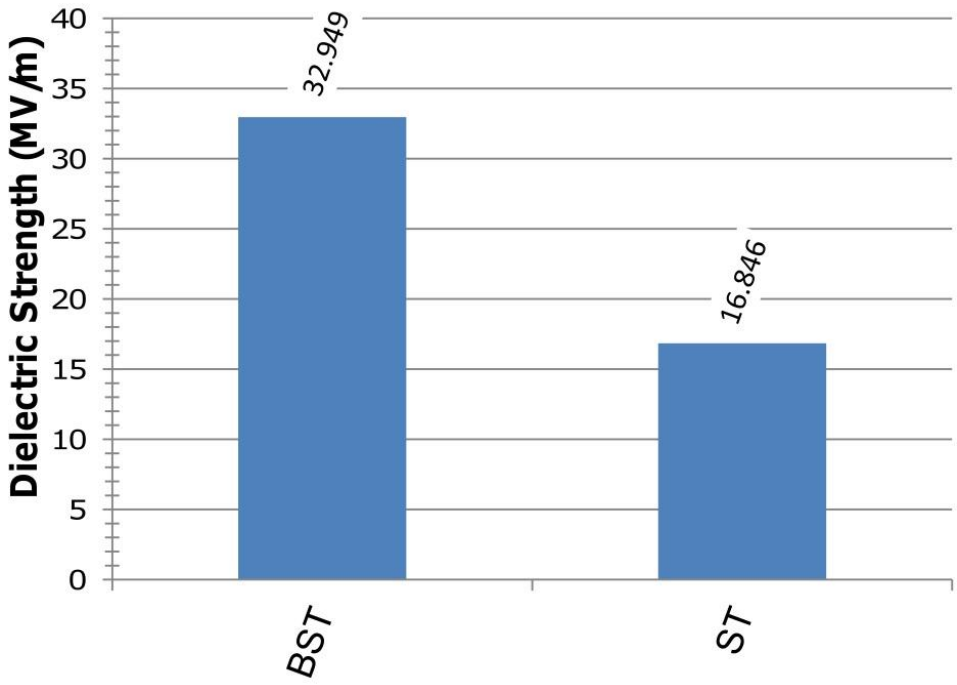

Figure 4. 40: The dielectric strength, 63% probability of breakdown, of ST and BST composites in a Teflon matrix will 70% by volume in MV/m

There was an unexpected result when the dielectric strengths of the composites were compared to the dielectric strengths of the bare plastics. Bare Teflon has twice the dielectric strength compared to bare PVDF, but the composites do not reflect this trend. The 70% BST filled Teflon had approximately 20% lower dielectric strength compared to the same PVDF material. As mentioned in the previous section, this trend could be because material interactions will be different between the different materials. Because of the different material interactions, the Teflon composites might not have mixed as well as the PVDF composites.

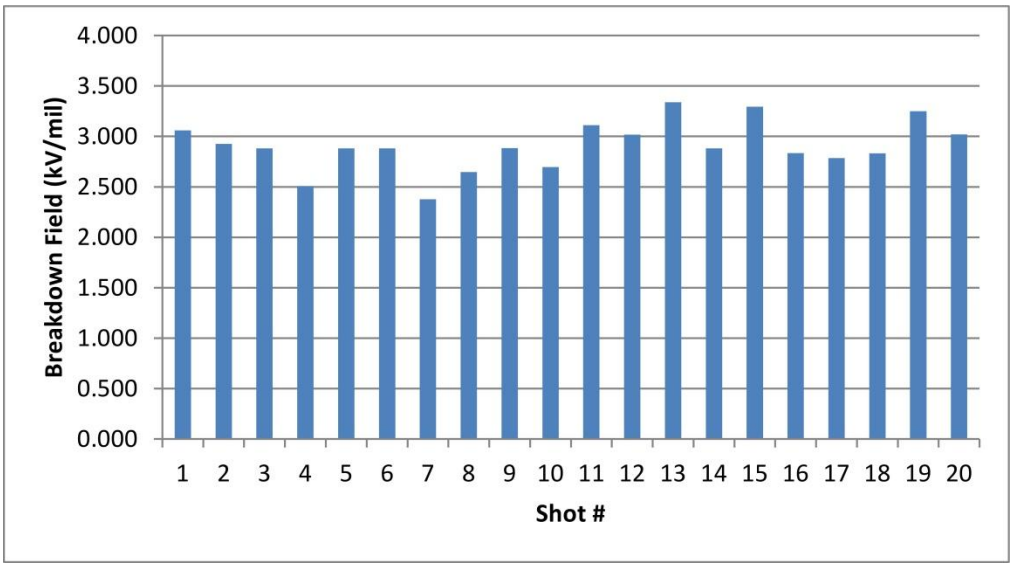

Figure 4. 41: Breakdown table of 0.508 mm (20 mil) HDPE in kV/mil

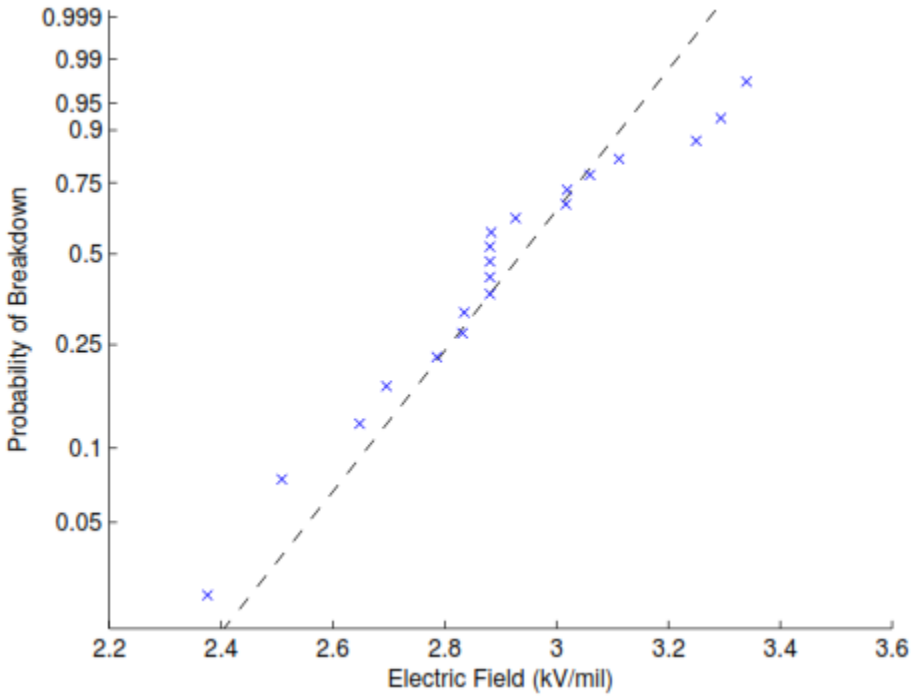

Figure 4. 42: Weibull probability breakdown plot of 0.508 mm (20 mil) HDPE in kV/mil

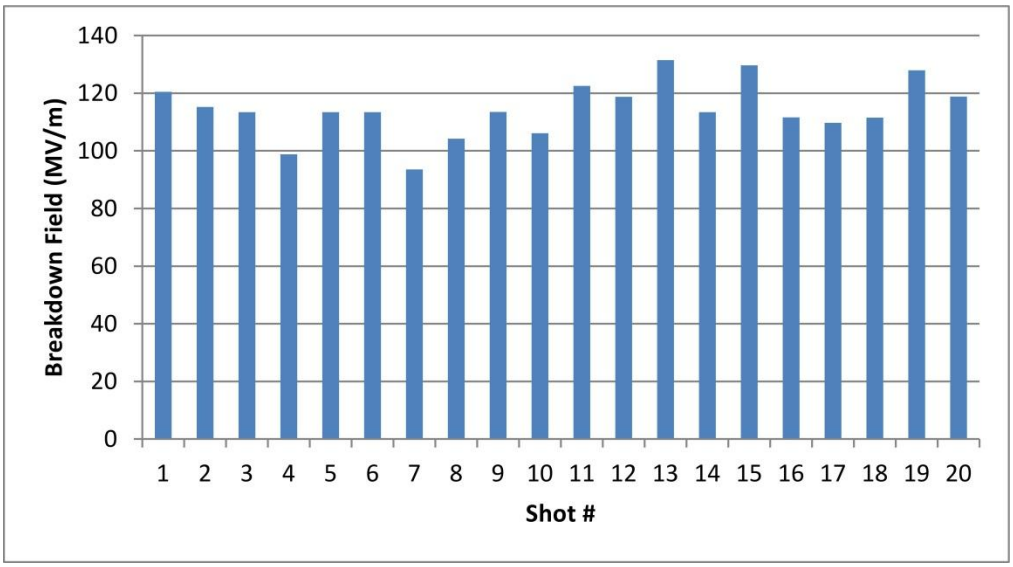

Figure 4. 43: Breakdown table of 0.508 mm (20 mil) HDPE in MV/m

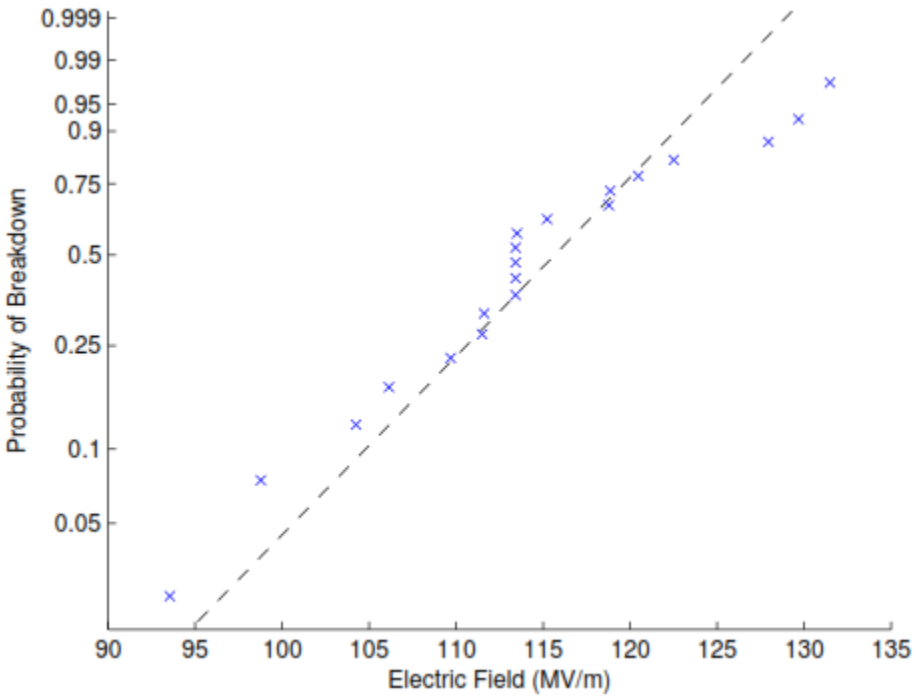

Figure 4. 44: Weibull probability breakdown plot of 0.508 mm (20 mil) HDPE in MV/m

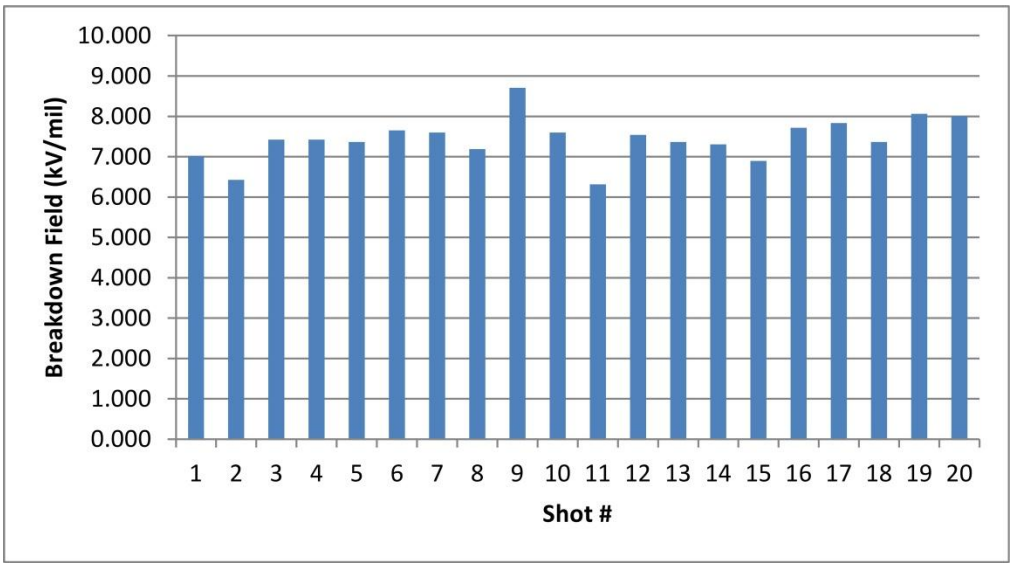

Figure 4. 45: Breakdown table of 0.127 mm (5 mil) Kapton in kV/mil

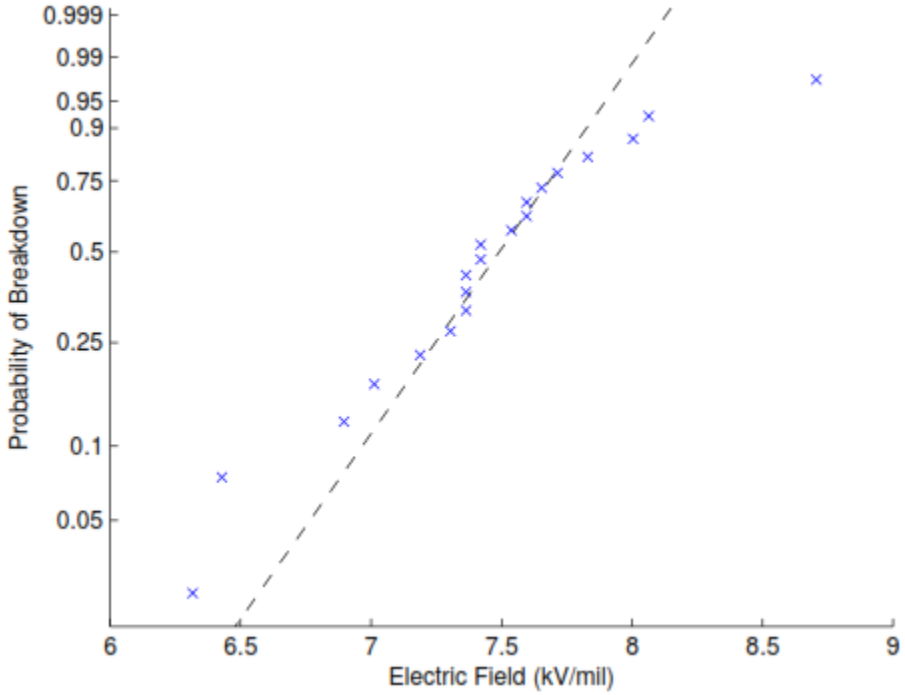

Figure 4. 46: Weibull probability breakdown plot of 0.127 mm (5 mil) Kapton in kV/mil

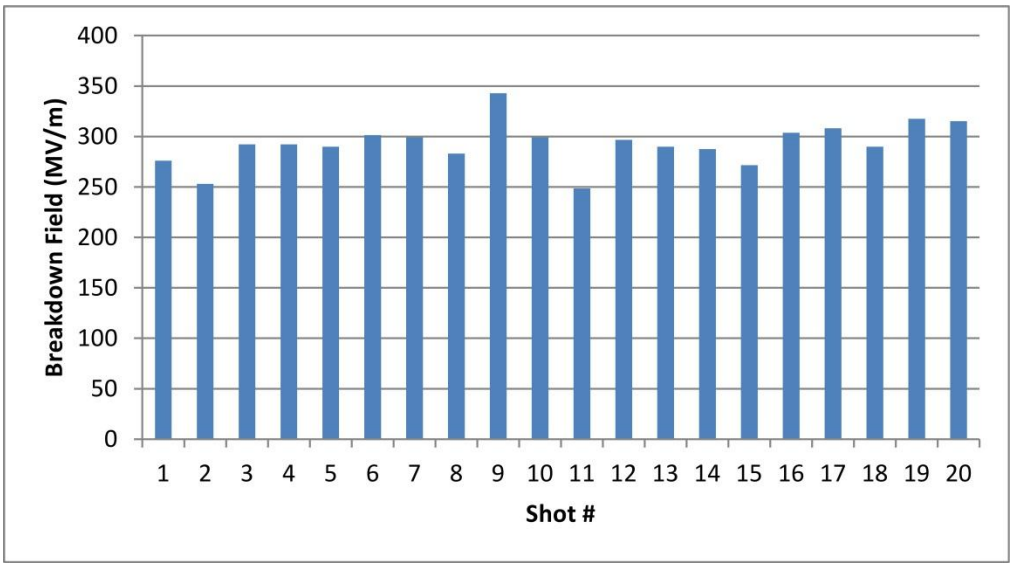

Figure 4. 47: Breakdown table of 0.127 mm (5 mil) Kapton in MV/m

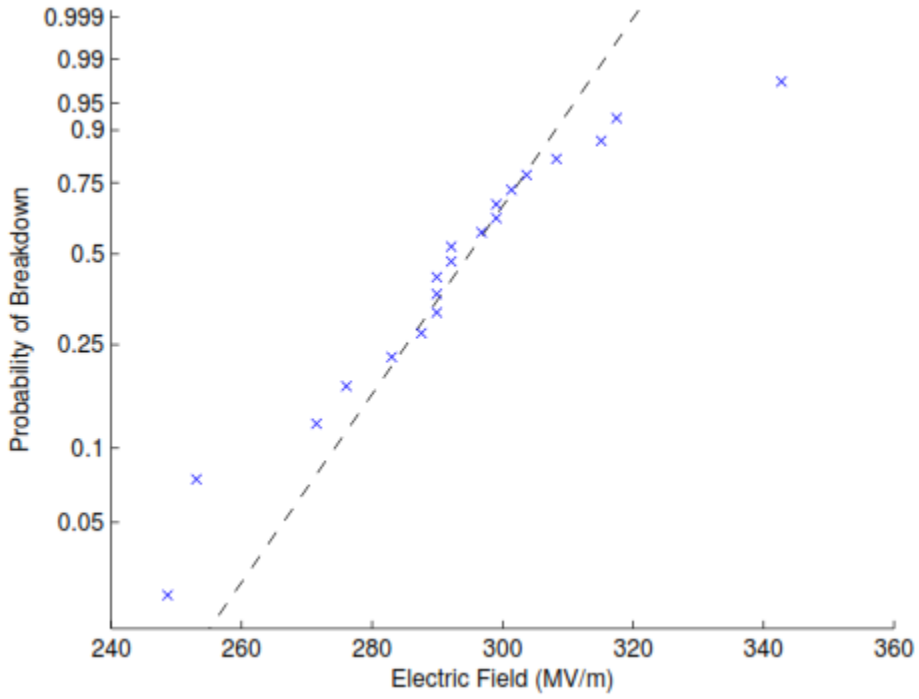

Figure 4. 48: Weibull probability breakdown plot of 0.127 mm (5 mil) Kapton in MV/m

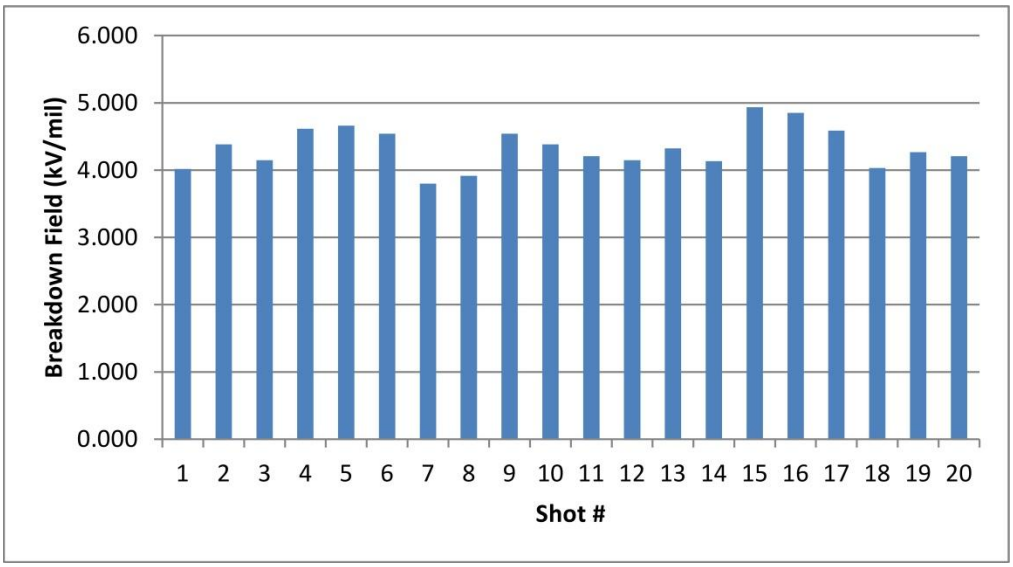

Figure 4. 49: Breakdown table of 0.127 mm (5 mil) Mylar in kV/mil

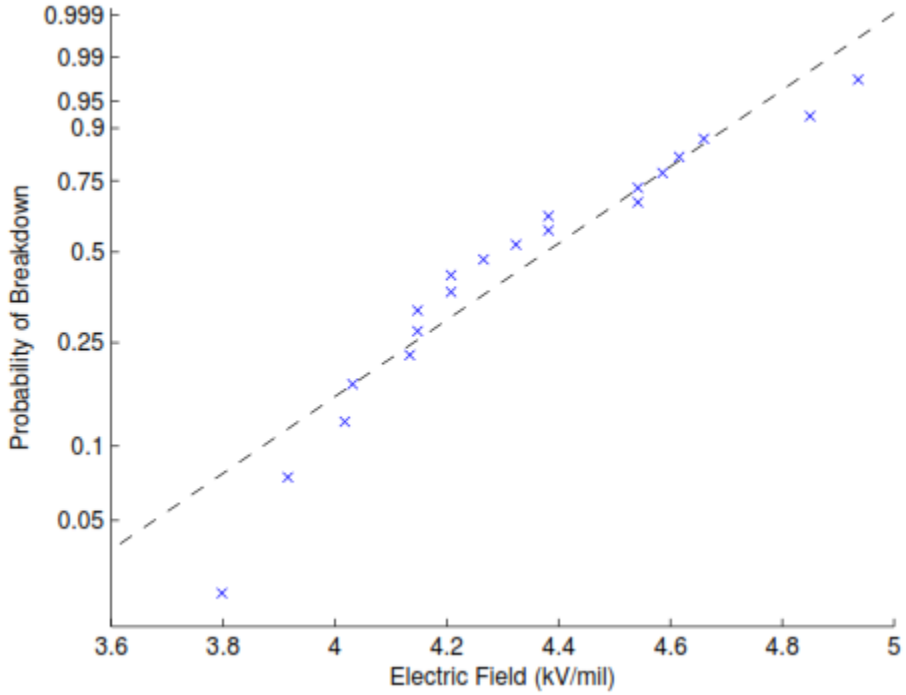

Figure 4. 50: Weibull probability breakdown plot of 0.127 mm (5 mil) Mylar in kV/mil

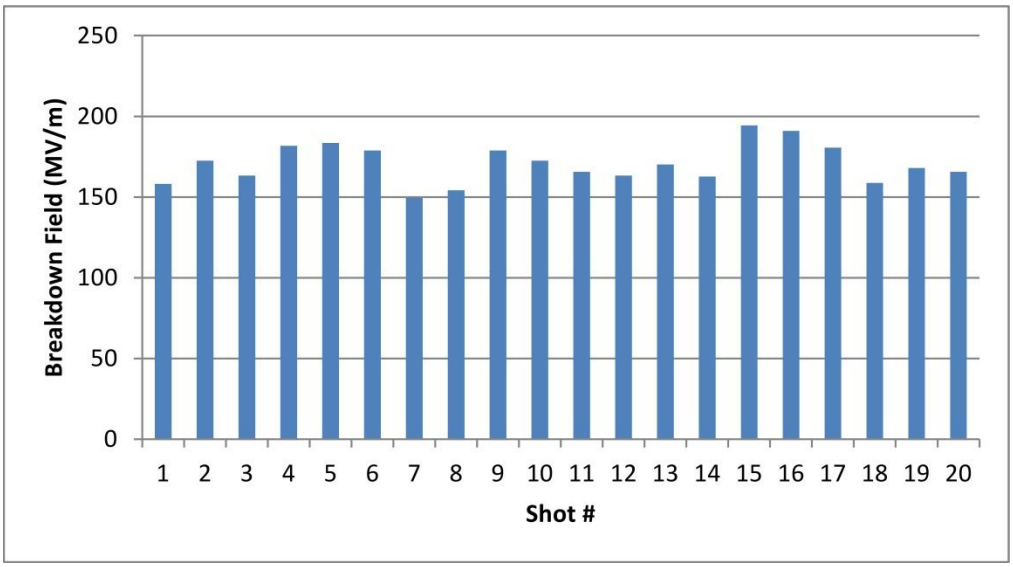

Figure 4. 51: Breakdown table of 0.127 mm (5 mil) Mylar in MV/m

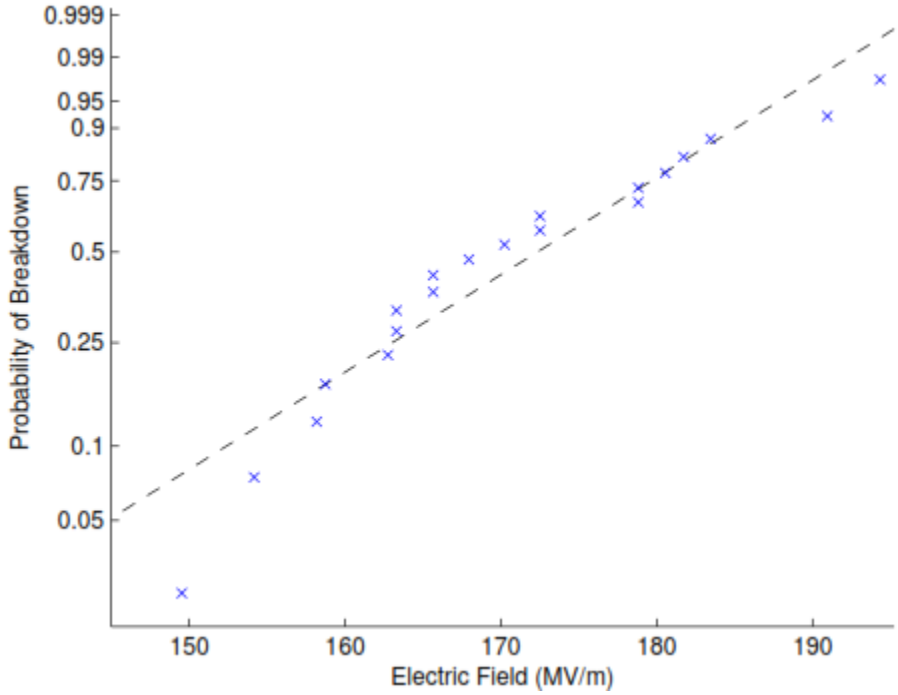

Figure 4. 52: Weibull probability breakdown plot of 0.127 mm (5 mil) Mylar in MV/m

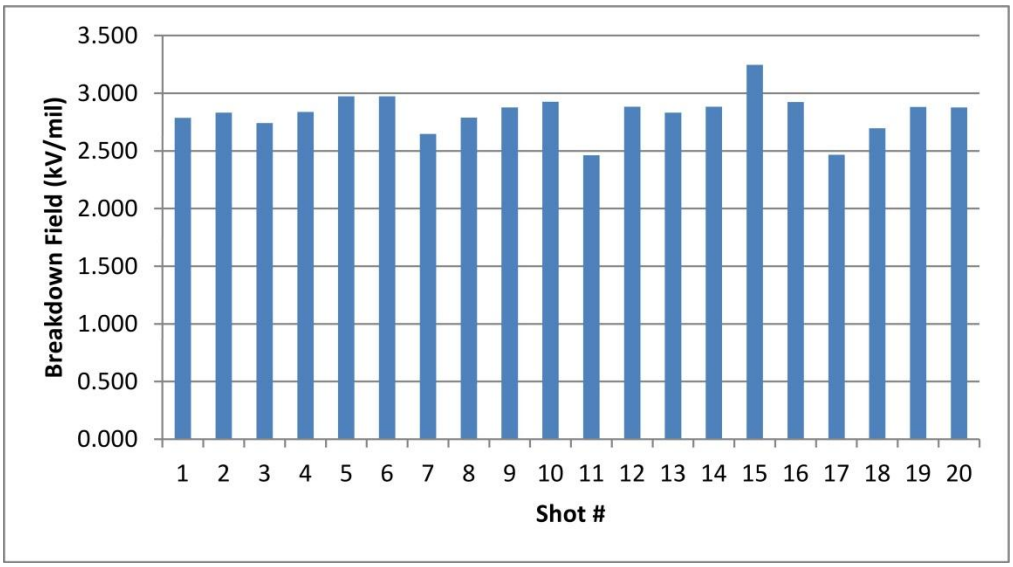

Figure 4. 53: Breakdown table of 0.508 mm (20 mil) Mylar in kV/mil

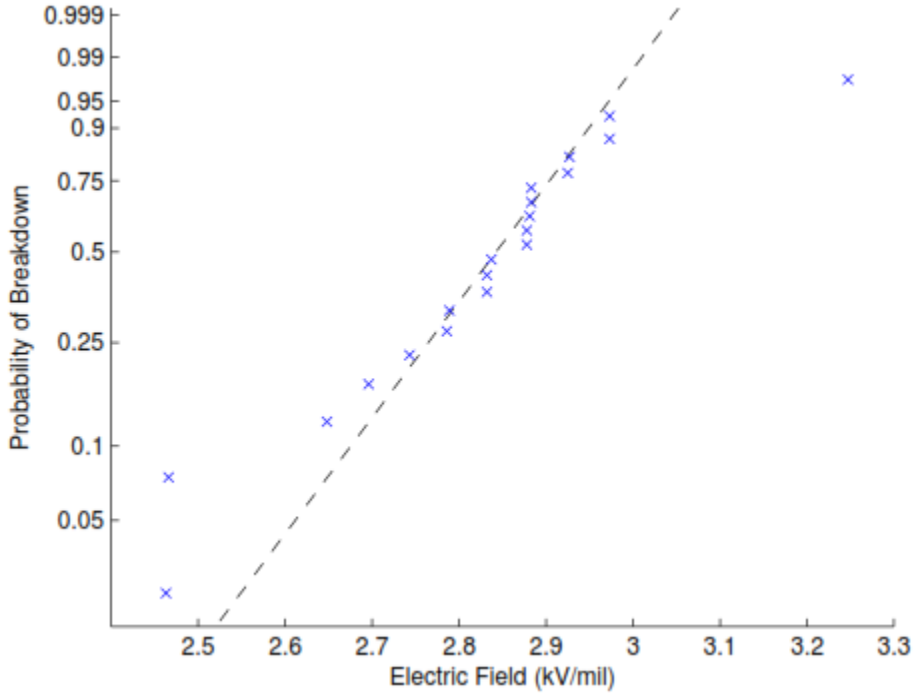

Figure 4. 54: Weibull probability breakdown plot of 0.508 mm (20 mil) Mylar in kV/mil

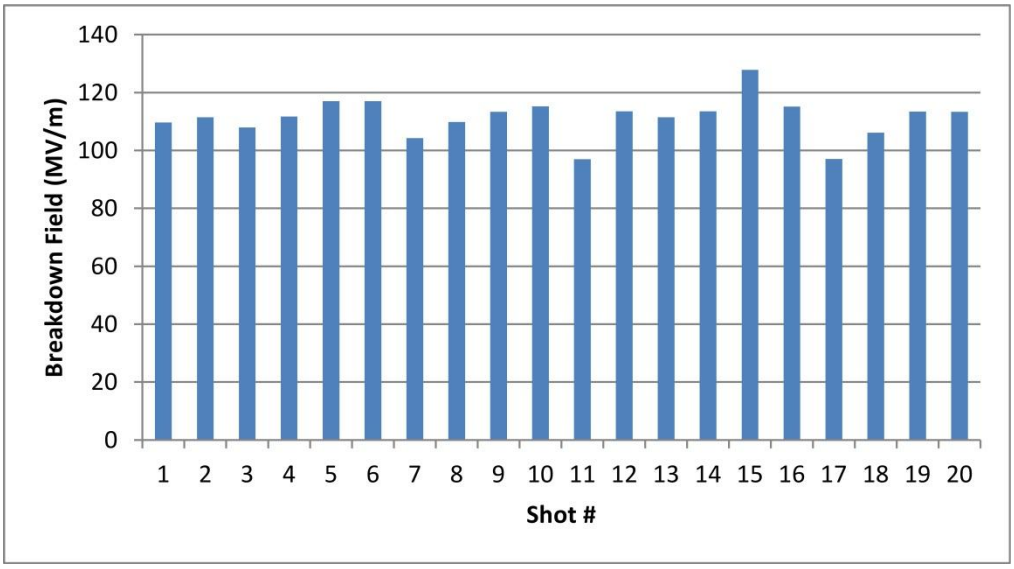

Figure 4. 55: Breakdown table of 0.508 mm (20 mil) Mylar in MV/m

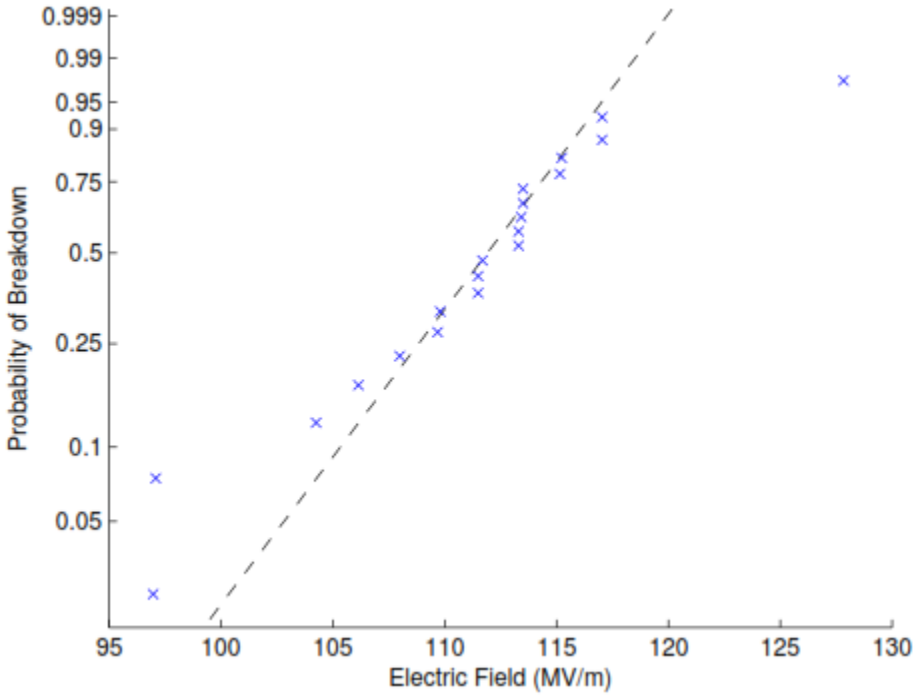

Figure 4. 56: Weibull probability breakdown plot of 0.508 mm (20 mil) Mylar in MV/m

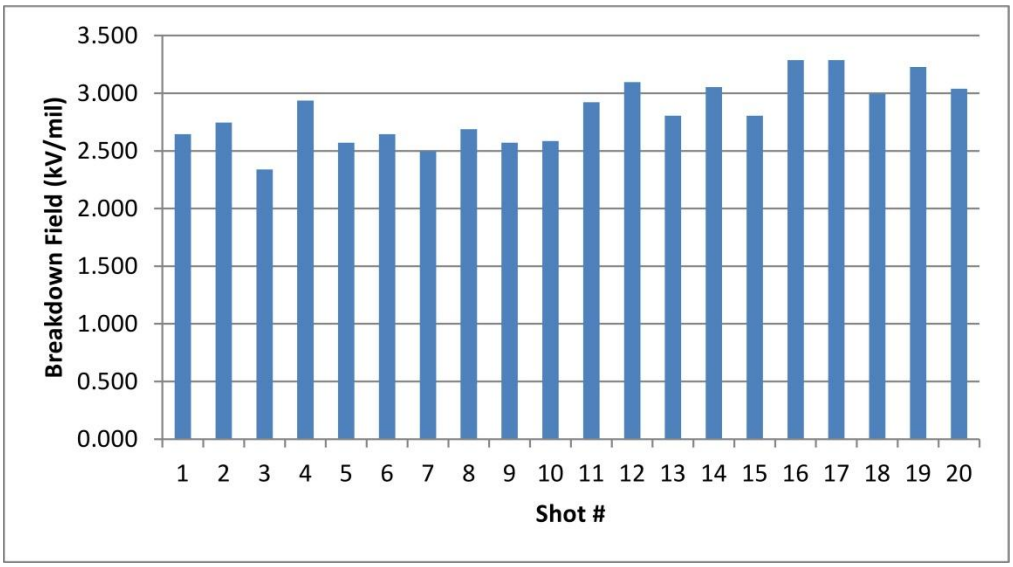

Figure 4. 57: Breakdown table of 0.254 mm (10 mil) Nylon in kV/mil

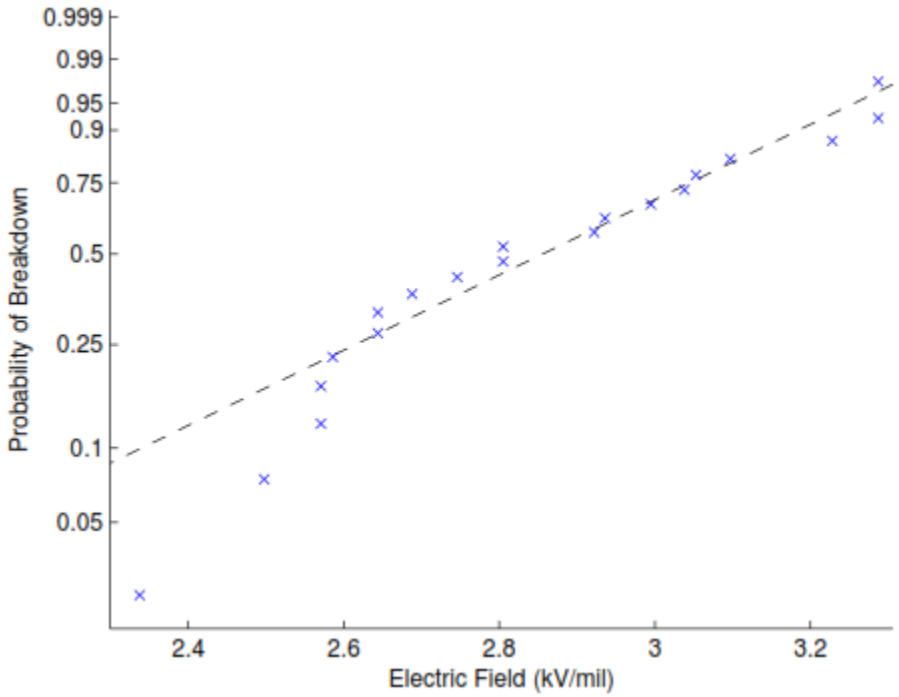

Figure 4. 58: Weibull probability breakdown plot of 0.254 mm (10 mil) Nylon in kV/mil

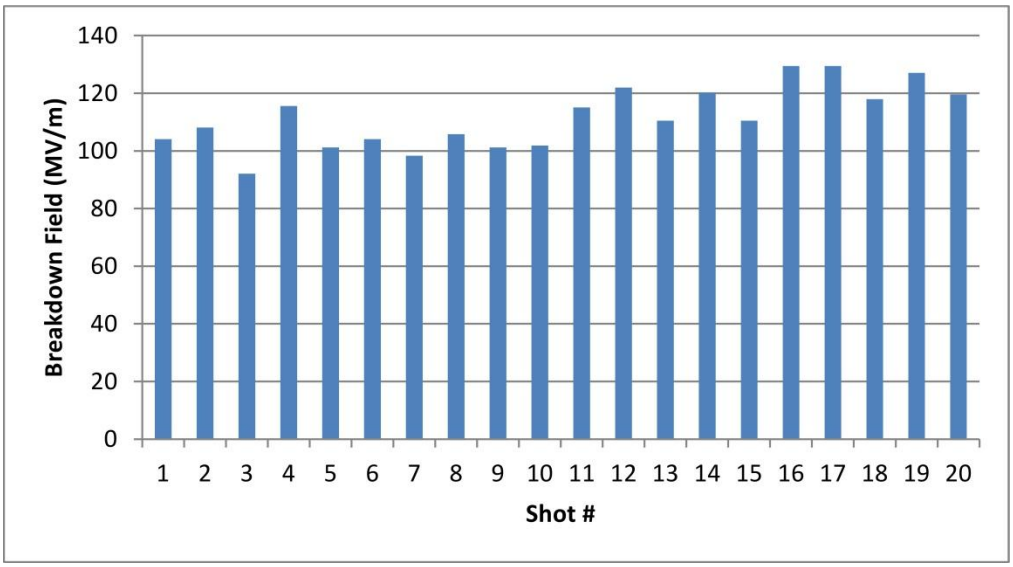

Figure 4. 59: Breakdown table of 0.254 mm (10 mil) Nylon in MV/m

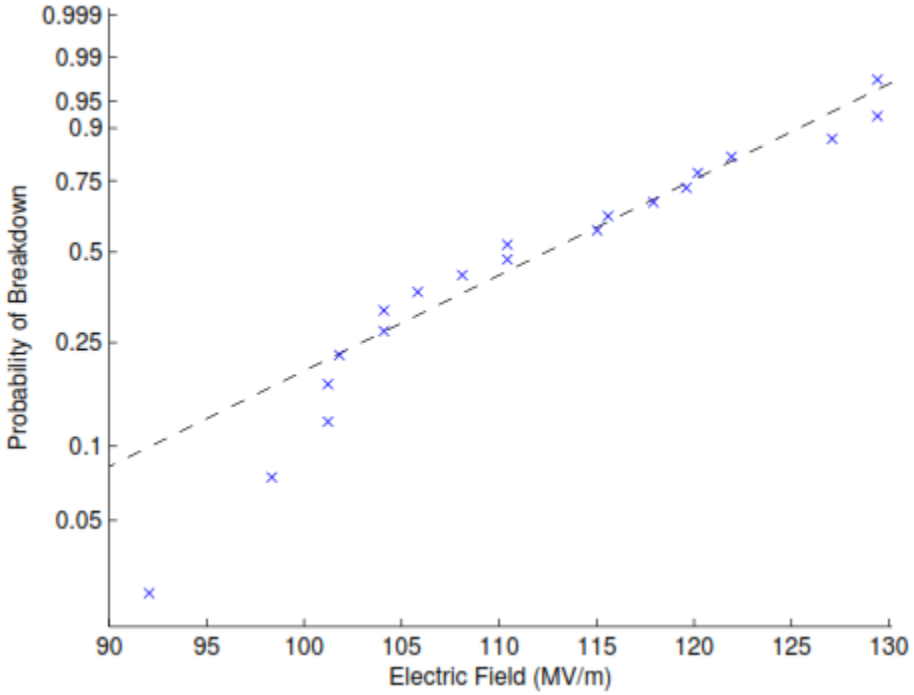

Figure 4. 60: Weibull probability breakdown plot of 0.254 mm (10 mil) Nylon in MV/m

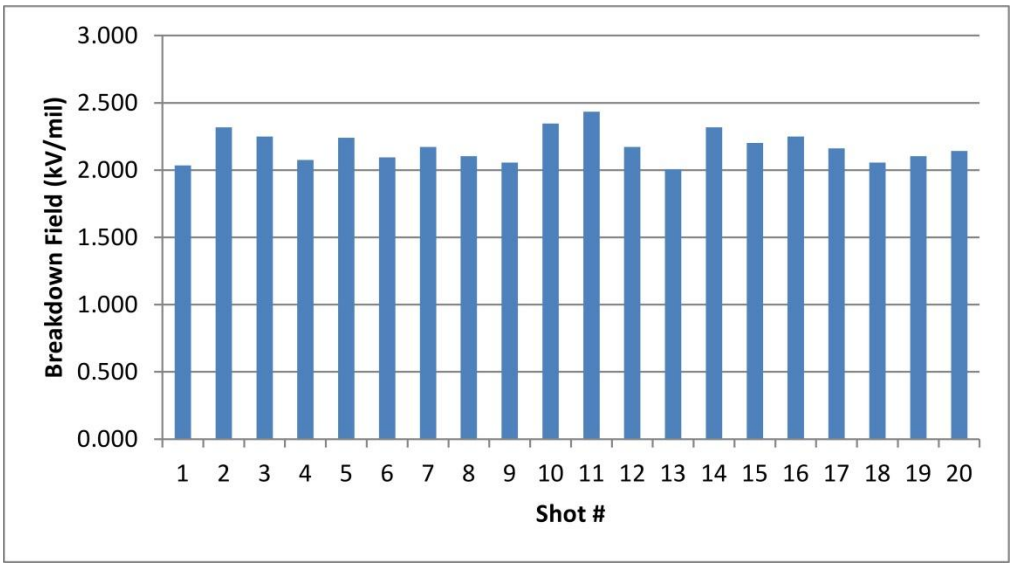

Figure 4. 61: Breakdown table of 0.381 mm (15 mil) Nylon in kV/mil

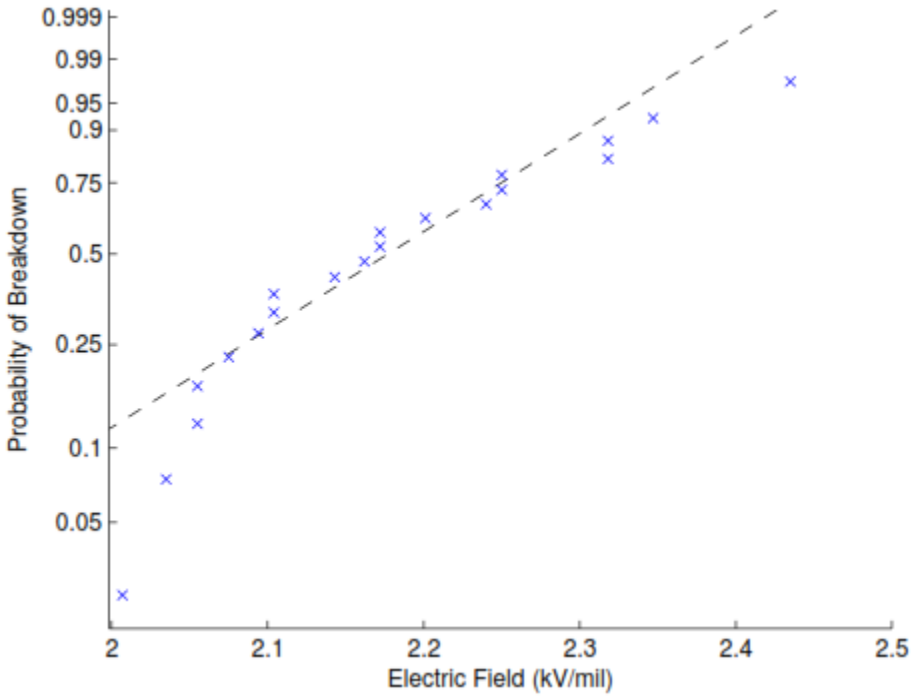

Figure 4. 62: Weibull probability breakdown plot of 0.381 mm (15 mil) Nylon in kV/mil

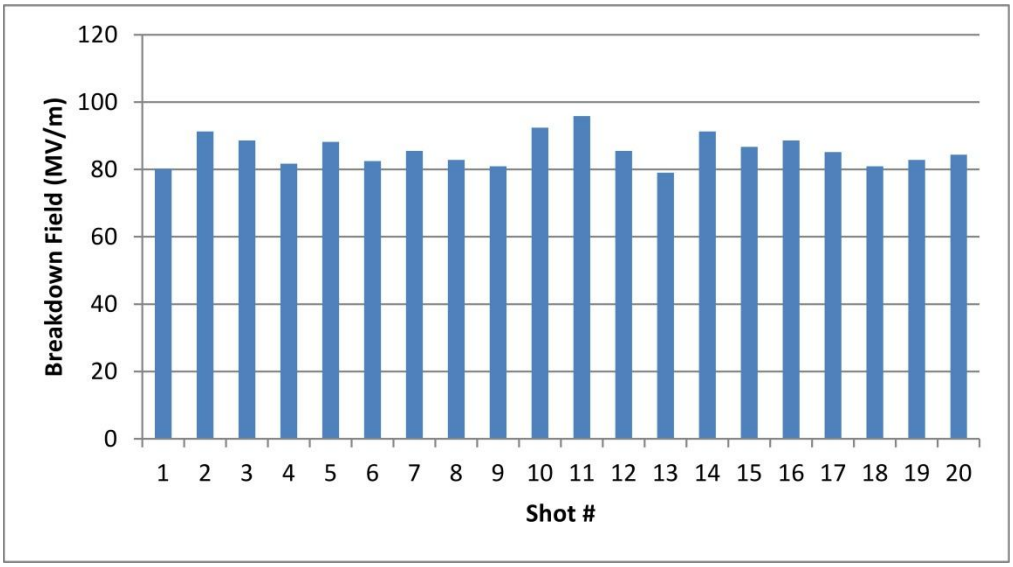

Figure 4. 63: Breakdown table of 0.381 mm (15 mil) Nylon in MV/m

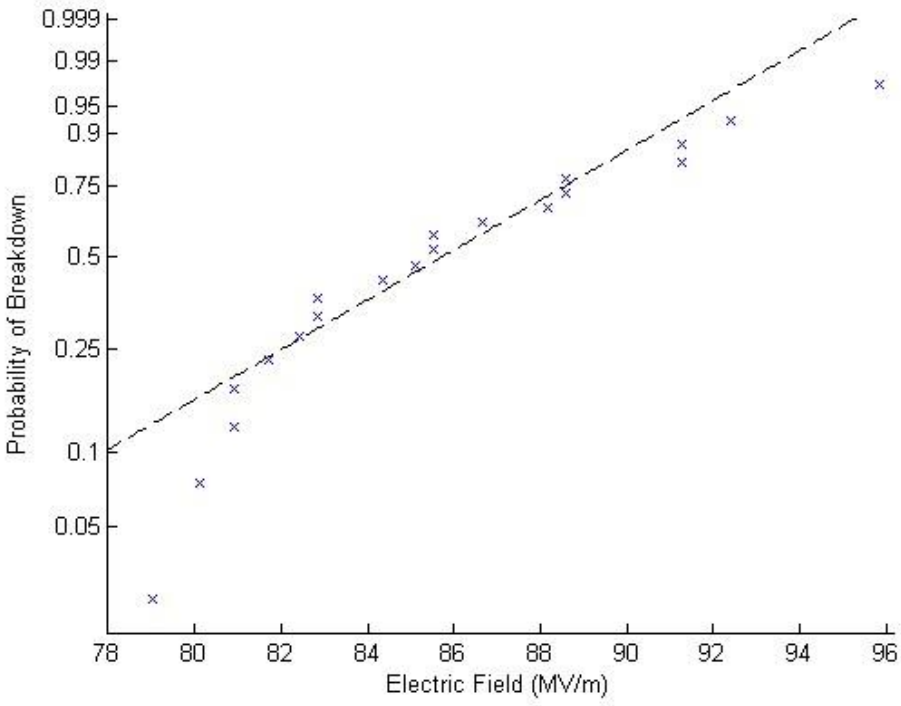

Figure 4. 64: Weibull probability breakdown plot of 0.381 mm (15 mil) Nylon in MV/m

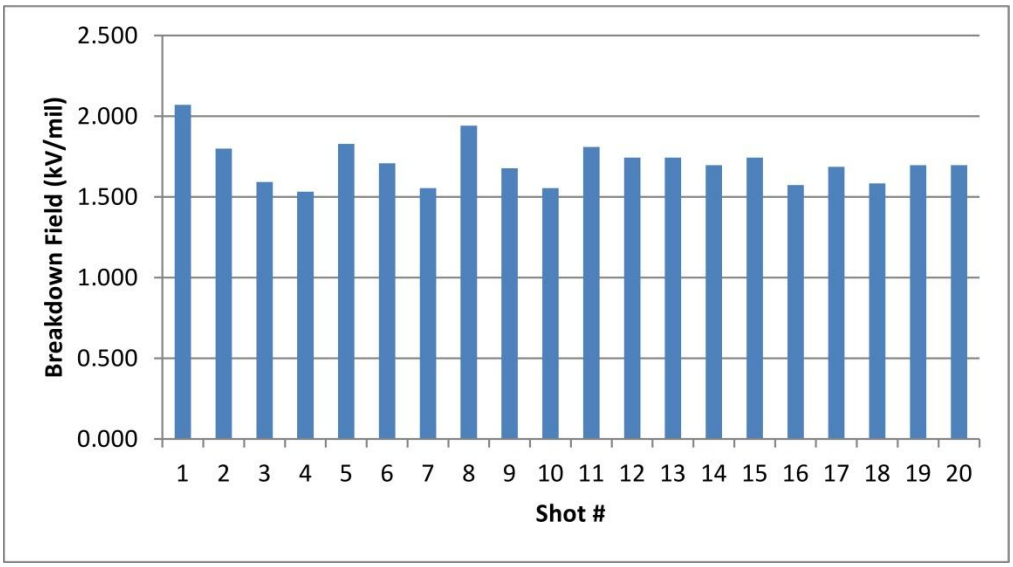

Figure 4. 65: Breakdown table of 0.788 mm (31 mil) Nylon in kV/mil

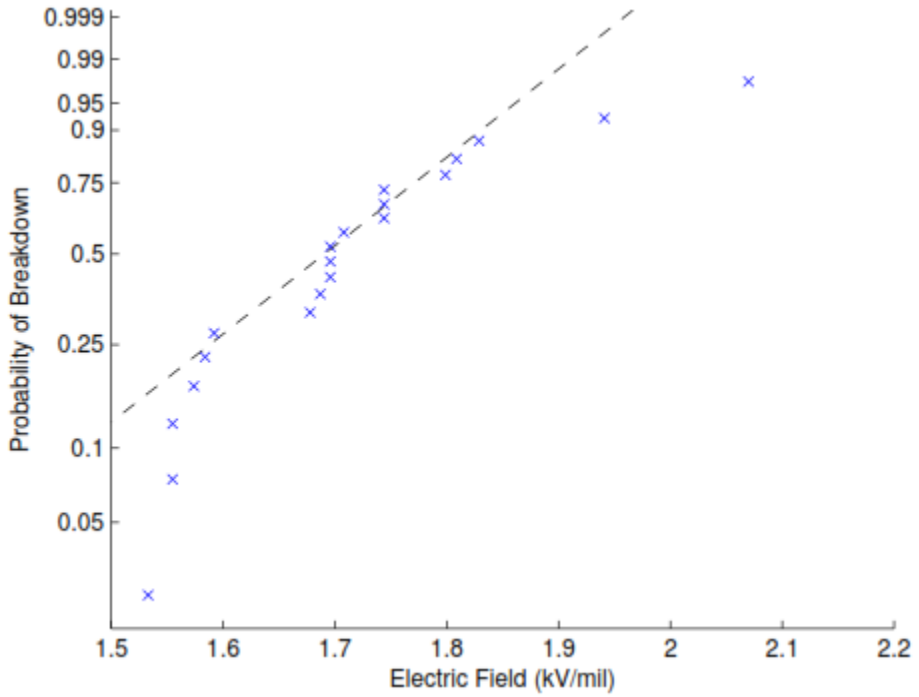

Figure 4. 66: Weibull probability breakdown plot of 0.788 mm (31 mil) Nylon in kV/mil

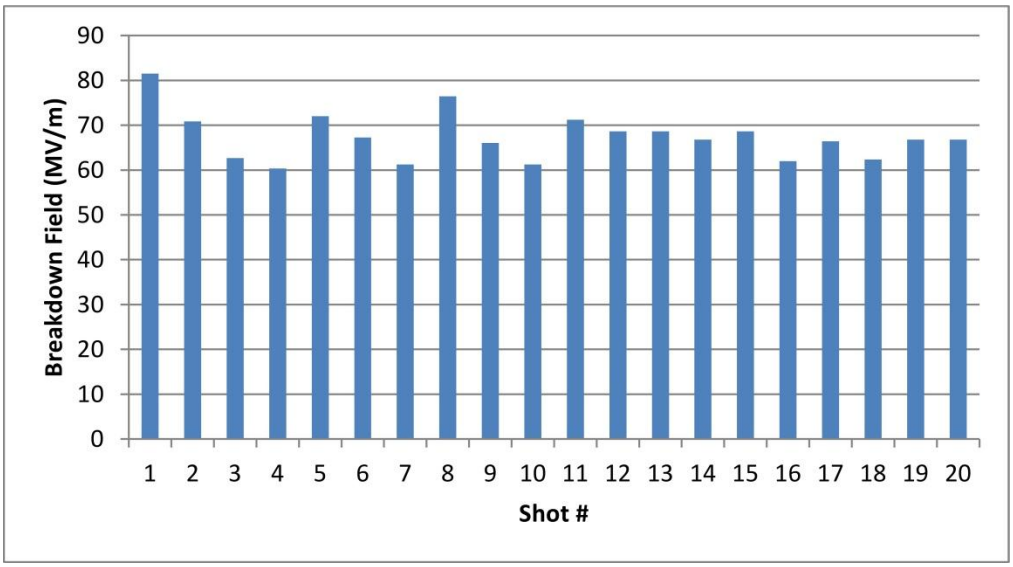

Figure 4. 67: Breakdown table of 0.788 mm (31 mil) Nylon in MV/m

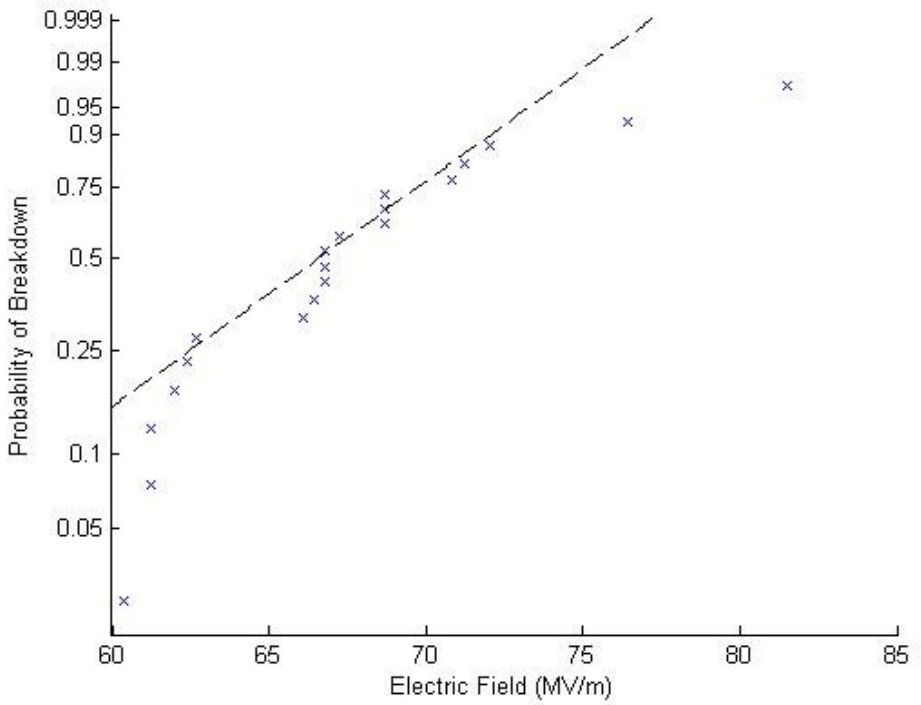

Figure 4. 68: Weibull probability breakdown plot of 0.788 mm (31 mil) Nylon in MV/m

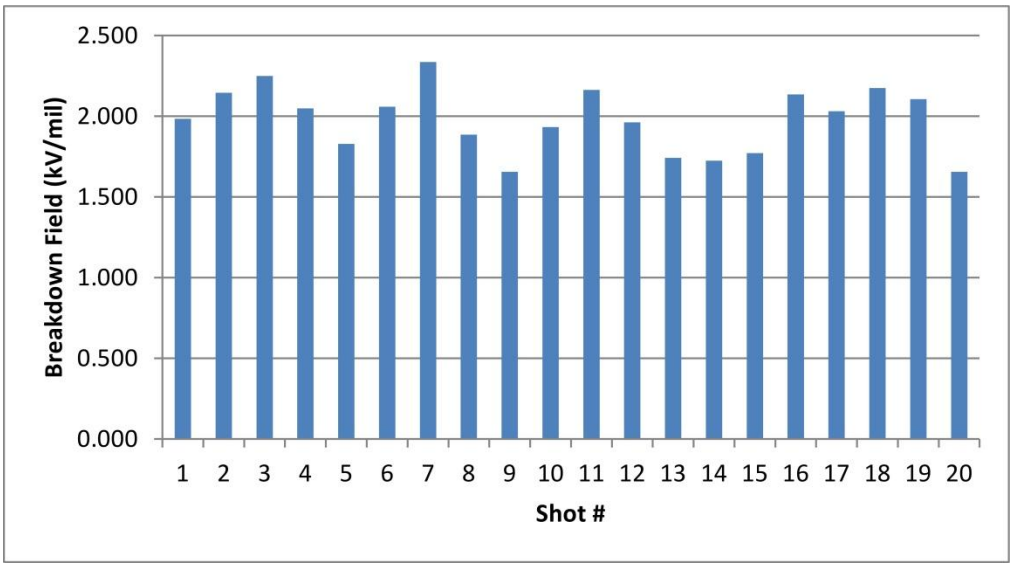

Figure 4. 69: Breakdown table of 0.508 mm (20 mil) Nylon in kV/mil

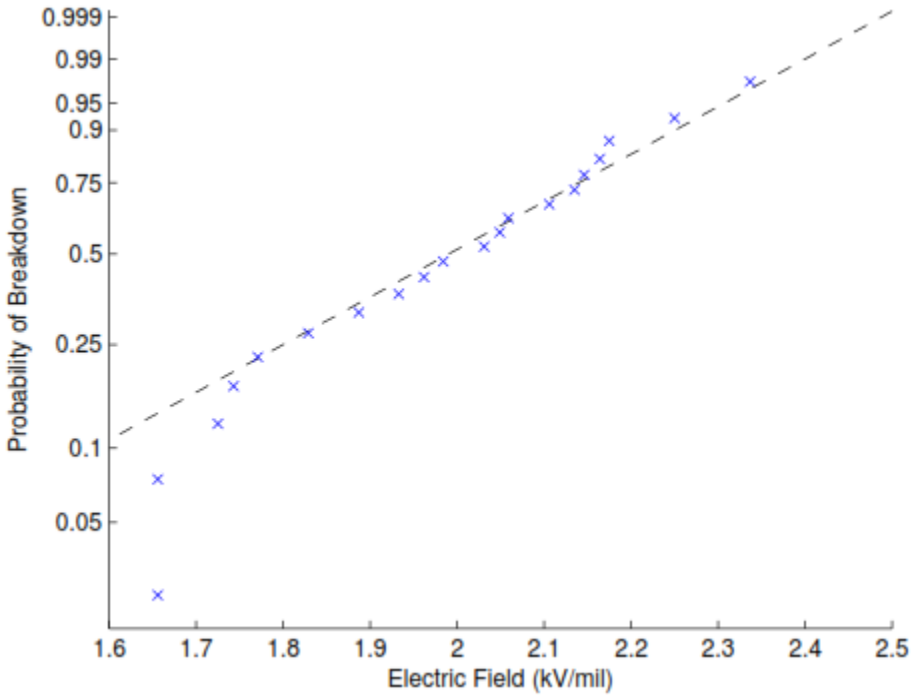

Figure 4. 70: Weibull probability breakdown plot of 0.508 mm (20 mil) Nylon in kV/mil

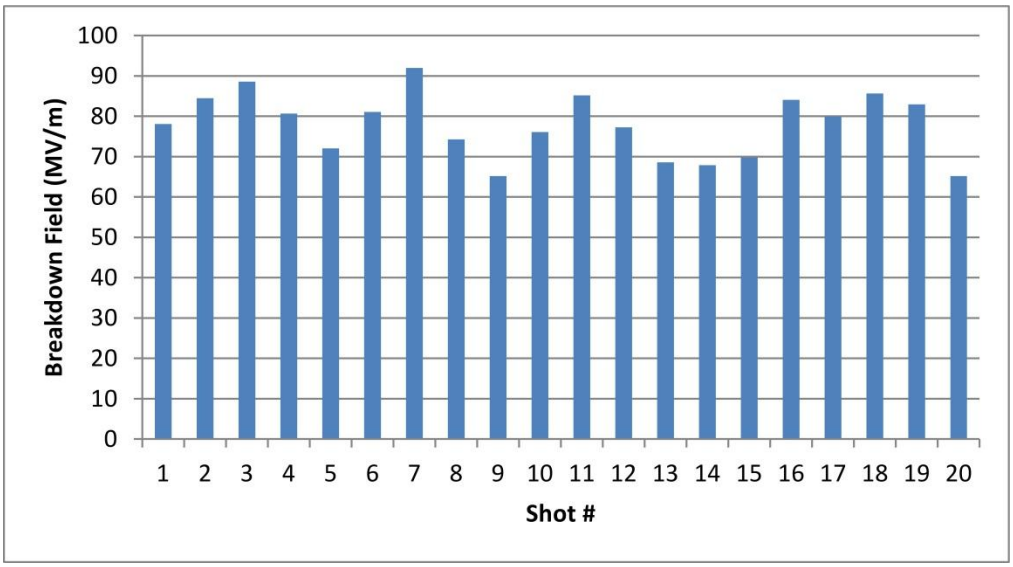

Figure 4. 71: Breakdown table of 0.508 mm (20 mil) Nylon in MV/m

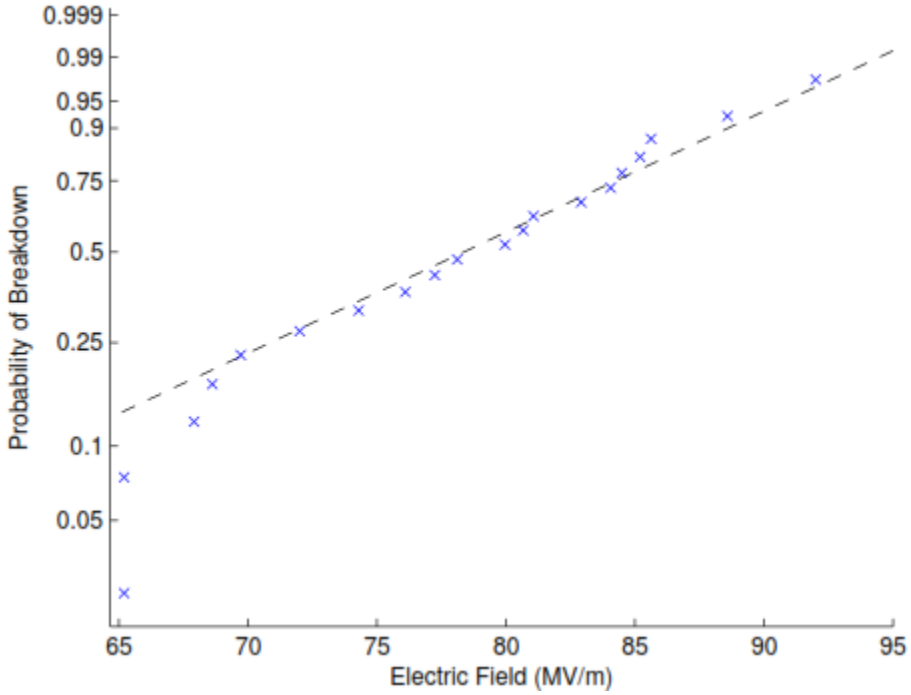

Figure 4. 72: Weibull probability breakdown plot of 0.508 mm (20 mil) Nylon in MV/m

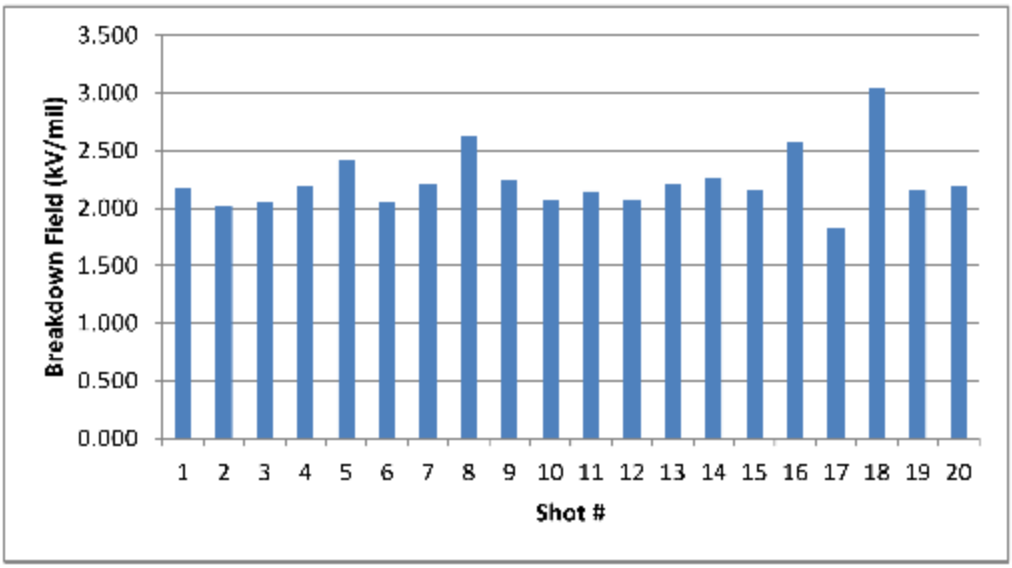

Figure 4. 73: Breakdown table of 0.254 mm (10 mil) PVDF in kV/mil

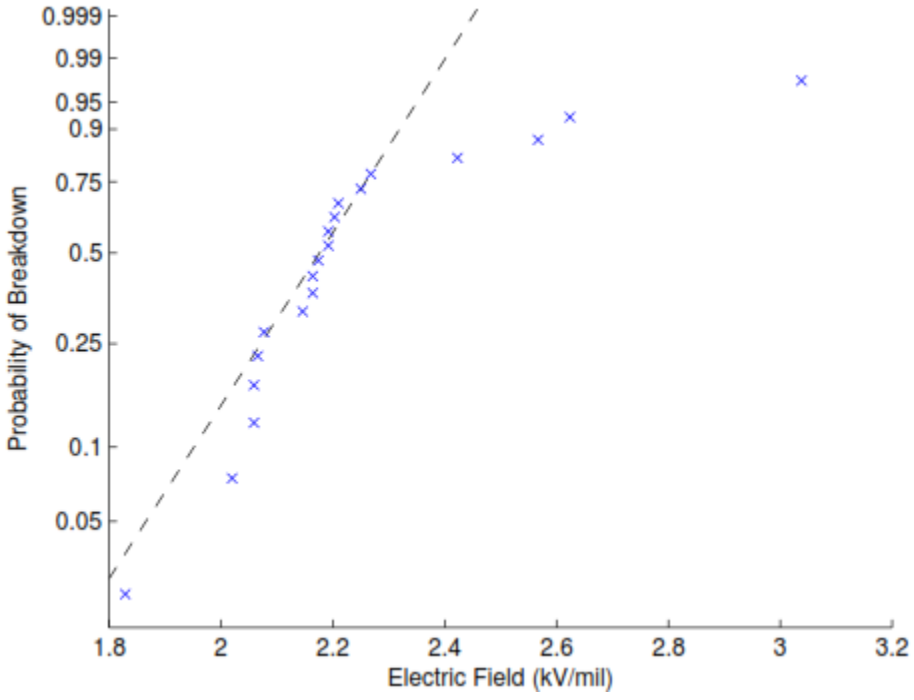

Figure 4. 74: Weibull probability breakdown plot of 0.254 mm (10 mil) PVDF in kV/mil

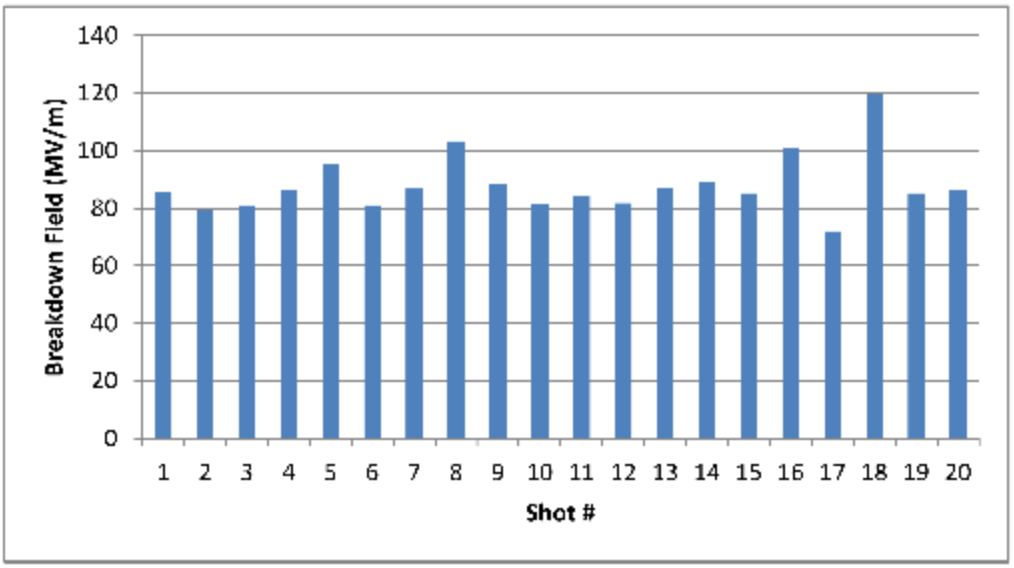

Figure 4. 75: Breakdown table of 0.254 mm (10 mil) PVDF in MV/m

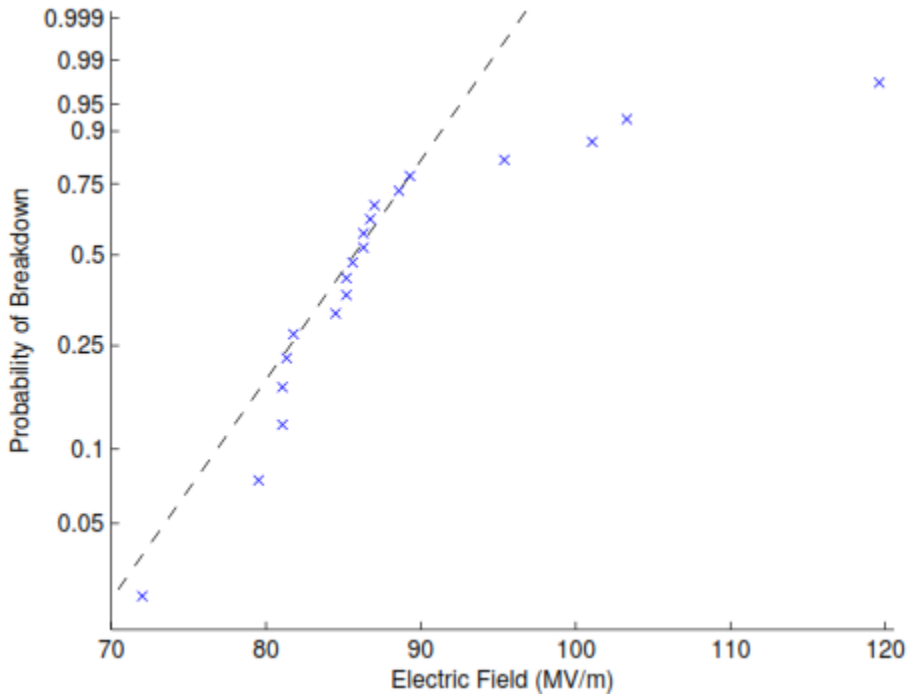

Figure 4. 76: Weibull probability breakdown plot of 0.254 mm (10 mil) PVDF in MV/m

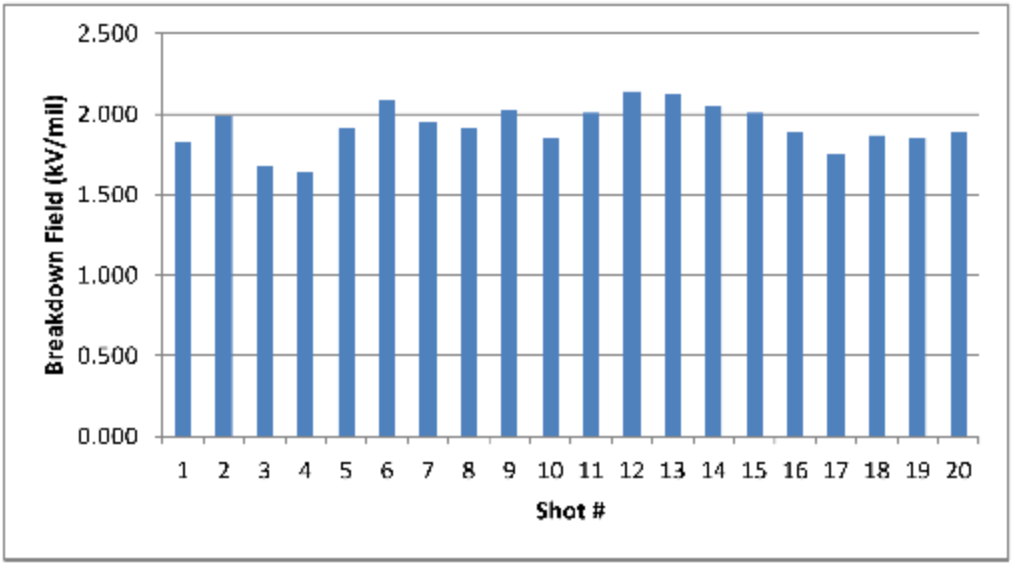

Figure 4. 77: Breakdown table of 0.381 mm (15 mil) PVDF in kV/mil

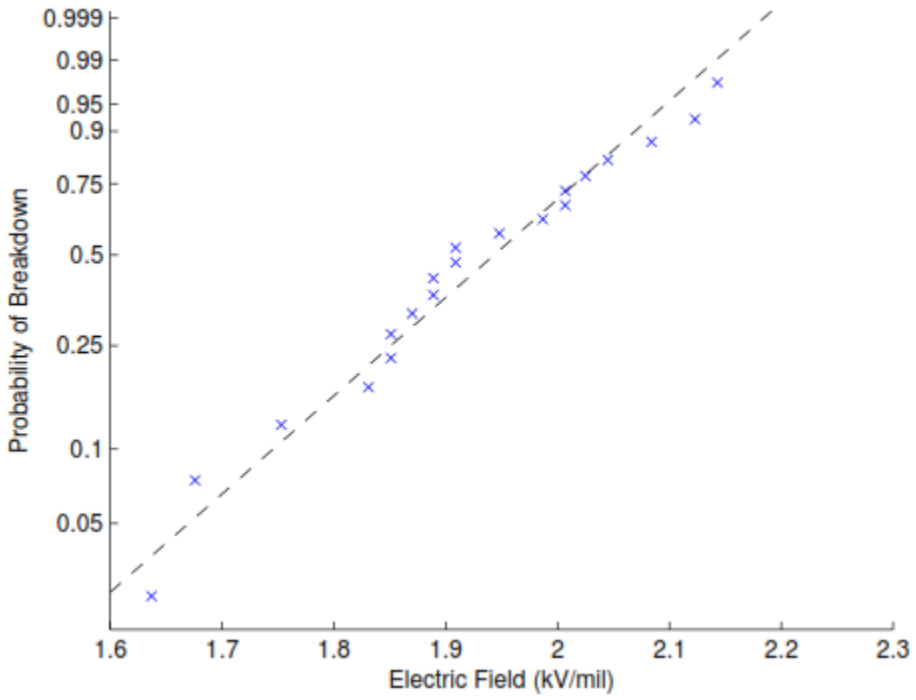

Figure 4. 78: Weibull probability breakdown plot of 0.381 mm (15 mil) PVDF in kV/mil

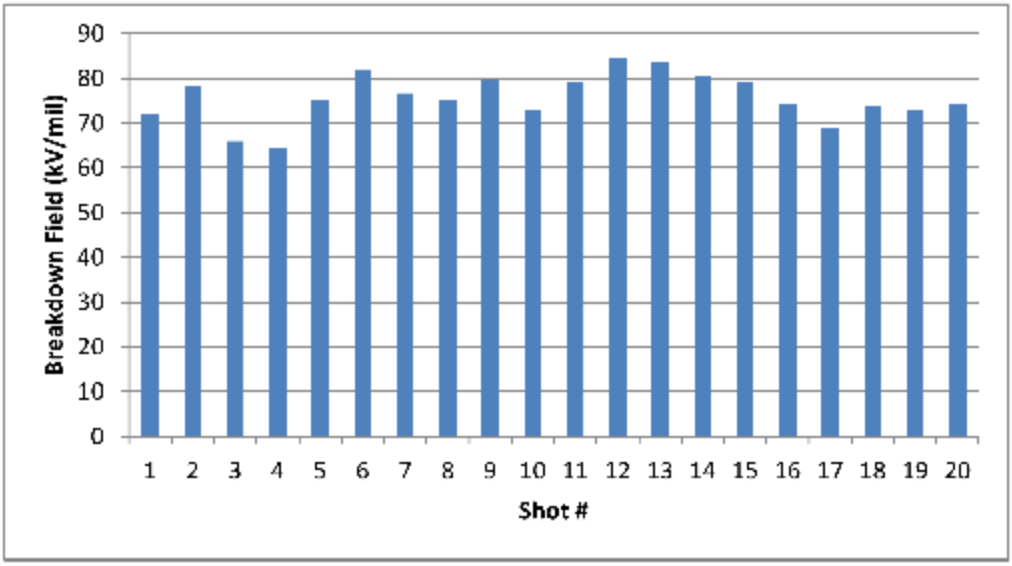

Figure 4. 79: Breakdown table of 0.381 mm (15 mil) PVDF in MV/m

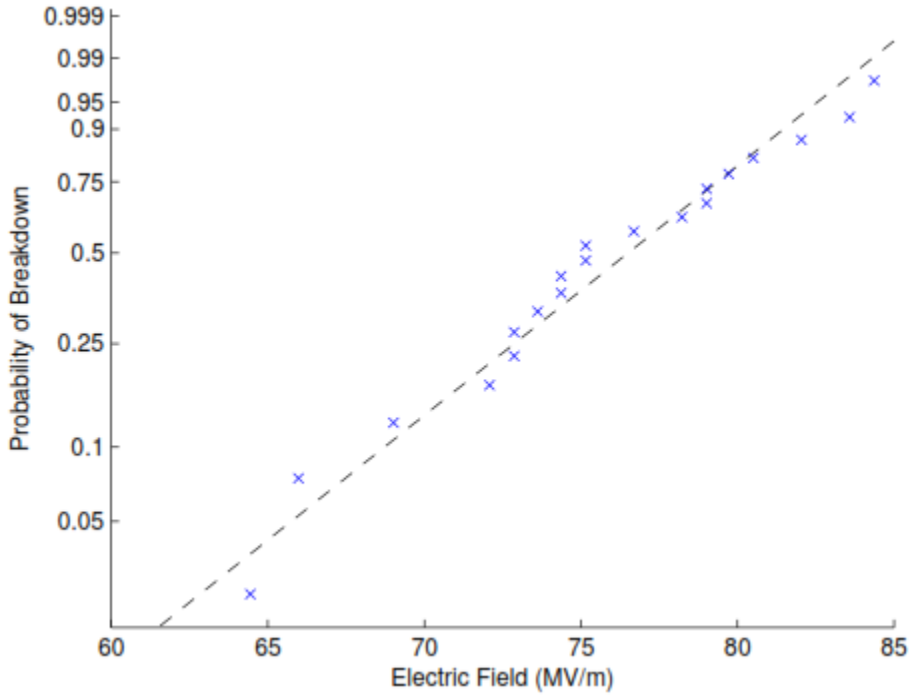

Figure 4. 80: Weibull probability breakdown plot of 0.381 mm (15 mil) PVDF in MV/m

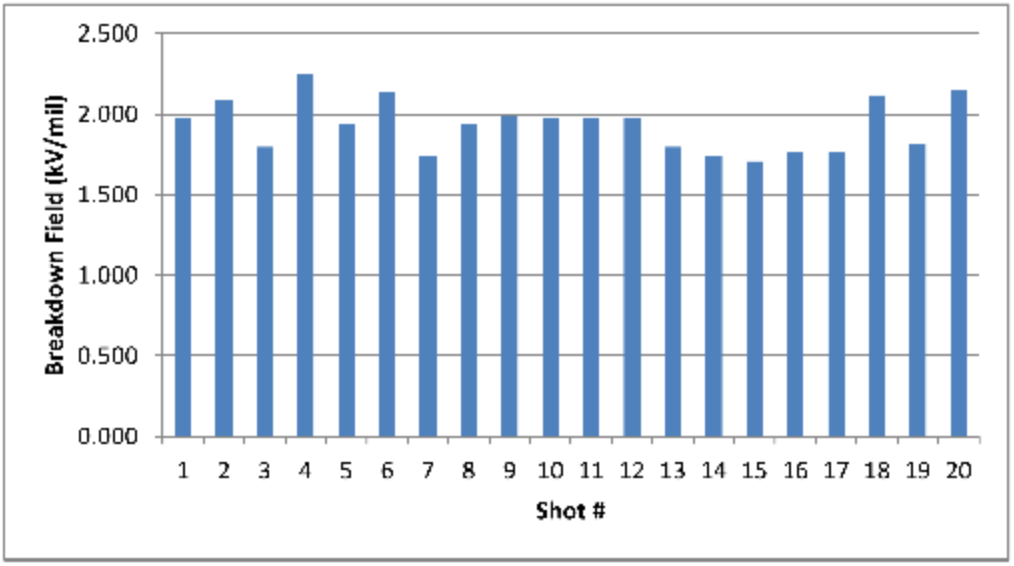

Figure 4. 81: Breakdown table of 0.508 mm (20 mil) PVDF in kV/mil

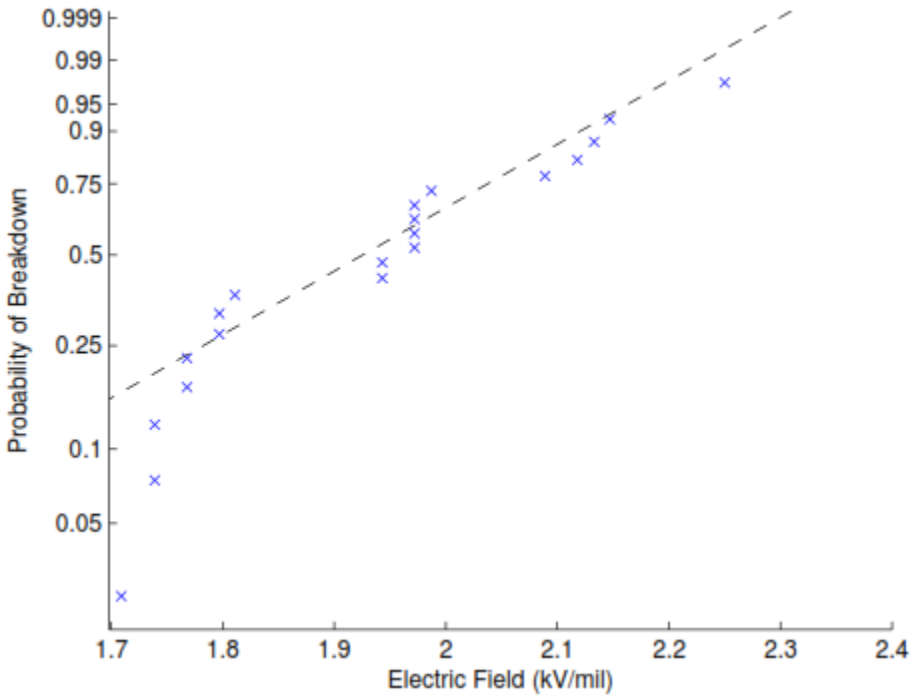

Figure 4. 82: Weibull probability breakdown plot of 0.508 mm (20 mil) PVDF in kV/mil

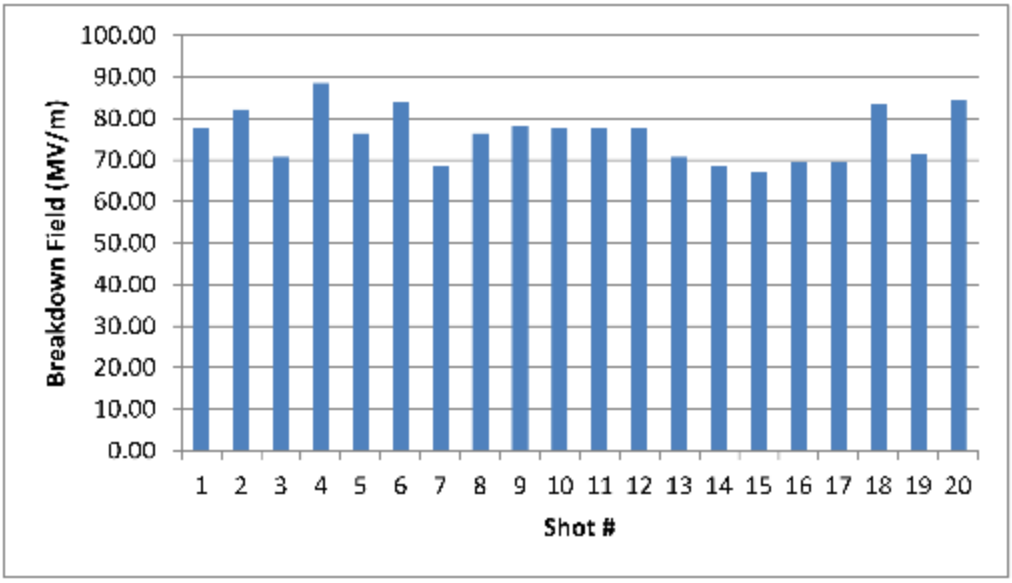

Figure 4. 83: Breakdown table of 0.508 mm (20 mil) PVDF in MV/m

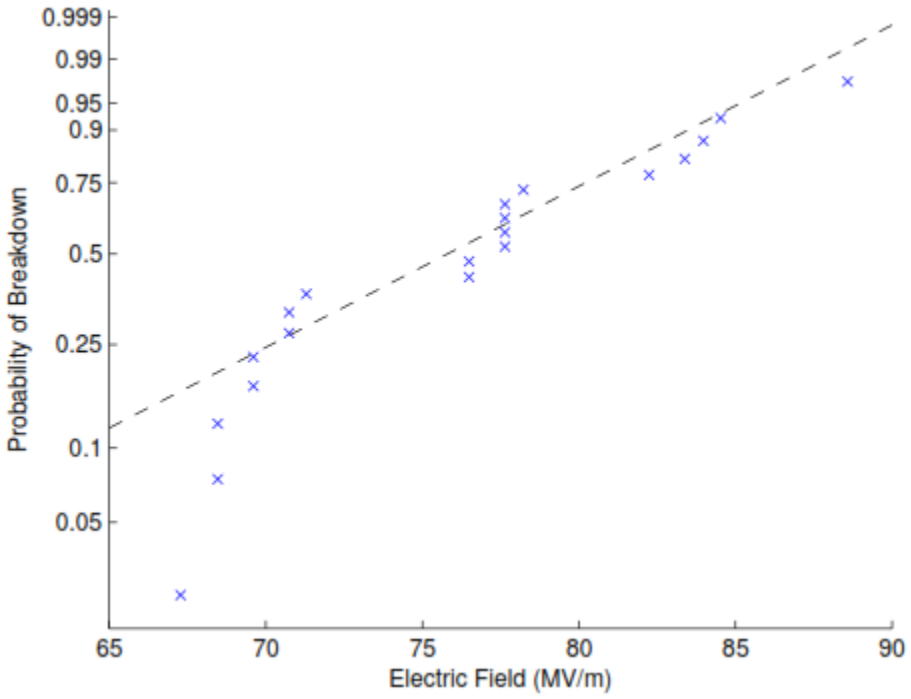

Figure 4. 84: Weibull probability breakdown plot of 0.508 mm (20 mil) PVDF in MV/m

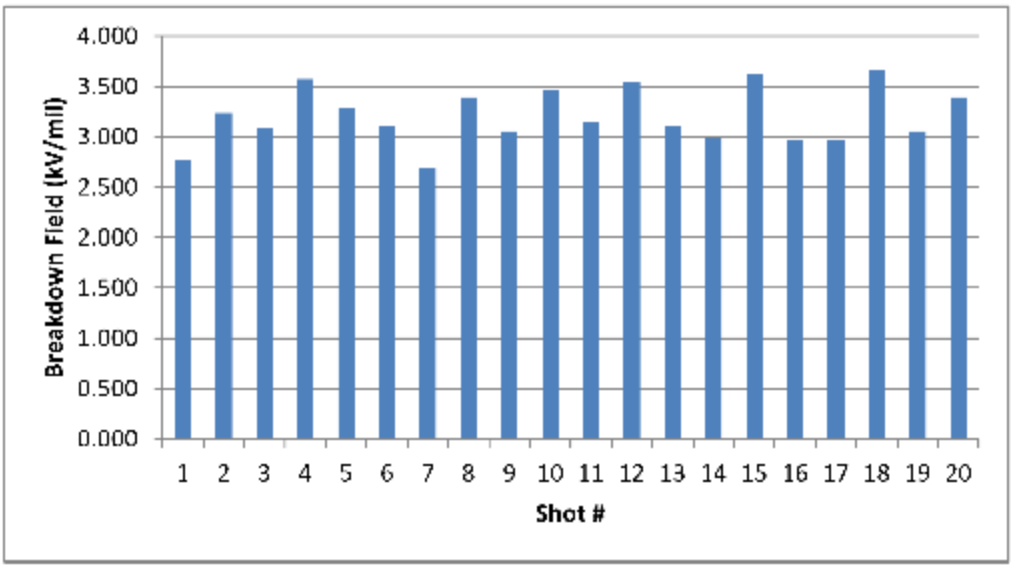

Figure 4. 85: Breakdown table of 0.508 mm (20 mil) Teflon in kV/mil

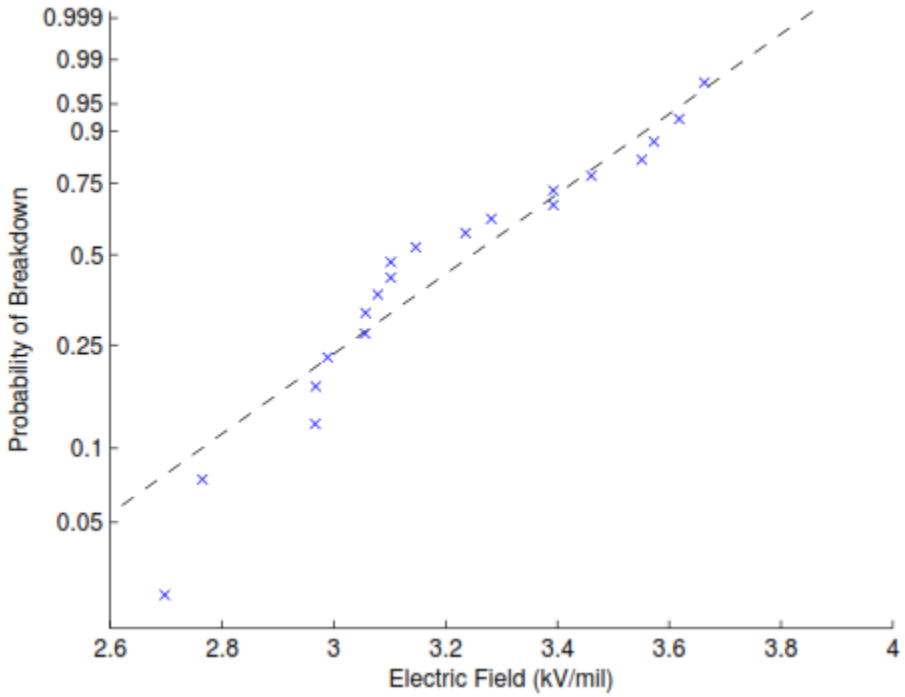

Figure 4. 86: Weibull probability breakdown plot of 0.508 mm (20 mil) Teflon in kV/mil

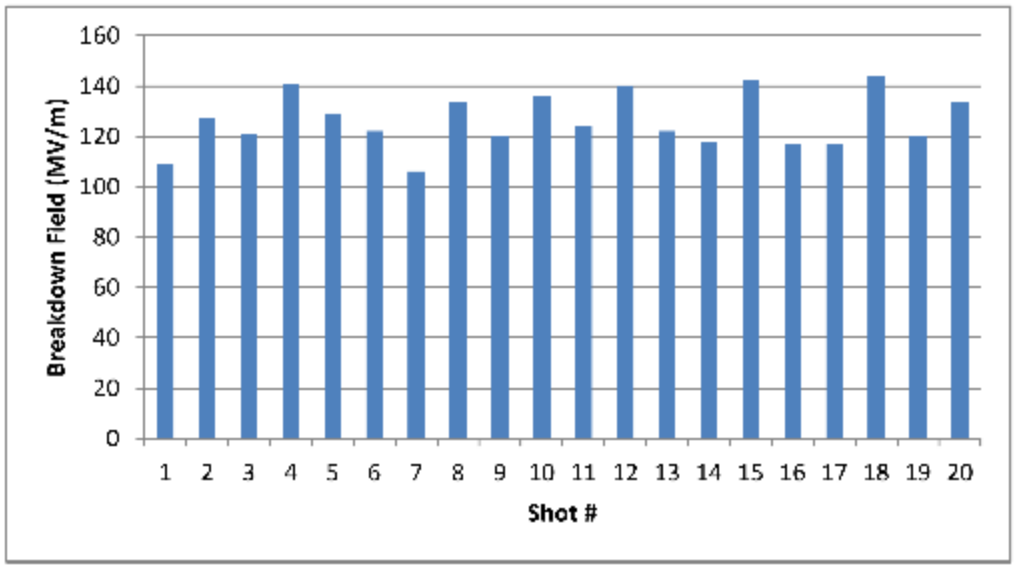

Figure 4. 87: Breakdown table of 0.508 mm (20 mil) Teflon in MV/m

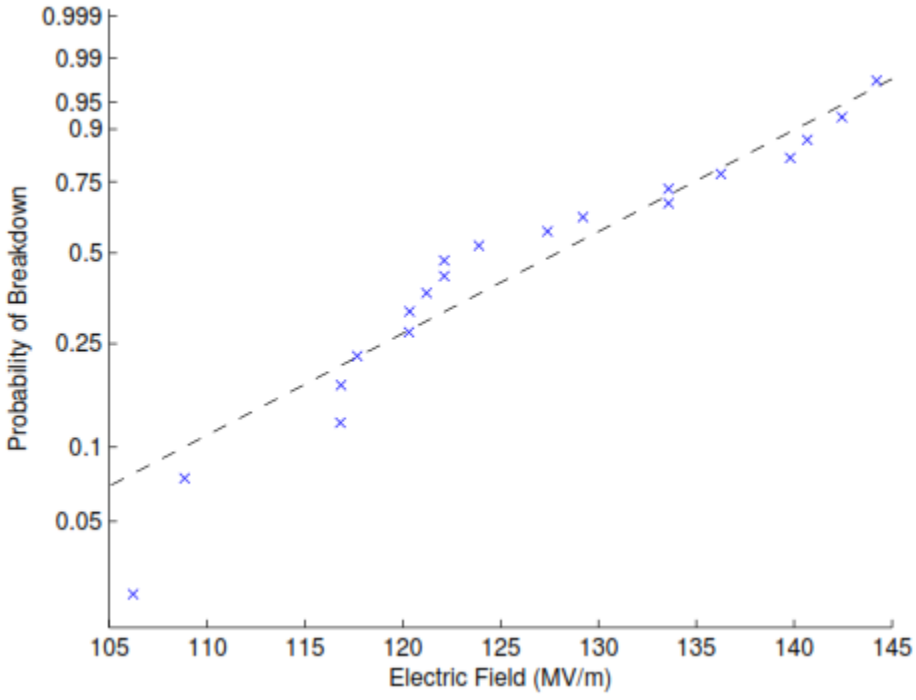

Figure 4. 88: Weibull probability breakdown plot of 0.508 mm (20 mil) Teflon in MV/m

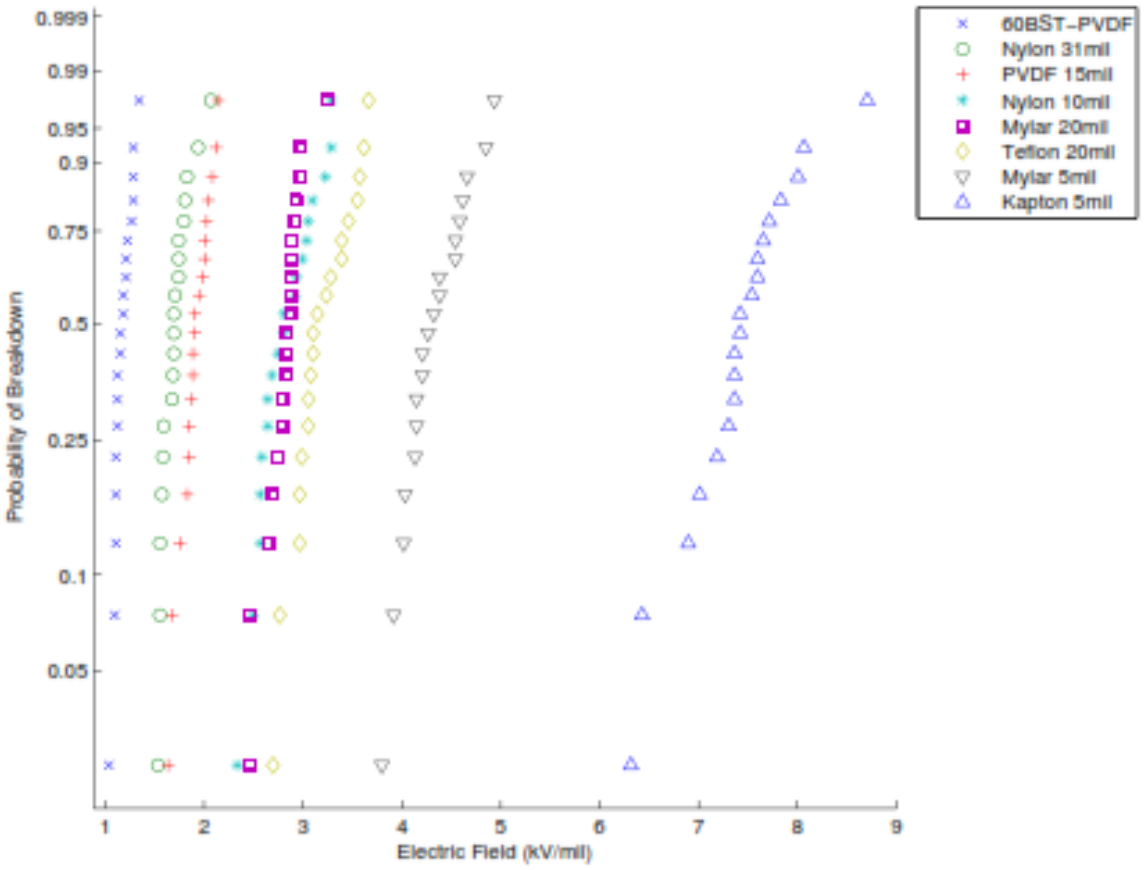

Figure 4. 89: A Weibull plot of some commercial dielectrics compared to 60% BST by volume in a PVDF matrix in kV/mil. Some of the different thicknesses of the commercial dielectrics were excluded from the plot to make it more readable.

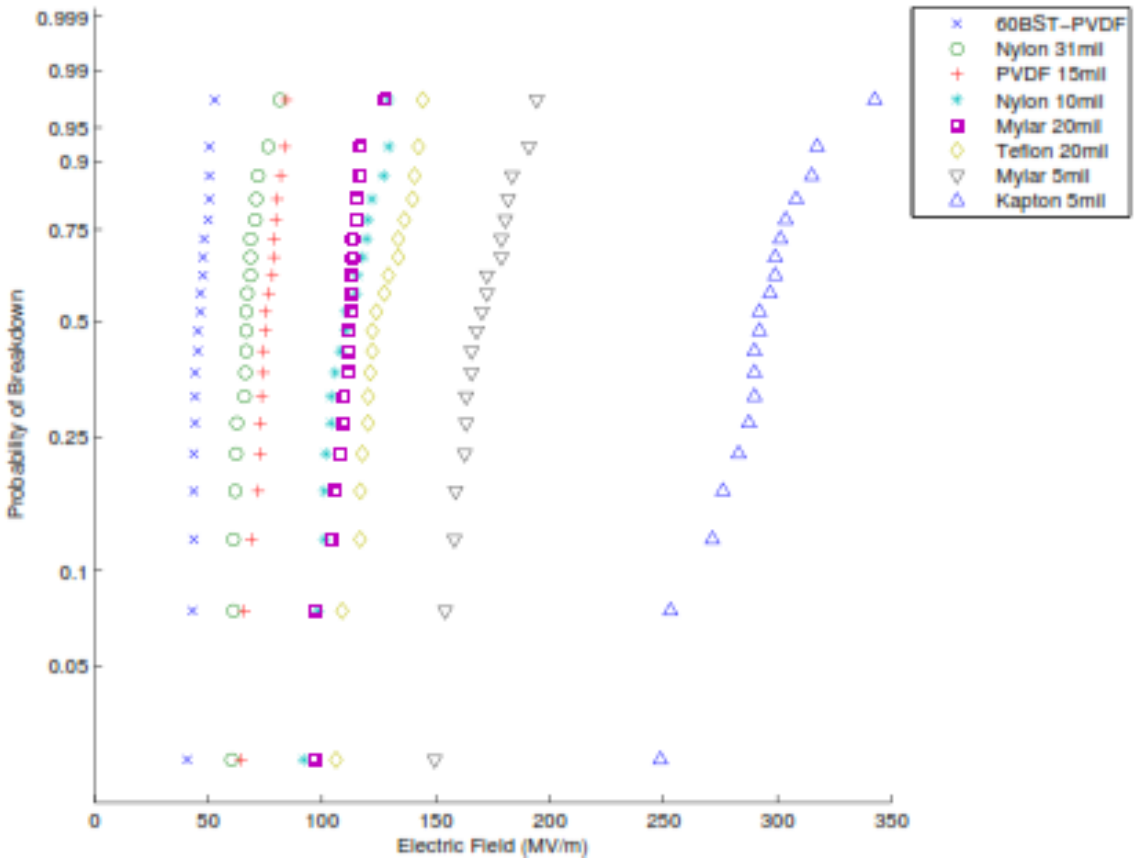

Figure 4. 90: A Weibull plot of some commercial dielectrics compared to 60% BST by volume in a PVDF matrix in MV/m. Some of the different thicknesses of the commercial dielectrics were excluded from the plot to make it more readable.

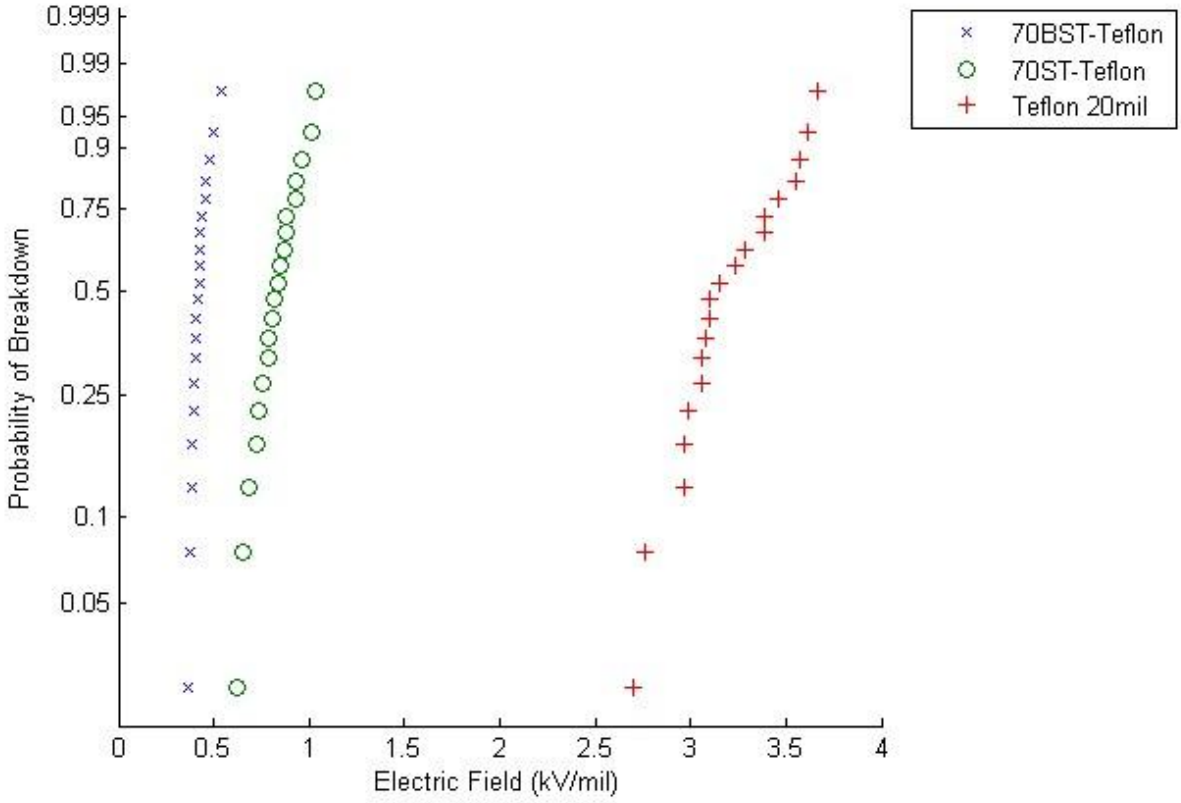

Figure 4. 91: A Weibull plot of the breakdown values in kV/mil of the 0.508 mm (20 mil) thick ST and BST composites mixed with Teflon compared to commercial 0.508 mm (20 mil) Teflon

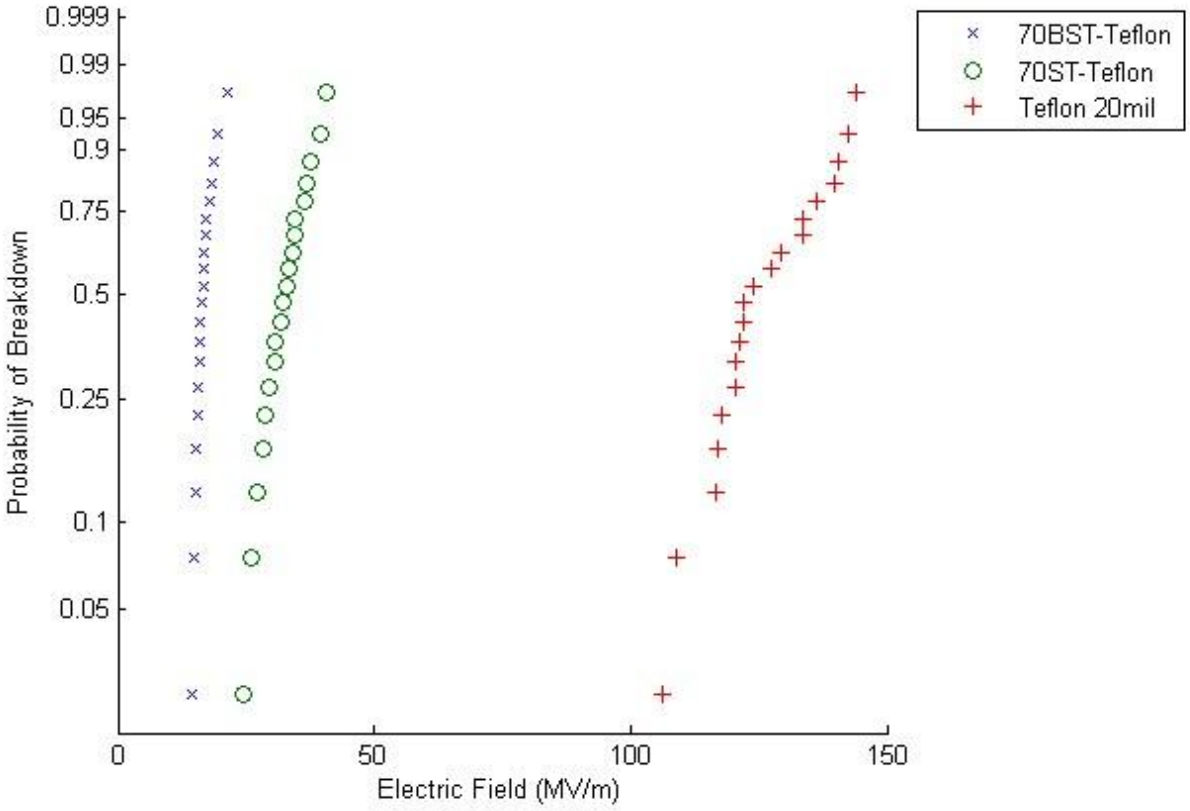

Figure 4. 92: A Weibull plot of the breakdown values in MV/m of the 0.508 mm (20 mils) thick ST and BST composites mixed with Teflon compared to commercial 0.508 mm (20 mils) Teflon

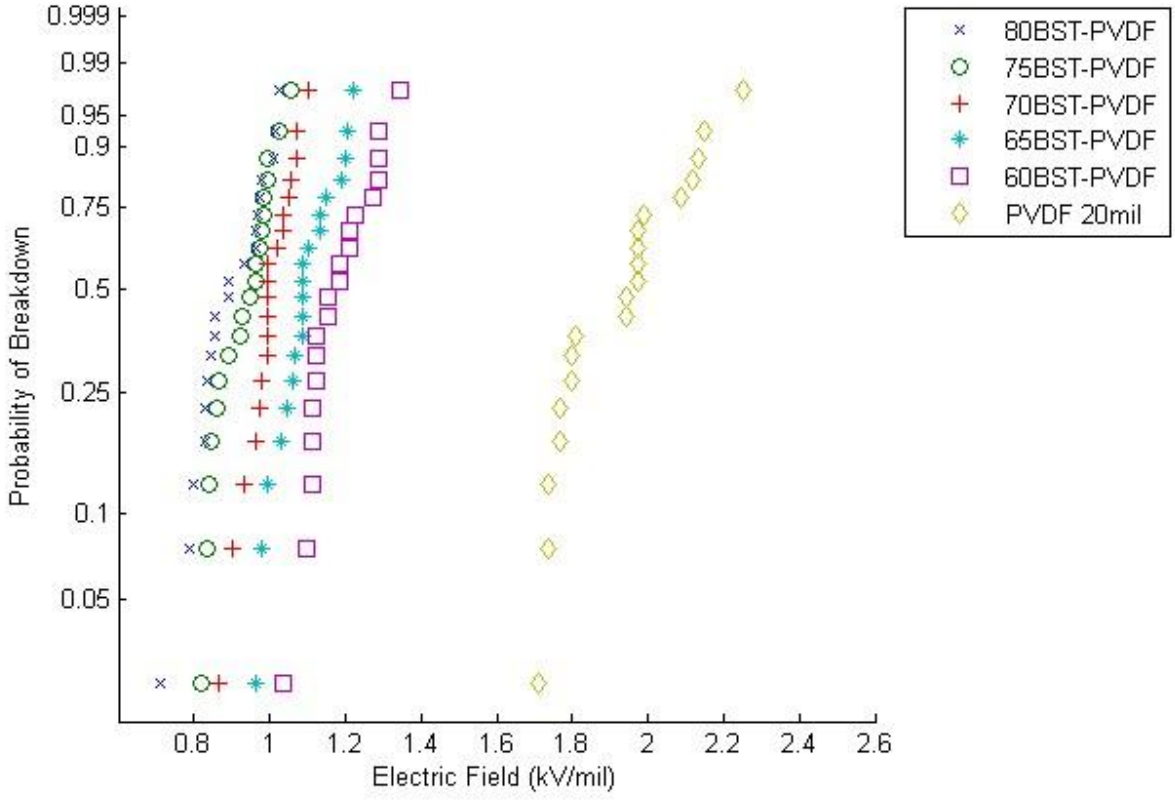

Figure 4. 93: A Weibull plot of the breakdown values in kV/mil of the 0.508 mm (20 mils) thick BST composites mixed with PVDF compared to commercial 0.508 mm (20 mils) PVDF

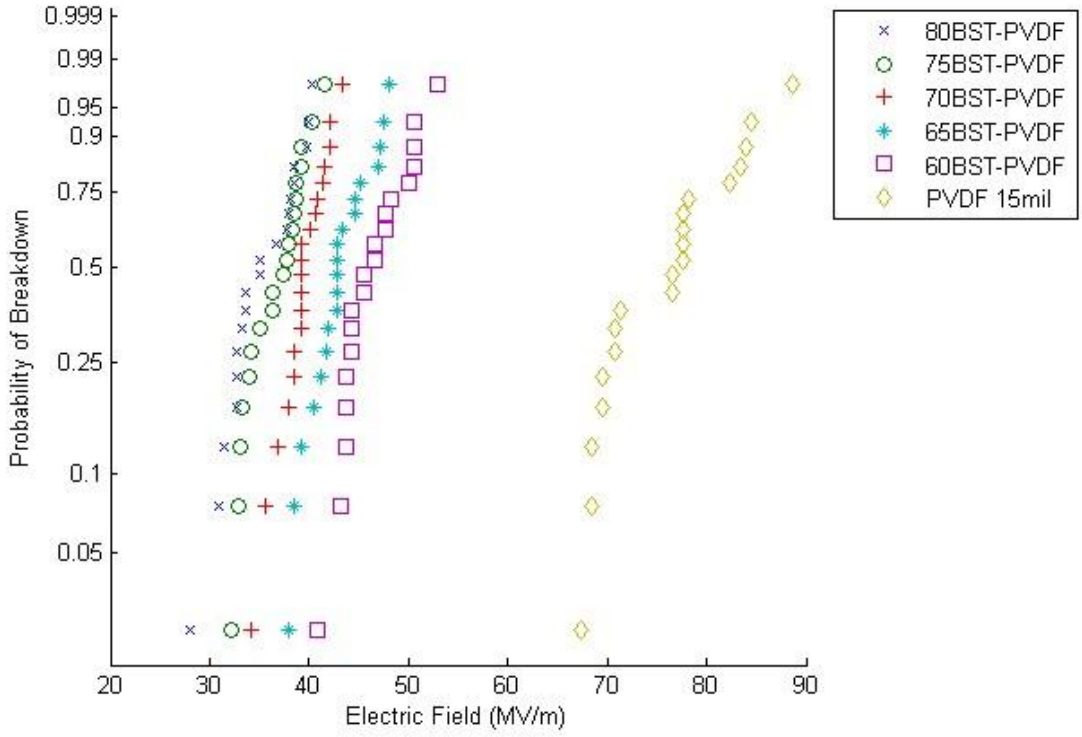

Figure 4. 94: A Weibull plot of the breakdown values in MV/m of the 0.508 mm (20 mils) thick BST composites mixed with PVDF compared to commercial 0.508 mm (20 mils) PVDF

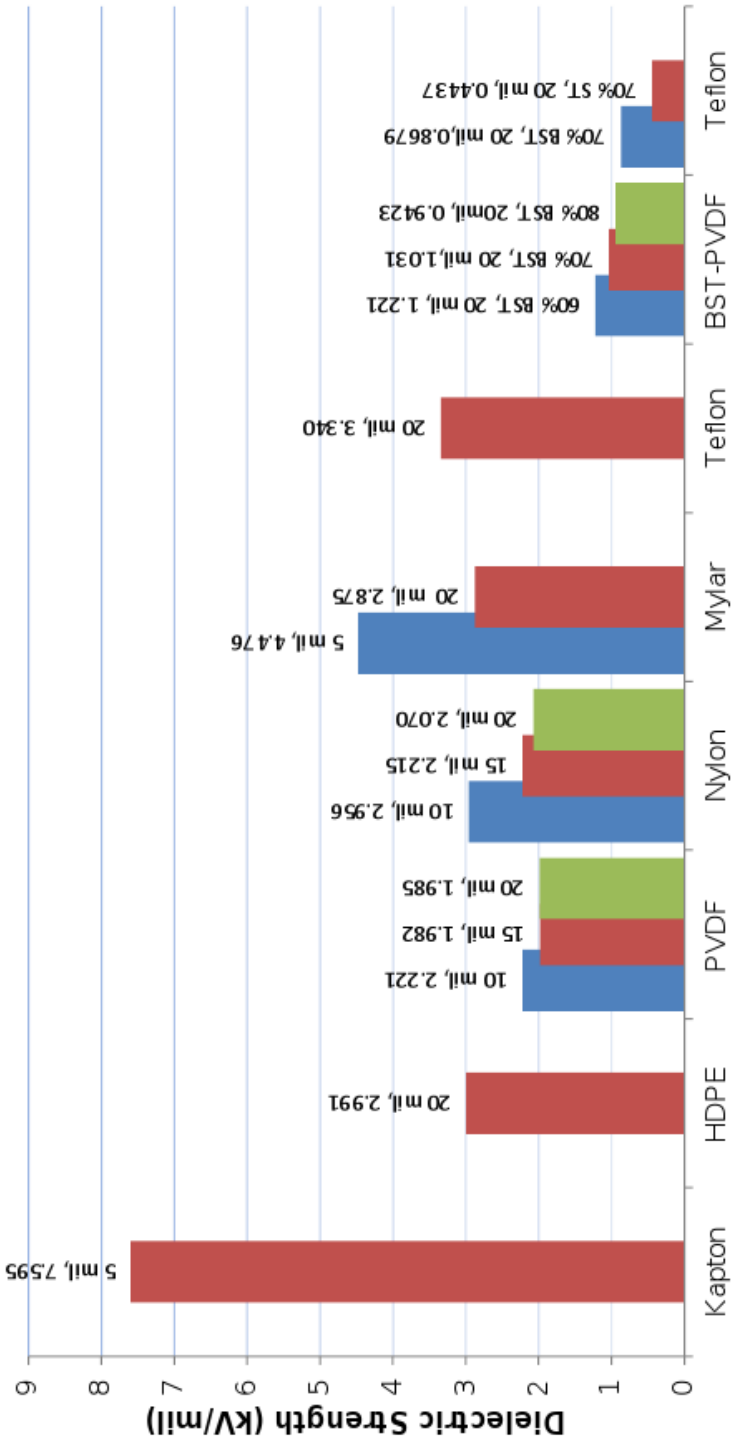

Figure 4.95: The dielectric strengths of the nanocomposites compared to commercial plastics in kV/mil

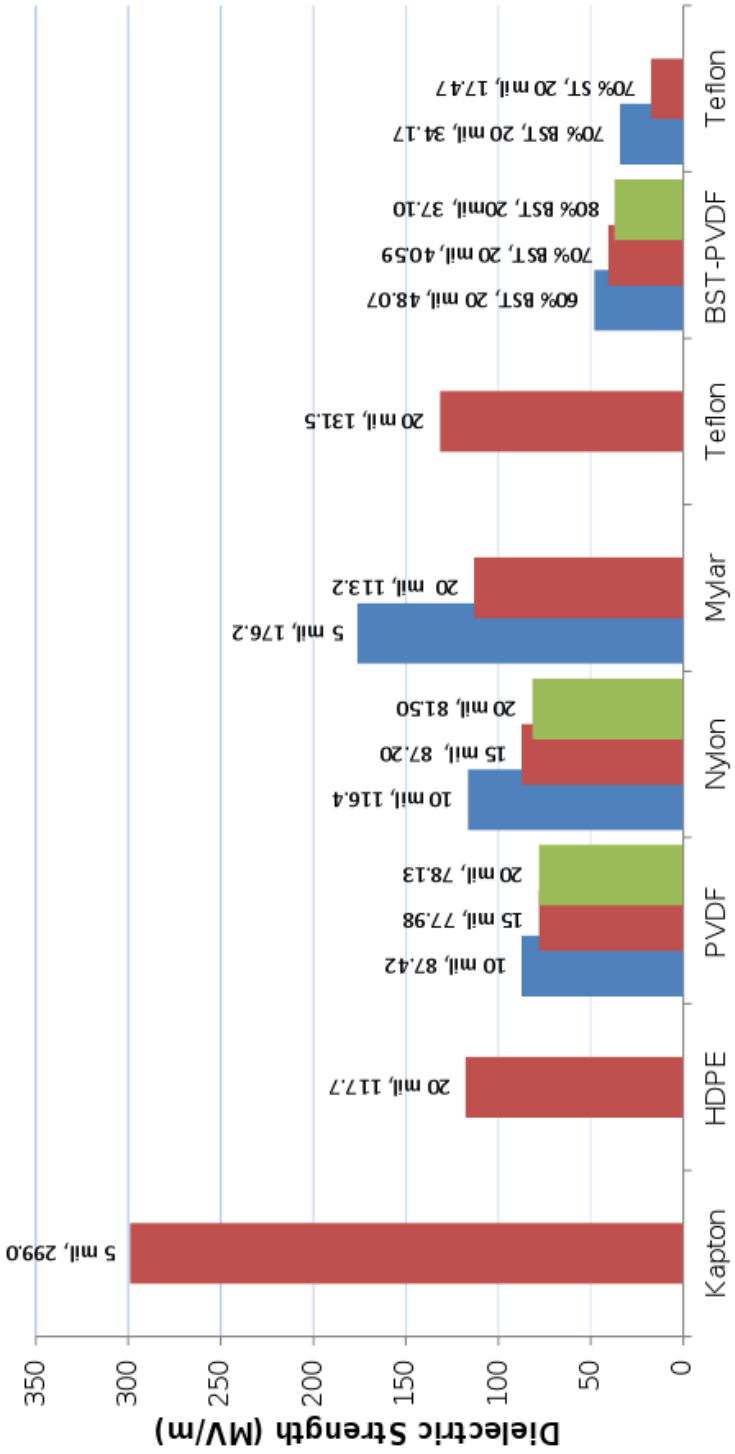

Figure 4.96: The dielectric strengths of the nanocomposites compared to commercial plastics in MV/m

Figure 4.97: A picture of the surface of 75% filler by volume BST-PVDF composite

4.5 SEM Images of Nanocomposites

A scanning electron microscope (SEM) was utilized to observe the level of mixing that the ceramic powder and the plastic matrix underwent. The SEM images, represented in Figures 4.98 through 4.100, show a significant amount of clumping of the ceramic material within the plastic matrix. The white circles are the clumped BST particles and the dark space in between is the plastic matrix material. Since the grain size of the nanopowder is on the order of 50 nm, it is clear that the ceramic did not mix effectively. This incomplete mixing could significantly reduce the dielectric constant of the composite. A picture of the surface of a 75% BST by volume filled PVDF composite is shown in Figure 4.97. This picture shows spotting on the surface of the composite disk, which is further evidence of the incomplete mixing of the two materials.

SEM images of the dry BST particles were also taken and are represented in Figures 4.101 through 4.104. The pictures show that the BST particles are already clumped together before they are mixed with the plastic matrix. This pre-clumping could indicate some sort of bonding that takes place when the powder is dried. This bonding could be the reason that the composites did not mix effectively, which in turn, would cause a significant decrease in the dielectric constant of the composites and the dielectric strength.

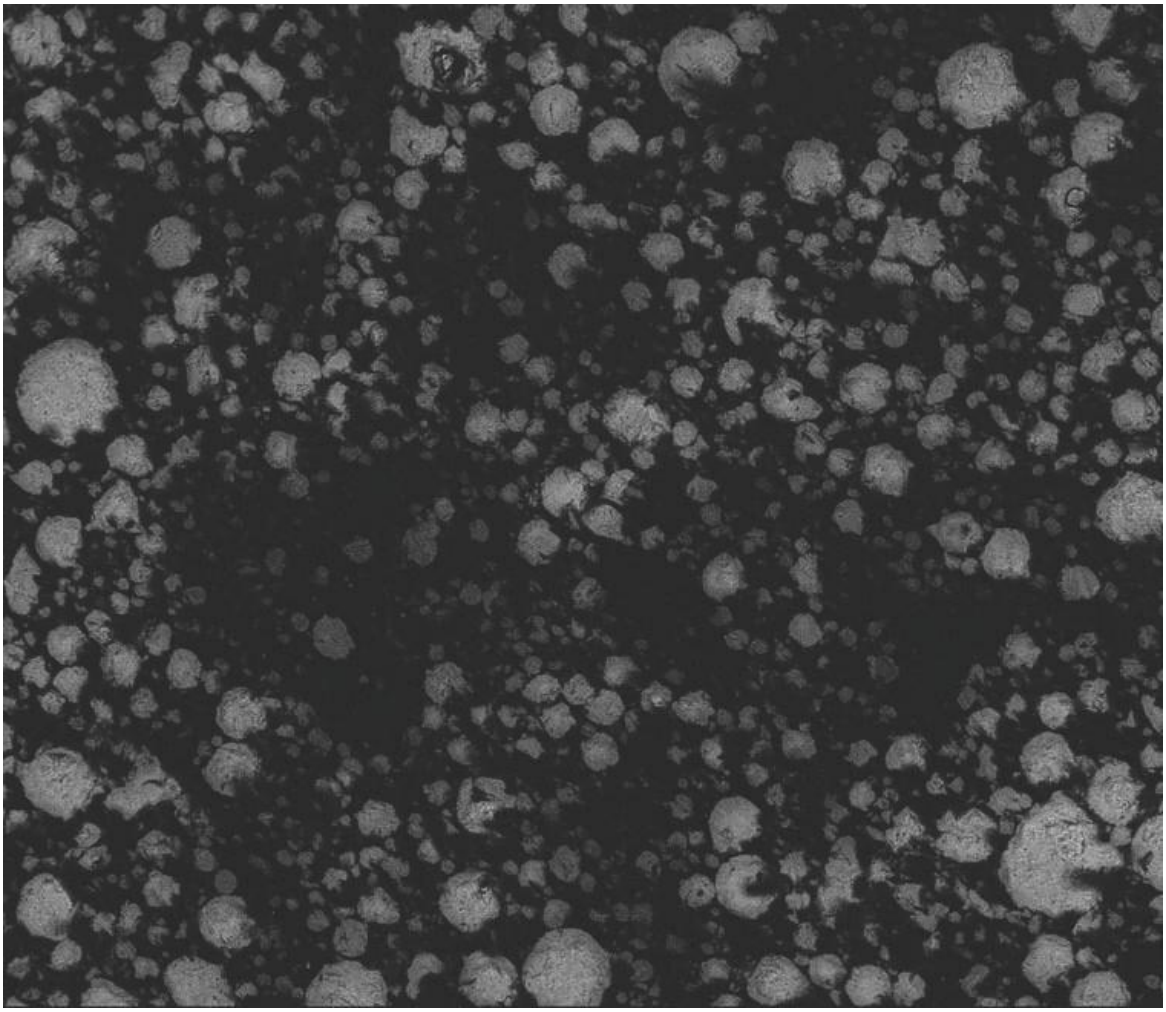

Figure 4. 98: SEM images of the PVDF-BST nanocomposite with 60% of BST fill by volume

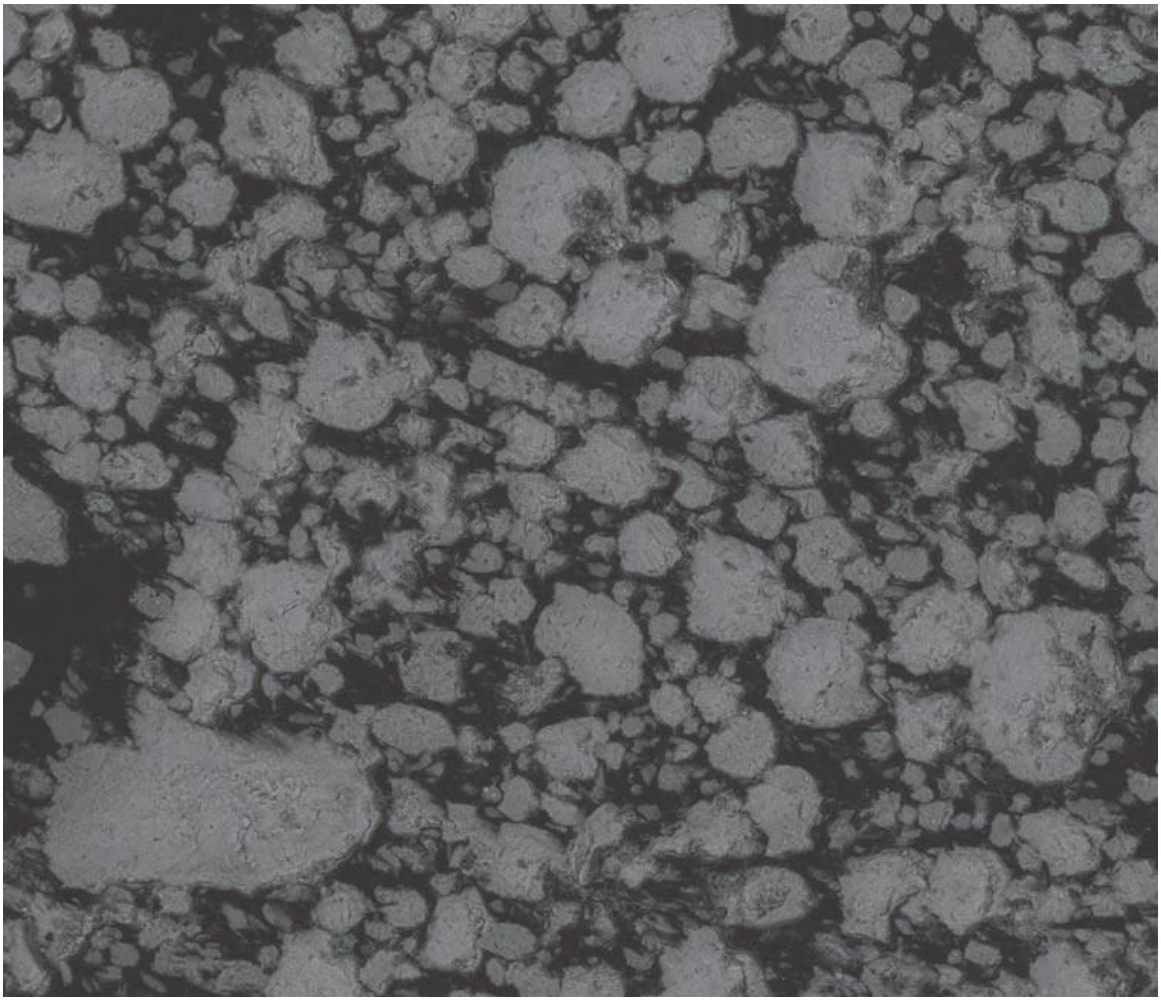

Figure 4. 99: SEM images of the PVDF-BST nanocomposite with 70% of BST fill by volume

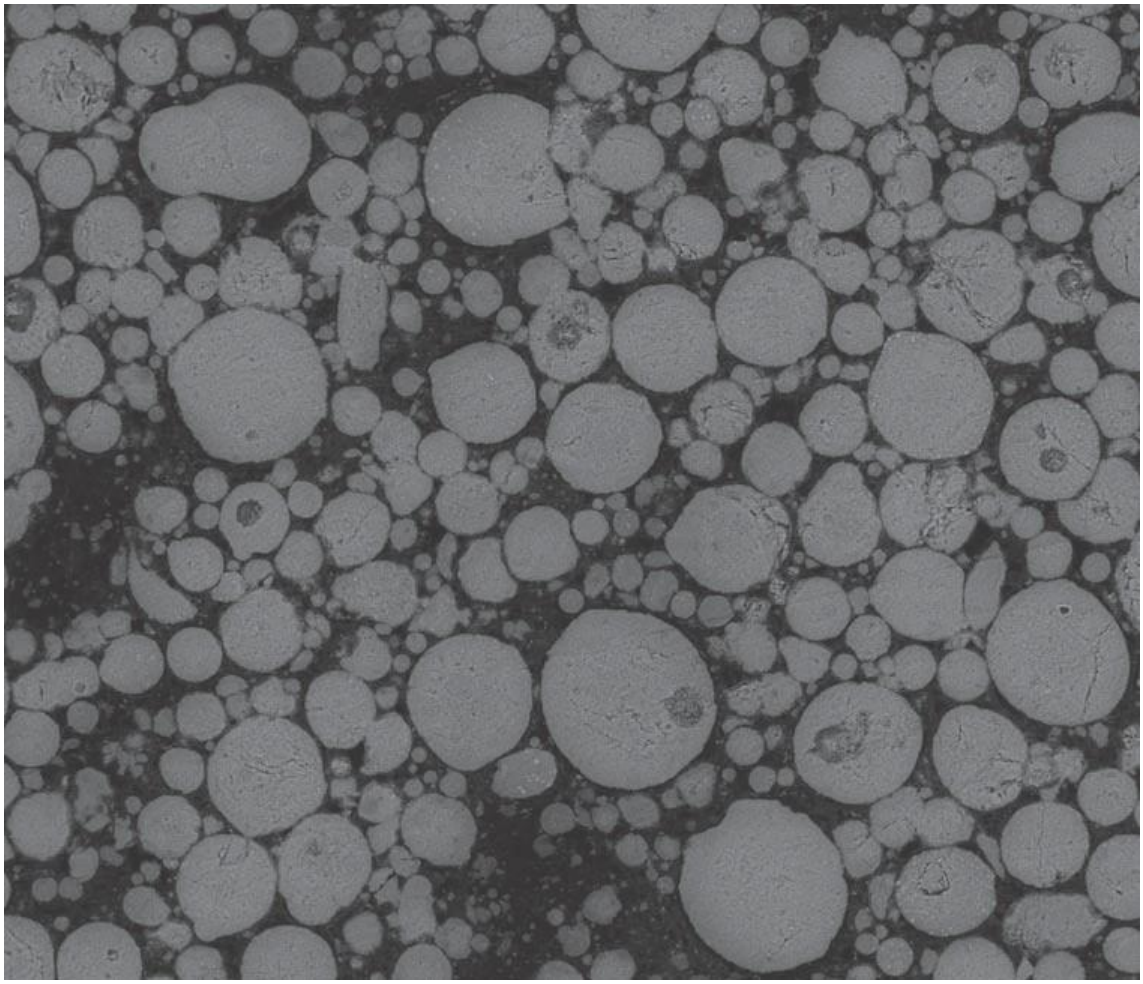

Figure 4. 100: SEM images of the PVDF-BST nanocomposite with 80% of BST fill by volume

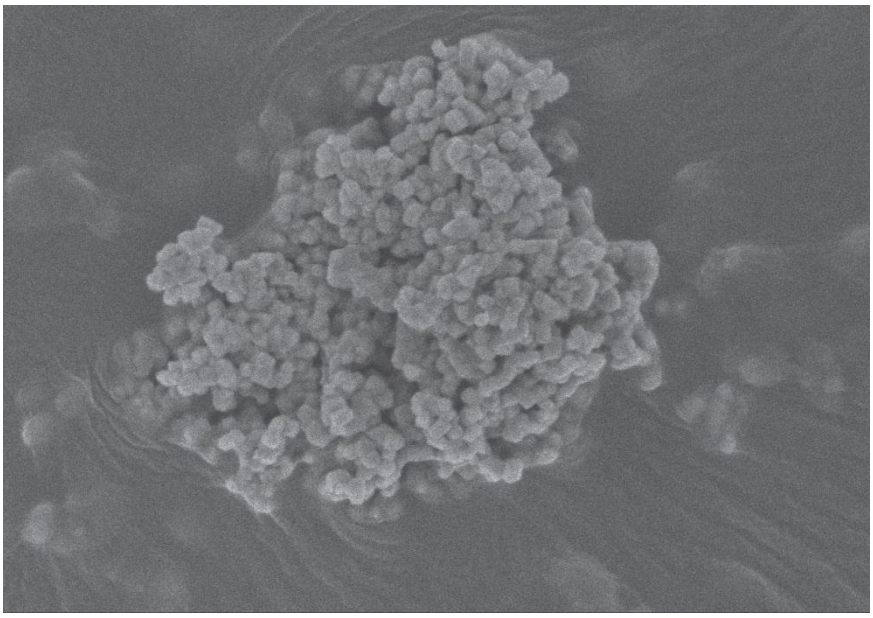

Figure 4. 101: SEM images of dry BST powder before mixing at different magnifications.

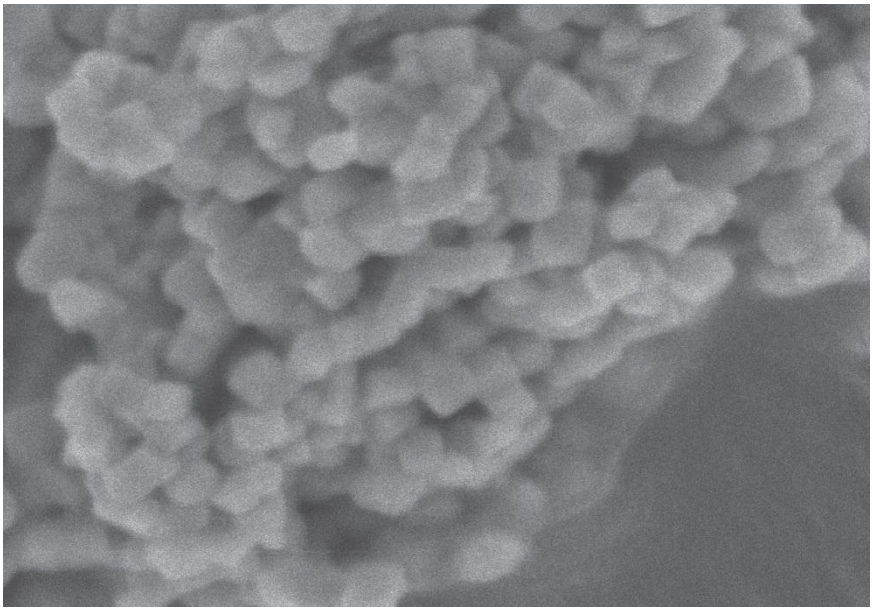

Figure 4. 102: SEM images of dry BST powder before mixing at different magnifications.

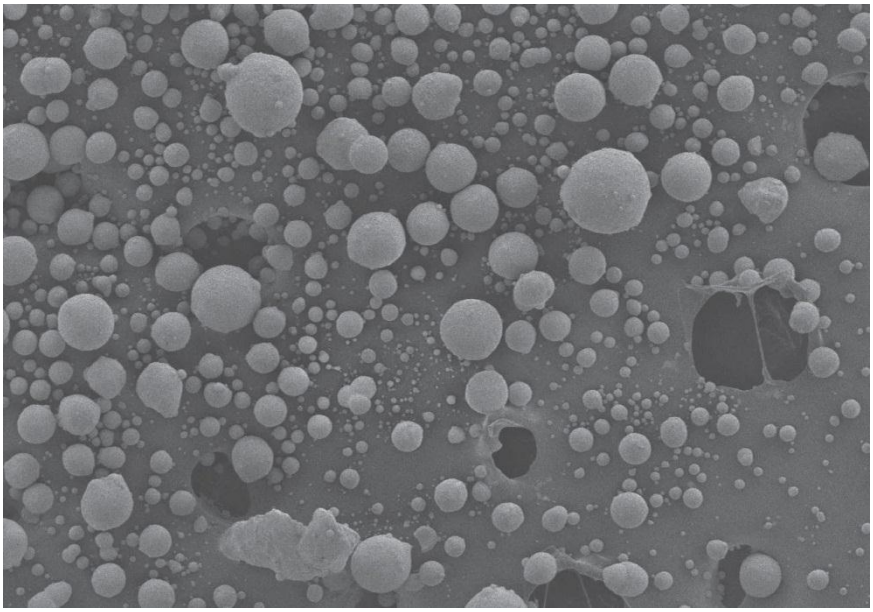

Figure 4. 103: SEM images of dry BST powder before mixing at different magnifications.

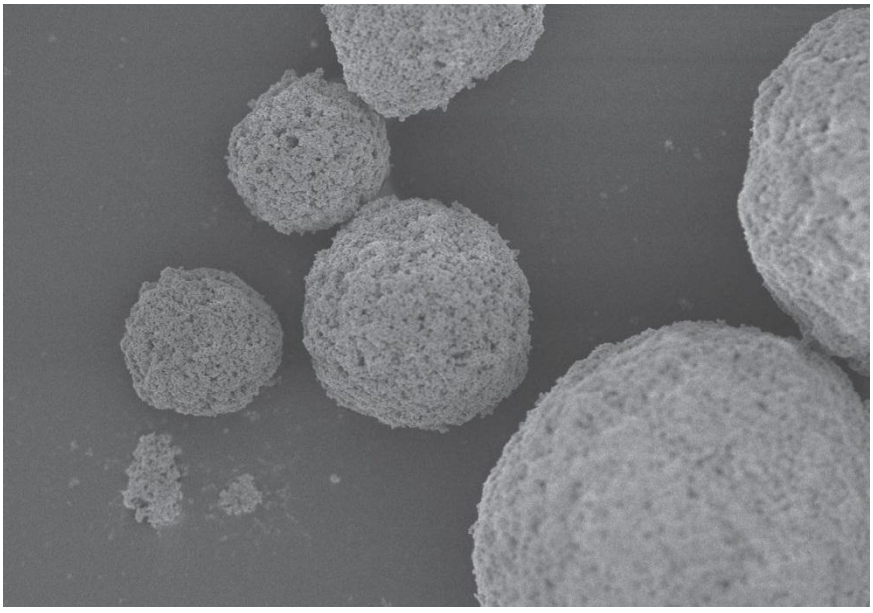

Figure 4. 104: SEM images of dry BST powder before mixing at different magnifications.

4.6 Conclusion and Future Investigations

Two ceramic powders, BST and ST, were added to two different plastics, Teflon and PVDF, by a commercial manufacturer in order to increase the dielectric constant of plastic materials. The addition of the ceramic did increase the dielectric constant compared to the bare plastic material, but the increase was not as much as expected. The SEM images show that the ceramic particles did not evenly disperse in the plastic matrix which seems to be the cause of the less than expected dielectric constant. Poor interphase bonding could have led to the condition displayed in the SEM images. This poor bonding could be a result of the two materials tendency to bond with itself rather than the other phase of the material.

A number of changes could be made to increase the interphase bonding and de- crease the clumping of the ceramic particles. The SEM images of the dry powder show that the particles are already clumped together, which is a product of the drying process or the particle preparation. The formation and the processing of the particles occurs in an aqueous solution. If the mixing of the plastic and the ceramic particles took place when the ceramic was still in the aqueous solution, the pre-clumping of the ceramic particles might be avoided.

Another possibility is using an aqueous plastic monomer. One could mix an aqueous plastic monomer to the aqueous ceramic nanoparticles with a sonicator and then add a catalyst that would polymerize the plastic in situ.

If pre-clumping of the dried ceramic powder represents a bonding between the particles themselves. A surfactant could be added to the mixing process that would help break up the particles and better disperse them within the plastic matrix. There are a number of commercial surfactants that could be used for this purpose.

It seems that the smaller the grain size of the ceramic particles, the harder it is to effectively mix them together. Using a ceramic powder with a larger grain size might help in the mixing process. The larger grain size would lower surface area to volume ratio which would lower the dielectric constant of the powder, but the increase of the effectiveness of the mixing process might outweigh that decrease.

The BST filler material increased the dielectric constant of the Teflon composites by more than a factor of two. This seems to indicate that the BST ceramic particles are a better choice for a high dielectric constant nanocomposite. This was expected because the dielectric constant of BST is intrinsically higher than that of ST at room temperature.

The BST/Teflon composite had approximately 50% higher dielectric constant than the BST/PVDF composite for the same volume fraction of the filler. This was un- expected since the dielectric constant of bare PVDF is four times that of Teflon. This was probably due to the Teflon composite, which mixed better than the PVDF composite. This does not necessarily mean that Teflon is a better candidate. If the mixing techniques can be corrected, the higher initial PVDF dielectric constant could still help it to outperform Teflon.

4.7 BIBLIOGRAPHY FOR CHAPTER 4

[1] Teflon PTFE 612A, DuPont, Wilmington, Delaware.

[2] H. T. Vo and F. G. Shi, "Towards model-based engineering of optoelectronic packaging materials: dielectric constant modeling," Microelectronics Journal, vol. 33, pp. 409–415, 2002.

[3] N. Lombardo, "A two-way particle mapping for calculation of the effective dielectric response of graded spherical composites," Composites Science and Technology, vol. 67, 2007.

[4] M. Todd and F. Shi, "Complex permittivity of composite systems: a comprehensive interphase approach," IEEE Transactions on Dielectrics and Electrical Insulations, vol. 12, no. 3, pp. 601–611, 2005.

[5] M. G. Todd and F. G. Shi, "Characterizing the interphase dielectric constant of polymer composite materials: effect of chemical coupling agents," Journal of Applied Physics, vol. 94, no. 7, pp. 4551–4557, 2003.

[6] P. Murugaraj, D. Mainwaring, and N. Mora-Huertas, "Dielectric enhancement in polymer-nanoparticle composites through interphase polarizability," Journal of Applied Physics, vol. 98, 2005.